



HAL
open science

Exocytose : analyse de la cinétique du développement du pore de fusion et de la libération sécrétoire associée

Lihui Hu

► To cite this version:

Lihui Hu. Exocytose : analyse de la cinétique du développement du pore de fusion et de la libération sécrétoire associée. Chimie analytique. Université Paris sciences et lettres, 2018. Français. NNT : 2018PSLEE087 . tel-03405382

HAL Id: tel-03405382

<https://theses.hal.science/tel-03405382>

Submitted on 27 Oct 2021

HAL is a multi-disciplinary open access archive for the deposit and dissemination of scientific research documents, whether they are published or not. The documents may come from teaching and research institutions in France or abroad, or from public or private research centers.

L'archive ouverte pluridisciplinaire **HAL**, est destinée au dépôt et à la diffusion de documents scientifiques de niveau recherche, publiés ou non, émanant des établissements d'enseignement et de recherche français ou étrangers, des laboratoires publics ou privés.

THÈSE DE DOCTORAT

de l'Université de recherche Paris Sciences et Lettres
PSL Research University

Préparée à l'Ecole Normale Supérieure

**Deciphering exocytosis: kinetic analysis of fusion pore
development and its associated secretory release**

**Exocytose : analyse de la cinétique du développement du pore
de fusion et de la libération sécrétoire associée**

Ecole doctorale n°388

Chimie physique et chimie analytique de Paris Centre

Spécialité Chimie analytique

**Soutenue par Lihui HU
le 23/11/2018**

Dirigée par **Christian AMATORE**
et **Jérôme DELACOTTE**

COMPOSITION DU JURY :

Mme. SZUNERITS Sabine
Université de Lille, Rapporteur

M. SOJIC Neso
Ecole Nationale Supérieure de Chimie et
de Physique de Bordeaux, Rapporteur

Mme. LOJOU Elisabeth
CNRS, Examineur

M. BEDIUI Fethi
Chimie ParisTech, Examineur

M. AMATORE Christian
Ecole Normale Supérieure, Directeur de
thèse

M. DELACOTTE Jérôme
Ecole Normale Supérieure, Co-encadrant
de thèse



Résumé en français

Exocytose : analyse de la cinétique du développement du pore de fusion et de la libération sécrétoire associée

LIHUI HU

Introduction

Exocytose

Les cellules, en tant qu'entités élémentaires constituant les êtres vivants, assurent des fonctions physiologiques à l'échelle de l'organisme via la communication intercellulaire. Cette communication repose de façon générale sur un échange de signaux. L'exocytose vésiculaire est une voie de signalisation qui consiste en la libération de messagers chimiques ou biochimiques tels que les hormones et les neurotransmetteurs dans le milieu extracellulaire. Les molécules messagères contenues à l'intérieur de vésicules intracellulaires sont libérées suite à la fusion de la membrane vésiculaire avec la membrane cellulaire pour induire une réponse physiologique. L'exocytose, compte tenu de son rôle crucial en biologie cellulaire et de son implication dans certaines pathologies, a fait l'objet de nombreuses études au cours de ces dernières décennies et de deux prix Nobel.

De façon générale, le processus de sécrétion vésiculaire peut être divisé en quatre étapes principales décrites dans la figure 1. Les messagers biochimiques sont chargés dans les vésicules qui migrent ensuite vers la membrane. La troisième étape est l'arrimage de la vésicule à la membrane cellulaire puis l'exocytose débute par la fusion des membranes vésiculaires et cellulaires. La libération des molécules contenues dans la vésicule se produit initialement par le pore de fusion ainsi formé.

Après l'expansion du pore de fusion rendant possible la libération des molécules intravésiculaires, la vésicule peut être recyclée par fermeture du pore. Ce scénario prédomine dans le cas de la sécrétion régulée. Une alternative à la fermeture du pore est la fusion permanente de la membrane vésiculaire dans la membrane cellulaire (fusion complète). Ces deux modes d'exocytose aboutissent respectivement à une libération partielle et totale du contenu des vésicules.

Les modèles cellulaires habituellement dédiés à l'étude de la sécrétion de neuromédiateurs incluent les neurones et les cellules chromaffines. Au cours des vingt dernières années, les cellules chromaffines ont été supplantées par les cellules PC12 issues d'une tumeur (phéochromocytome) des glandes surrénales du rat. Les cellules PC12 peuvent en effet être cultivées et manipulées pharmacologiquement ce qui les rend d'un usage plus aisé que des cellules chromaffines prélevées sur un animal. De plus, la différenciation des cellules PC12 en cellule neurosécrétoire est possible par traitement au facteur de croissance. Les cellules PC12 ont donc été adoptées comme modèle dans ce travail de thèse.

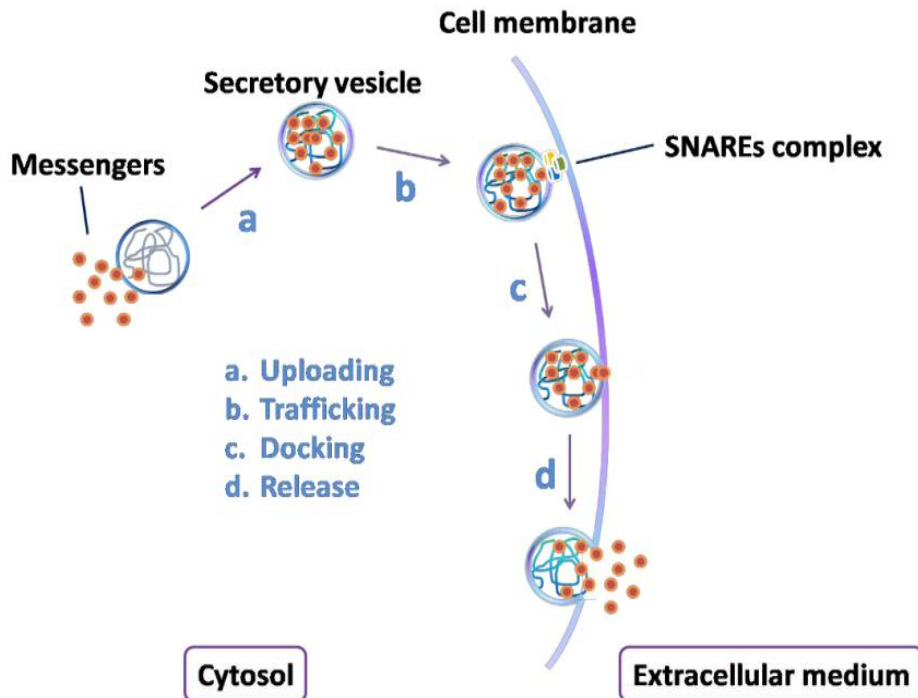


Fig 1. Représentation schématique des quatre étapes principales de sécrétion : chargement des vésicules, migration des vésicules, arimage, des vésicules, libération à travers le pore de fusion.

Réseau d'actine corticale et protéines associées

In vivo, le cytosquelette est composé de filaments polymériques d'actine et des protéines associées. Ces protéines liées à l'actine sont impliquées dans la polymérisation, la dépolymérisation, le branchement et le mouvement relatif des filaments (myosines). Le cortex d'actine aussi appelé le cortex d'actomyosin est situé sur la face interne de la membrane cellulaire et s'étend sur une épaisseur de quelques centaines de nanomètres. Après la migration des vésicules sécrétoires au voisinage de la membrane, ce réseau d'actine cortical peut réguler l'accès à la membrane et pourrait donc également être impliqué dans la régulation des étapes d'arrimage des vésicules. Au cours de cette thèse, nous nous sommes intéressés au rôle du moteur moléculaire myosine II dans la libération des neuromédiateurs et dans l'évolution du pore de fusion.

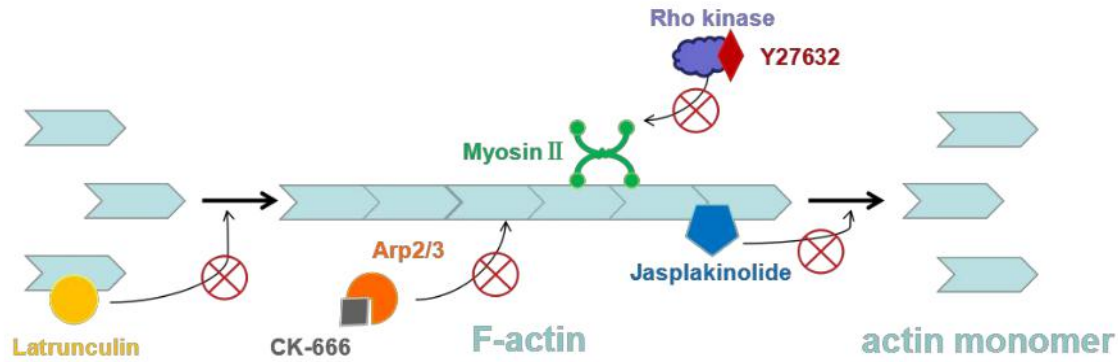


Fig 2. Représentation schématique du mode d'action des inhibiteurs utilisés pour perturber la polymérisation (latrunculine) , la dépolymérisation (Jasplakinolide) de l'actine ou le branchement des filaments (inactivation du complexe Arp2/3 nécessaire au branchement).

Le rôle de l'actine est habituellement étudié en utilisant des toxines et des agents pharmacologiques qui interfèrent avec la polymérisation, la dépolymérisation et le réarrangement des filaments d'actine. Les modes d'action des inhibiteurs les plus usuels et utilisables avec des cellules non fixées sont représentés schématiquement sur la figure 2. La latrunculine inhibe la polymérisation en séquestrant les monomères d'actine. La dépolymérisation conduit alors à la déstabilisation du réseau de filaments d'actine. La Jasplakinolide stabilise les filaments d'actine empêchant la dépolymérisation. Les moteurs moléculaires myosine II peuvent être inactivés indirectement par inhibition de la rho-kinase qui catalyse la phosphorylation des myosine II.

Méthodes analytiques pour l'étude de l'exocytose

Les méthodes développées pour l'analyse de l'exocytose sont principalement de nature optique et électrique. En particulier, l'ampérométrie sur microélectrode permet le suivi de la libération des neuromédiateurs et leur quantification. La dynamique de l'exocytose peut être suivie par microscopie de fluorescence, imposant alors le marquage luminal ou membranaire de la vésicule.

Nous décrivons brièvement ci-dessous, le principe des méthodes ampérométriques et de la microscopie de fluorescence à réflexion totale (TIRFM) ainsi que les stratégies de marquage couramment utilisées

pour le suivi de l'exocytose par microscopie de fluorescence.

Ampérométrie

Le suivi ampérométrique de l'exocytose repose sur l'oxydation des neuromédiateurs libérés à la surface d'une électrode positionnée en contact avec la cellule (distance de l'ordre de 100 nm). Le potentiel de l'électrode est maintenu à un potentiel permettant l'oxydation du neuromédiateur libéré. Un événement exocytotique est alors détecté comme un pic de courant (Figure 3).

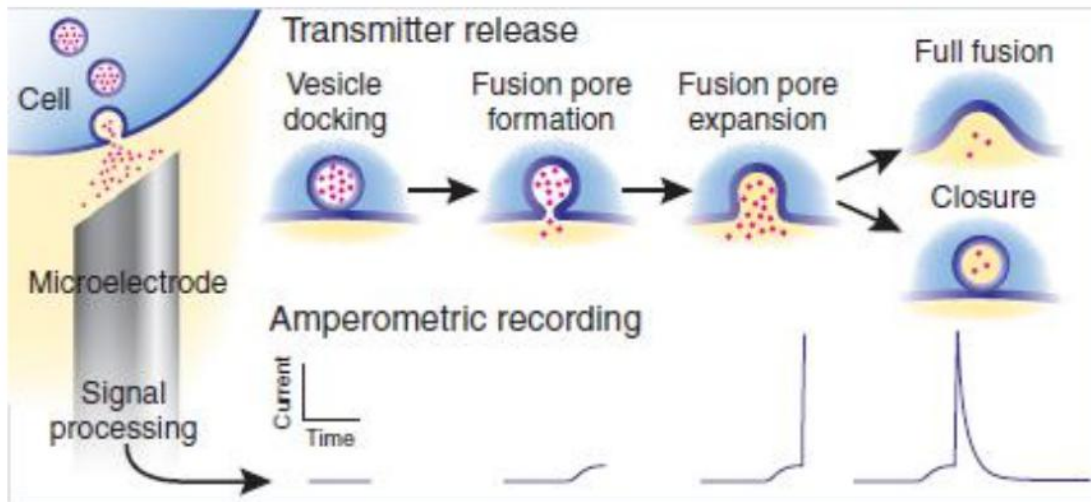


Fig 3. Détection d'un événement d'exocytose par ampérométrie sur microélectrode. La libération des neuromédiateurs à travers le pore de fusion se traduit par une légère augmentation du courant (pied de pic). La libération des neuromédiateurs résultant de l'ouverture du pore entraîne ensuite l'apparition d'un pic de courant.

Le courant est mesuré avec une résolution temporelle de quelques dizaines de microsecondes. La quantité de neuromédiateurs libérés, de l'ordre de 10^4 à 10^5 molécules, est proportionnelle à la charge détectée sur l'ensemble du pic de courant. Une analyse plus fine du pic de courant permet également de caractériser la dynamique de la libération des neurotransmetteurs sur une durée de quelques dizaines de millisecondes.

Microscopie de fluorescence à réflexion totale (TIRFM)

L'illumination par réflexion totale présente l'intérêt d'exciter sélectivement les fluorophores situés à

quelques centaines de nanomètres de l'interface sur laquelle la lumière est réfléchi. Pour le suivi de l'exocytose, la réflexion totale du faisceau d'illumination à l'interface substrat/échantillon permet d'imager sélectivement la membrane basale de la cellule où se produit l'exocytose. Le bruit de fond dû aux fluorophores présents dans les parties supérieures de la cellule est ainsi éliminé. Cette amélioration du rapport signal/bruit s'accompagne également d'une diminution de la phototoxicité en comparaison avec la microscopie confocale ou en épifluorescence. D'autre part, la résolution temporelle est supérieure à celle accessible en microscopie confocale avec des valeurs de quelques dizaines de millisecondes.

La figure 4 illustre le principe de formation du champ évanescent à l'interface substrat/échantillon. Le substrat présente un indice de réfraction supérieur à celui de l'échantillon. Il est alors possible de former un champ évanescent en illuminant l'interface sous un angle supérieur à l'angle critique au delà duquel le faisceau est réfléchi. En deçà de l'angle critique, le faisceau lumineux est transmis et illumine l'échantillon dans toute son épaisseur (épifluorescence).

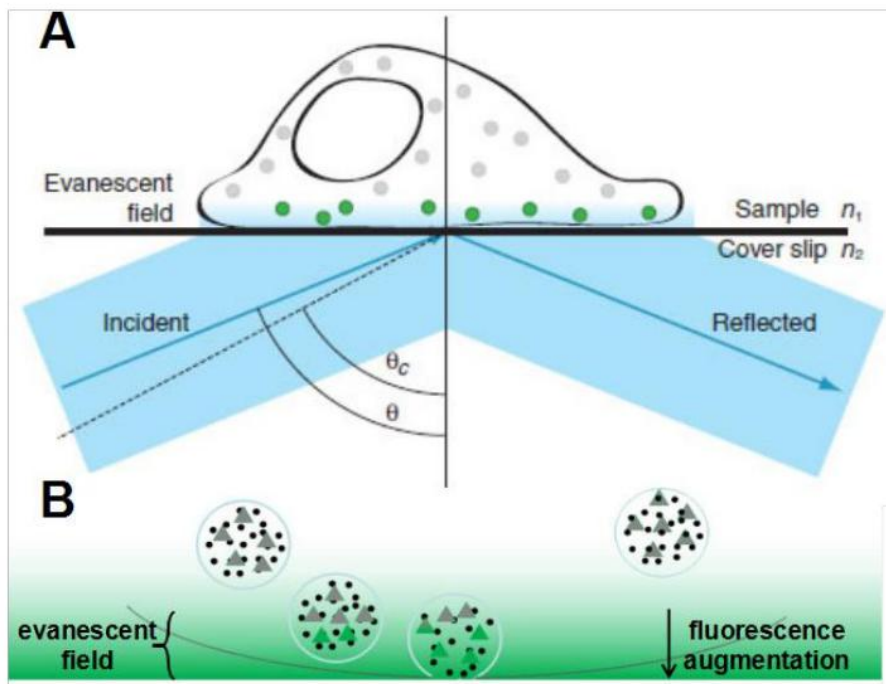


Fig. 4 A : Formation d'un champ évanescent à l'interface substrat/échantillon par un faisceau incident à un angle d'incidence supérieur à l'angle critique (θ_c). B : illumination sélective des fluorophores proches de l'interface substrat/échantillon.

Les vésicules peuvent être marquées par des sondes qui permettent leur visualisation avant l'exocytose ou encore de détecter l'ouverture du pore de fusion ainsi que sa fermeture éventuelle. Le suivi d'un évènement d'exocytose peut ainsi être réalisé sur une durée de plusieurs secondes (selon les propriétés du fluorophore utilisé) donnant des indications sur la libération du contenu des vésicules, l'état d'ouverture ou de fermeture du pore et le mélange de la membrane vésiculaire avec la membrane de la cellule.

Marquage fluorescent des vésicules

Parallèlement au développement des méthodes de microscopie de fluorescence, des sondes fluorescentes ont été élaborées afin de caractériser les propriétés des vésicules exocytotiques (pH, recyclage par endocytose) et la dynamique de l'exocytose. Les quatre principales stratégies de marquage des vésicules consistent à (i) insérer un fluorophore dans la membrane, (ii) lier un fluorophore à une protéine membranaire, (iii) internaliser une sonde dans le lumen, (iv) lier un fluorophore à un peptide intravésiculaire. La figure 5 illustre ces approches à travers des exemples d'utilisation de sondes fluorescentes dans l'étude de la dynamique de l'exocytose et des propriétés physico-chimiques des vésicules.

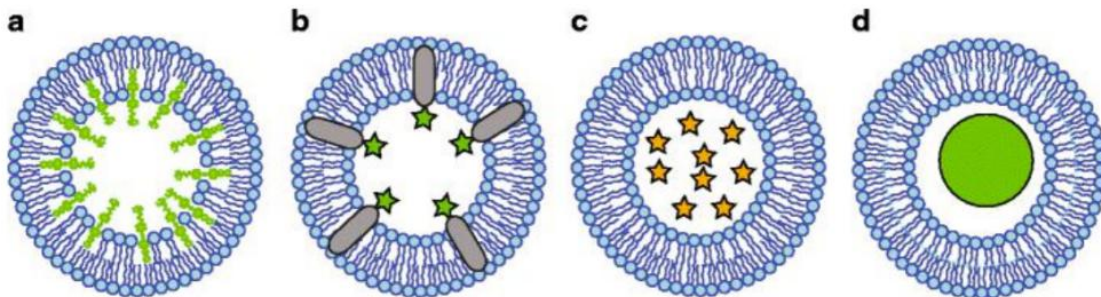


Fig. 5 A) Les sondes styryles s'insèrent dans le feuillet interne de la membrane par endocytose. B) Les protéines membranaires marquées par des sondes sensibles au pH permettent la mesure du pH intravésiculaire ou la détection de la formation du pore de fusion. C) Sondes fluorescentes concentrées à l'intérieur des vésicules. D) Des peptides marqués génétiquement encodés sont exprimés à l'intérieur des vésicules.

Objet de la thèse

Mon travail de thèse est centré sur l'étude des facteurs influençant la cinétique de libération lors de la sécrétion vésiculaire. Dans une première partie, l'électroactivité d'un faux neurotransmetteur fluorescent (FFN102) a été utilisée pour quantifier son internalisation dans les vésicules des cellules PC12. Nos analyses ampérométriques ont permis de montrer que cette sonde remplaçait une partie de la dopamine endogène stockée dans ces vésicules. La cinétique de libération du FFN102 reflétait également la structure "bi-phasique" du lumen des vésicules sécrétoires.

Dans une deuxième partie, le rôle du moteur moléculaire myosine II dans l'expansion du pore de fusion a été caractérisé. Une mesure ampérométrique de la cinétique d'ouverture du pore a permis de montrer que la myosine II contribuait à réguler l'expansion du pore lors de l'exocytose dans les cellules PC12. L'inhibition des myosines II entraîne une expansion plus rapide sans modifier la taille maximale atteinte par le pore.

Dans la dernière partie, nous avons réalisé le suivi d'évènements d'exocytose uniques dans leur intégralité. La libération du neuromédiateur a été caractérisée par ampérométrie et l'évolution de la membrane vésiculaire a été suivie simultanément par TIRFM sur cellule PC12. Dans la grande majorité des cas, le pore se referme et la vésicule est conservée. Dans une minorité de cas, la membrane vésiculaire s'intègre complètement à la membrane cellulaire.

Remplacement partiel de la dopamine par un faux neurotransmetteur fluorescent et électroactif dans les cellules PC12

La libération des neuromédiateurs, phase cruciale de l'exocytose, a été étudiée en utilisant un faux neurotransmetteur fluorescent sensible au pH (FFN102). Cette sonde, analogue synthétique de neuromédiateurs endogènes, a été précédemment utilisée comme sonde fluorescente pour signaler le début de l'exocytose qui se traduit par une augmentation de la fluorescence. Les propriétés électroactives de FFN102 avaient déjà été mises à profit pour suivre l'exocytose sur les cellules BON N13, par ampérométrie et par microscopie de fluorescence. L'utilisation de FFN102 minimise les perturbations imposées à la cellule. En effet, FFN102 présente un faible encombrement stérique comparé à celui des sondes fluorescentes liées à des protéines ou à des peptides. De plus, FFN102 est reconnu par les transporteurs des monoamines assurant le chargement des vésicules en monoamines. Il

en résulte une spécificité du marquage des vésicules.

La libération de neurotransmetteurs par des cellules PC12 uniques a été stimulée pour détecter sélectivement la dopamine seule ou la dopamine et le FFN102 (figure 6). Les traces ampérométriques ont été enregistrées en utilisant une microélectrode de carbone. Le potentiel de l'électrode a été maintenu au potentiel de 650 mV ou de 900 mV (vs Ag/AgCl) pour assurer une oxydation rapide de la dopamine seule ou de la dopamine et du FFN102.

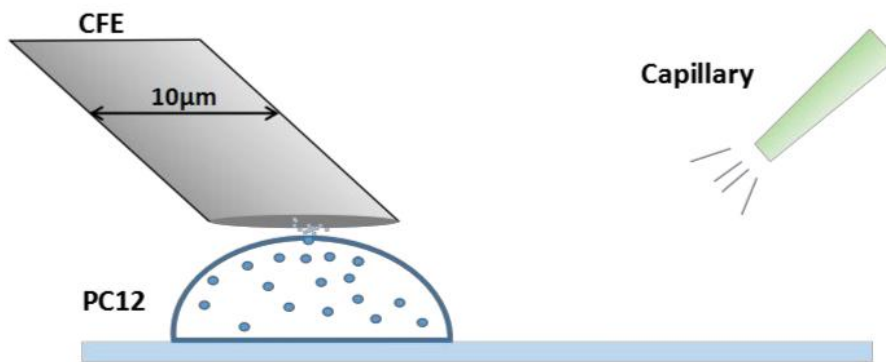


Fig. 6 Configuration d'une mesure ampérométrique dite de "synapse artificielle". L'électrode de carbone est au contact de la membrane apicale d'une cellule PC12 stimulée par injection d'un stimulant à proximité de la cellule.

La détection ampérométrique a été effectuée sur des cellules pré-incubées dans un milieu supplémenté en FFN102 et sur des cellules contrôle n'ayant pas subi de pré-incubation. Un nombre d'évènements d'exocytose supérieur à 300 a été détecté sur 16 cellules dans chacune des conditions expérimentales. Les pics ampérométriques ont été analysés individuellement à l'aide un programme développé au laboratoire. L'intensité maximale du courant, la durée du pic, la charge totale détectée ont été compilées. La comparaison de la charge détectée en oxydant sélectivement la dopamine seule ou la dopamine et le FFN102 montre que le FFN102 remplace partiellement la dopamine endogène stockée dans les vésicules (figure 7). La fraction de dopamine remplacée est de 10%.

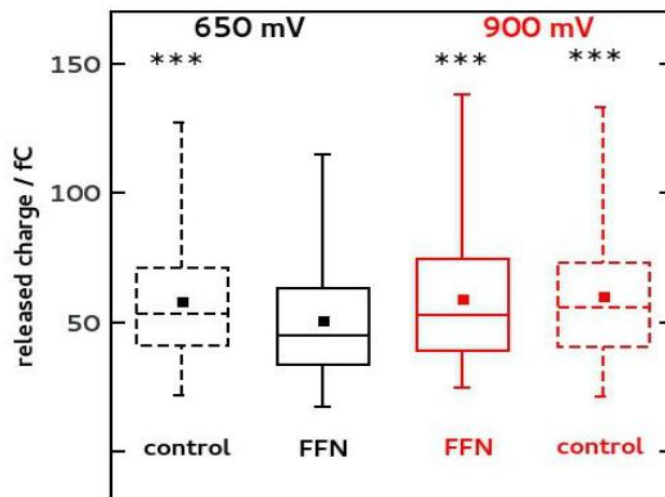


Fig. 7 Caractéristiques des distributions de charge détectées en oxydant la dopamine (650 mV vs Ag/AgCl) et par oxydation de la dopamine et du FFN102 (900 mV vs AG/AgCl) pour les cellules traitées (trait plein) et sur les cellules contrôle (trait pointillé). Les lignes horizontales correspondent aux trois premiers quartiles, les “moustaches” indiquent la gamme 5%-95%. Le point central indique la valeur moyenne.

De plus, l'analyse des pieds de pics indique que le FFN102 représente 30% des neuromédiateurs libérés à travers le pore de fusion initial (i.e. avant expansion de ce dernier). Cette observation suggère le stockage du FFN102 dans un compartiment des vésicules où le transport des neuromédiateurs est rapide.

Nous avons démontré que l'analogue de neurotransmetteur FFN102, associé au modèle cellulaire de neurosécrétion PC12, constitue un système adapté aux études bioanalytiques et pharmacologiques.

La dopamine stockée initialement dans les vésicules des cellules PC12 est remplacée par le FFN102 dans une proportion de 10%. Les potentiels d'oxydation différents de FFN102 et de la dopamine ont été utilisés pour quantifier le remplacement. La cinétique de libération du FFN102 reflète la structure “bi-phasique” des vésicules.

Role du moteur moléculaire myosin II dans la régulation du pore de fusion

Au cours de l'exocytose, l'expansion du pore de fusion permet la libération des neuromédiateurs dans le milieu extracellulaire. La mesure de la cinétique d'ouverture du pore de fusion à partir d'un pic ampérométrique a été récemment rendue possible par une méthode d'analyse développée précédemment au laboratoire.

Lorsque la libération des neuromédiateurs résulte d'une diffusion quasi stationnaire, il est possible de reconstruire la cinétique d'ouverture du pore de fusion à partir d'un pic ampérométrique. La taille du pore peut même être déterminée à un facteur de calibration près (figure 8).

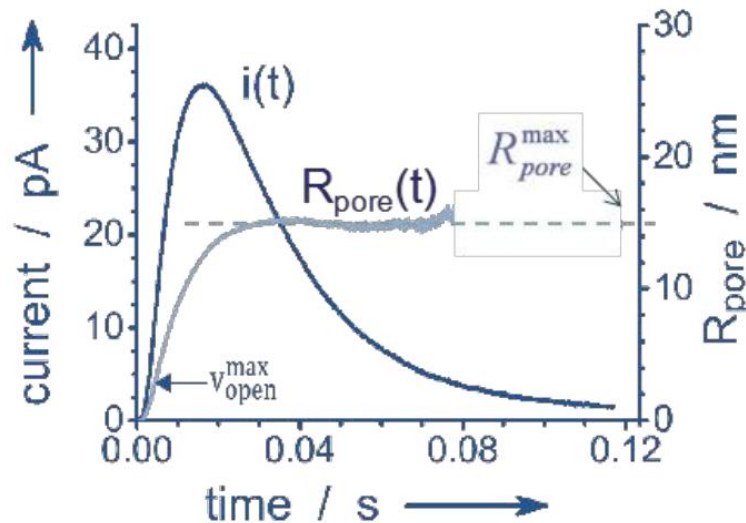


Fig. 8 Illustration de la reconstruction de la taille du pore et de la cinétique d'ouverture à partir d'un pic ampérométrique.

Cette méthode originale permettant de suivre l'évolution de la taille du pore durant la phase de libération des neuromédiateurs a été mise à profit pour évaluer l'influence du moteur moléculaire myosine II dans la régulation du pore.

Nous avons utilisé la configuration de synapse artificielle décrite plus haut et réalisé une analyse statistique portant sur plus de 100 événements obtenus sur 12 cellules contrôle et plus de cent événements sur 12 cellules traitées par un inhibiteur des myosines II (Y27632, 10 μ M, 10 min).

L'inhibition des myosines II a entraîné l'accélération de l'ouverture du pore (figure 9).

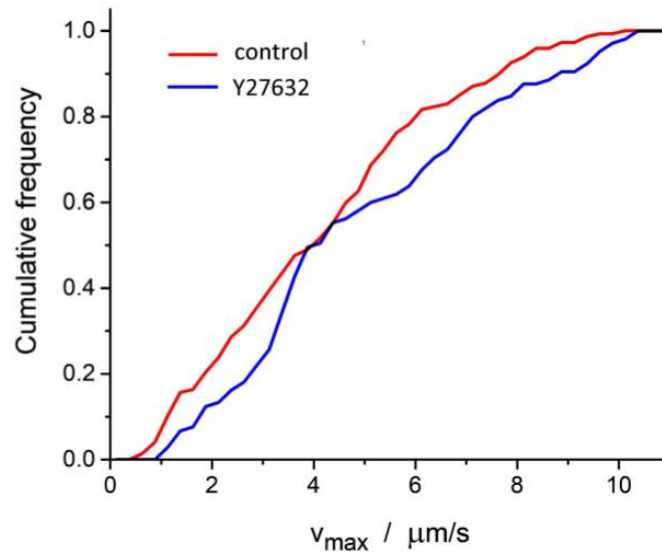


Fig. 9 Fonction de distribution cumulative des vitesses maximales d'expansion du pore pour les cellules contrôle (rouge) et pour les cellules traitées avec Y27632 (bleu). Les valeurs moyennes dans le groupe contrôle et dans le groupe traité sont respectivement $4.23\mu\text{m/s}$ et $4.97\mu\text{m/s}$.

Par ailleurs, la quantité de dopamine libérée et la taille maximale du pore sont restées inchangées par inhibition des myosines II. De façon notable, l'inhibition des myosines II a entraîné une augmentation du nombre de pics présentant un second temps caractéristique de libération. Cette observation suggère que l'inhibition des myosines II accélère la libération de la dopamine stockée dans les compartiments à diffusion rapide des vésicules. Il en résulterait une libération anticipée de la dopamine stockée dans les compartiments à diffusion lente vers les compartiments à diffusion rapide avant libération par le pore avec un temps caractéristique plus grand.

Suivi simultané de la libération des neurotransmetteurs et de l'évolution du pore de fusion

L'élargissement du pore de fusion pour la libération de petits neuromédiateurs comme la dopamine est suivi majoritairement d'une fermeture du pore. La vésicule est alors conservée et la libération en neuromédiateurs est partielle. Ce mode d'exocytose est qualifié de "kiss and run" ou "cavicapture". Une alternative à la fermeture consiste en une fusion complète de la membrane vésiculaire dans la

membrane cellulaire. La vésicule n'est alors pas conservée et le contenu vésiculaire est libéré en totalité . Ce mode d'exocytose est dit de “full fusion”.

L'ampérométrie et la microscopie à réflexion totale se complètent avantageusement en permettant un suivi de l'exocytose par la détection du contenu libéré et la visualisation de la membrane vésiculaire. Un évènement d'exocytose peut ainsi être observé dans son intégralité en suivant le devenir de la membrane vésiculaire aux temps longs en tirant bénéfice de la haute résolution de l'ampérométrie aux temps courts pour la détection des neuromédiateurs libérés.

Le suivi ampérométrique et par microscopie de fluorescence à réflexion totale interne ont été réalisées sur un microscope inversé à l'intérieur d'une cage de Faraday. Les cellules PC12 ont été cultivées sur le micro-dispositif élaboré au laboratoire. Préalablement à l'acquisition, le capillaire de stimulation a été placé à environ 20 μm de la cellule à stimuler (figure 10). La dopamine libérée par exocytose a été détectée par oxydation sur l'électrode transparente d'ITO (200 μm x 500 μm). Le signal de fluorescence a été détecté par une camera EMCCD à travers l'électrode transparente.

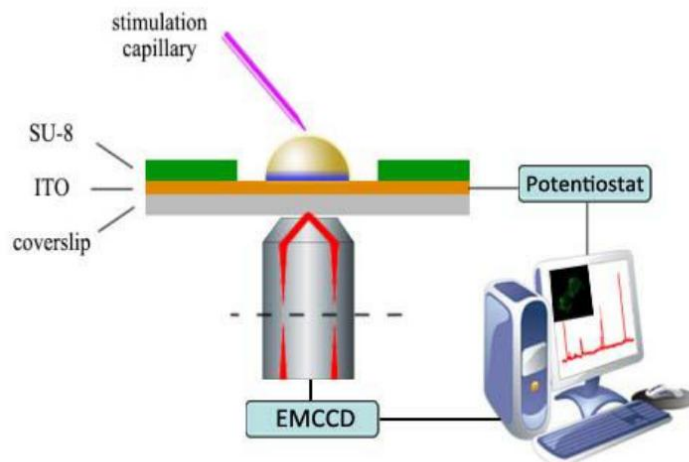


Fig 10. Schéma de principe du dispositif expérimental pour la détection ampérométrique et la visualisation en microscopies de fluorescence.

Le marquage de la membrane vésiculaire a été obtenu à l'aide d'une sonde génétiquement encodée et sensible au pH (pH-luorin) fusionnée au transporteur VMAT2. L'augmentation de pH due à l'ouverture du pore de fusion entraîne une augmentation de la fluorescence. Les évènements d'exocytose ainsi identifiés ont été mis en correspondance avec le signal ampérométrique. L'intensité moyenne a été

mesurée au cours du temps dans un cercle de 640 nm centré sur le point de fusion initial (ROI centrale) et dans la zone annulaire adjacente de diamètre interne 640 nm et de diamètre externe 1280 nm (ROI annulaire).

L'évolution de l'intensité de fluorescence dans ces deux zones a permis d'établir la signature des deux principaux modes d'exocytose rencontrés dans les cellules PC12 : "ouverture – fermeture" et "ouverture complète" (figure 12). Dans les deux cas, 4 phases d'évolution de l'intensité moyenne de fluorescence sont identifiables. Les phases 1 présentent augmentation de la fluorescence dans les deux ROIs, les phases 2 présentent une fluorescence décroissante au centre et croissante dans l'anneau périphérique alimenté par la région centrale. Les phases 4 présentent des intensités moyennes de fluorescence égales dans les deux ROIs. En revanche, les phase 3 sont différentes :

"ouverture et fermeture"

phase 3 : fluorescence à décroissance différente dans les deux régions sans alimentation de l'anneau périphérique par la région centrale en fluorophore.

"ouverture complète"

phase 3 : fluorescence décroissante dans la région centrale et croissante dans la région annulaire due à l'alimentation en VMAT-pHluorin résultant de l'expansion importante du pore.

Les quantités de dopamine détectées au cours des évènements " ouverture-fermeture " sont plus faibles que dans le cas " ouverture complète " . Dans la majorité des cas (17 évènements sur 21, avec 2 cellules), le pore s'est refermé après la libération de la dopamine. Ces observations sont en accord avec certaines hypothèses de la littérature qui rapportent un mode d'exocytose par " ouverture-fermeture " prédominant pour les cellules PC12.

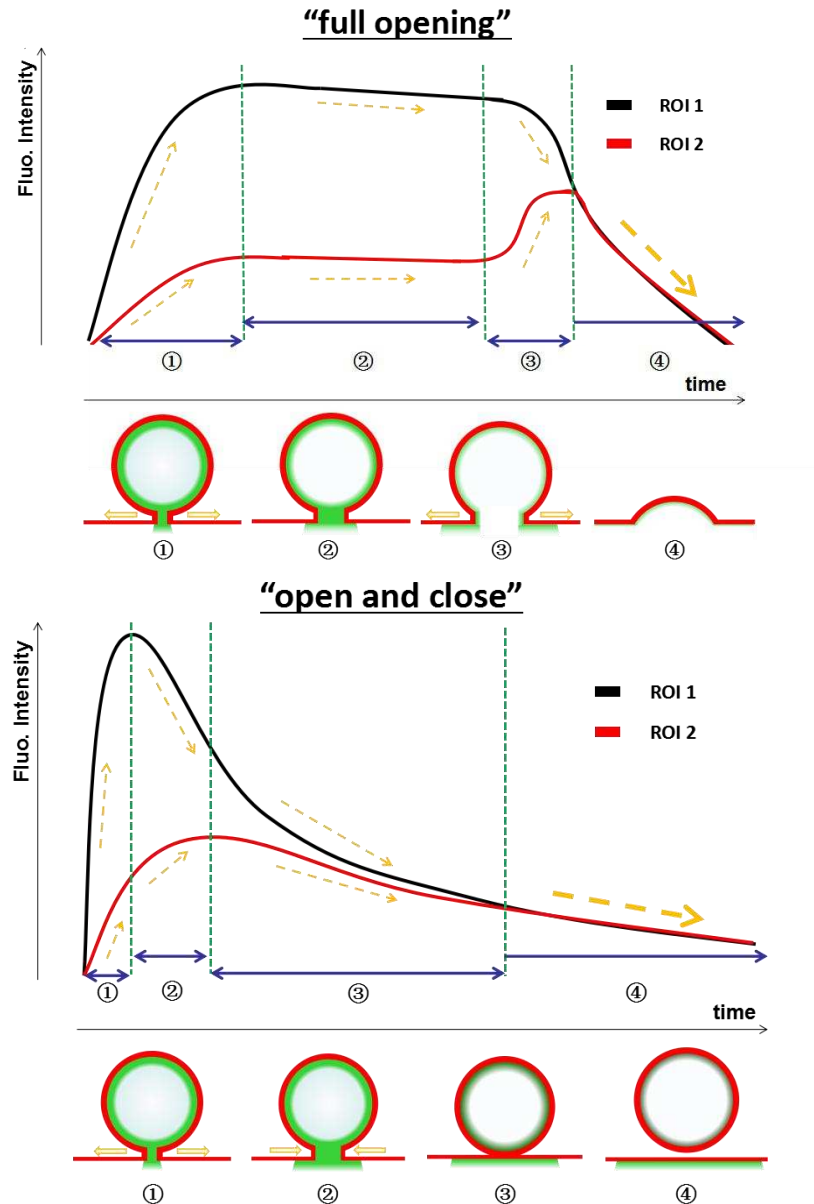


Fig 11. Signature en fluorescence de l'ouverture complète du pore et de son ouverture suivie de sa fermeture. Intensité moyenne de fluorescence dans la ROI centrale (noir) et dans la ROI annulaire (rouge).

Conclusions

L'exocytose, la dernière étape et but du processus de sécrétion, a été étudiée sur des cellules neuroendocrines modèles (PC12). Nous avons caractérisé l'internalisation d'un analogue synthétique de neurotransmetteur (FFN102) dans les vésicules des cellules PC12. La différence de potentiel

d'oxydation de la dopamine et de ce faux neurotransmetteur fluorescent a été exploitée pour montrer que l'internalisation de FFN102 s'effectue en remplaçant 10% de la dopamine endogène présente dans les vésicules. De plus, la cinétique de libération de FFN102 suggère son stockage dans un compartiment de la vésicule où sa diffusion est rapide. Cette sonde électroactive et fluorescente associée aux cellules PC12 constitue donc un système de choix pour des études bioanalytiques impliquant la libération de neurotransmetteurs par exocytose. L'exocytose débute par la formation d'un pore formé par la fusion de la membrane vésiculaire avec la membrane de la cellule. Les mécanismes de régulation de l'expansion du pore de fusion ne sont pas complètement connus. Nous avons montré que la myosine II limite la vitesse d'expansion du pore en détectant la libération de la dopamine par ampérométrie et en traitant les cellules PC12 avec un inhibiteur pharmacologique. La mesure de la cinétique d'ouverture du pore à l'aide d'un modèle développé récemment a montré que la myosine II ne modifie pas la taille maximale du pore au cours de la libération de neurotransmetteurs. Ce suivi ampérométrique de l'expansion du pore est limité à une durée de quelques dizaines de millisecondes; au déjà de laquelle le flux de neurotransmetteurs n'est plus détectable avec précision.

Afin d'étendre la durée du suivi de l'expansion du pore, nous avons réalisé des mesures simultanées de libération de la dopamine par ampérométrie et d'évolution de la membrane vésiculaire par TIRFM. La membrane des vésicules a été marquée par des protéines fluorescentes sensibles au pH et génétiquement encodées. Nous avons pu ainsi observer l'évolution du pore qui s'achève par une fermeture ou une expansion complète. La quantité de neurotransmetteurs détectée était plus importante dans le cas d'une expansion totale du pore.

Acknowledgements

First and foremost, I would like to thank China Scholar Council for the PhD's financial support. I really appreciate the opportunity to stay in Paris for these four years, experiencing the colorful life and making numerous lovely friends. Here I want to give my sincerely gratitude to all those who helped me during this period.

I would like to express my great gratitude to my supervisor Prof. Christian Amatore, who kindly accepted me as one of the members in his laboratory family. I am impressed by his intelligence, rigorous scientific attitude, active mind and continuous spirit of exploration. Many thanks to his generous guidance and warm encouragement during these four years. His words benefit me greatly including but not limit to academic research. It will be beneficial for all my future endeavors.

Alongside, I am immensely grateful to Dr. Jérôme Delacotte as my co-supervisor. I am greatly touched by his passion for scientific research, impressive problem-solving ability and his kindness. I appreciate his patient instruction and kind assistance during my entire PhD. For me, he is not only my supervisor, but also a friend. It's his encourage and support that gave me the strength to keep going on and overcome the difficulties encountered in the project. I will never forget the efforts he made for correcting my PhD manuscript.

I acknowledge all the members in my defense jury: Prof. Sabine Szunerits and Prof. Neso Sojic for the precious evaluation of this work and Dr. Elisabeth Lojou and Dr. Fethi Bedioui for assessing the examination of this thesis.

Special thanks to everyone who helped and contributed in the development of my projects. Many thanks to Dr. Frédéric Lemaître and Dr. Manon Guille-Collignon for their valuable instruction in electrochemistry and experience sharing. I would like to acknowledge Dr. Laurence Grimaud and Alexandra Savy, who devoted to the synthesis of our dual signal probe. I extend my thank to Dr. Alexander I. Oleinick for his generous support of theoretical simulation in this thesis. I also feel grateful to Marie-Aude Plamont, who enlightened me a lot in both cell culture and transfection manipulation. Thanks to Dr. Yong Chen, who kindly allowed me manipulating in his ultra-clean room.

I would like to thank all my dearest friends in our group. I owe a special gratitude to Dr. Xiaoqing Liu, the former PhD in our group. In terms of life, she helped me a lot for getting adapted to the new environment far away from my hometown. While in terms of PhD's project, she not only

taught me all the manipulations hand in hand but also proposed countless valuable advice. The equivalent appreciation owes to Dr. Damien Quinton, for his optimistic attitude and patience which infected me greatly. I also derived massive knowledge and innovative suggestions from those interesting discussions with him. Special thanks to Adnan Sayegh, who spent 3 years and a half with me as my dear teammate struggling for PhD title together. I sincerely thank Justine Pandard for accompanying me when I was in trouble. Her zealous assistance helped me a lot. Thank Léna Beauzamy for a great deal of funny talks and experience sharing.

I am deeply indebted to all the other friends in this department: Marina (for sharing time in cell culture room), all the members in organic chemistry group: Baptiste, Lucas, Indira, Nana, Pierre-Adrien (for sharing the office and organizing wonderful social activities), Chenge (for creating unforgettable memory in Paris and interpretation of French in some cases), Ana (for lots of funny topics), all the members in microfluidic group: Yadong Tang, Bin Wang, Jin Wei, Xiaolong Tu, Li Wang (for their help and suggestions in microfabrication), Ruikang Zhang (for answering my stupid questions in physical aspect), Lidia, Mathieu, Vincent, Guillaume, Eric, Raquel, Yun, etc.

Special thanks to the group named “energetic youngster in ENS”. I really cherish the coffee time with you to share my joy and sorrow. Our wonderful moment such as hiking, weekend traveling will be embedded in my memory forever.

Last but definitely not least, I want to thank my parents, who always remind me to follow my heart when making decisions and be responsible for my own life. Without your support and love, I would not have the chance to chase my PhD in Paris.

Table of contents

Chapter 1: Introduction.....	1
1.1 Vesicular exocytosis.....	1
1.1.1 Principle of exocytosis.....	1
1.1.2 Types of exocytosis.....	2
1.1.3 Cell models for exocytosis study.....	3
1.2 Actin cytoskeleton.....	5
1.2.1 Functions of actin in exocytosis.....	6
1.2.2 Actin associated proteins.....	8
1.2.3 Pharmacological drugs for arresting actin dynamics.....	10
1.3 Ultramicroelectrode in electrochemistry.....	11
1.3.1 Ultramicroelectrode geometry.....	12
1.3.2 Specific properties of UME.....	12
1.3.3 Types of UMEs applied in exocytosis study.....	15
1.4 Analytical techniques for exocytosis investigation.....	19
1.4.1 Electrical methodology.....	20
1.4.2 Optical methodology.....	28
1.4.3 Coupling of optical and electrochemical methods.....	31
1.5 Single vesicles' labeling for tracking exocytosis.....	35
1.5.1 Optical probe for visualization.....	36
1.5.2 Electro-active probe for electrochemical recording.....	37
1.5.3 Collaborative marker for optical and electrochemical detection.....	38
1.6 Research objectives.....	39
1.7 Reference.....	40
Chapter 2: Fluorescent and electroactive false neurotransmitter partially replaces dopamine in PC12 cell vesicles.....	50
2.1 Introduction.....	50
2.2 Materials and methods.....	51

2.3 Results and discussion.....	53
2.4 Conclusion and perspective.....	66
2.5 Reference.....	67
Chapter 3: Exploration of myosin II' s role in regulation of fusion pore opening.....	69
3.1 Introduction.....	69
3.2 Materials and methods.....	70
3.3 Results and discussion.....	73
3.4 Conclusion and perspective.....	85
3.5 Reference.....	86
Chapter 4: Simultaneous monitoring of both neurotransmitter release and fusion pore development.....	88
4.1 Introduction.....	88
4.2 Materials and methods.....	89
4.3 Results and discussion.....	95
4.4 Conclusion and perspective.....	111
4.5 Reference.....	112
Chapter 5: General conclusion and perspective.....	115
Supporting information.....	117
I. Quantitative extraction of fusion pore expansion from amperometric spikes by means of simulation.....	117
II. Cell transfection and selection.....	123

Chapter 1: Introduction

1.1 Vesicular exocytosis

Single cells, the fundamental units in various life systems, cannot stand alone as an independent machine for maintaining the operation of entire biological system. Indeed, cells keep constant communication with their surroundings. Generally speaking, intercellular communication is achieved through the transmission of chemical molecules from an emitting cell to a target cell to initiate the subsequent physiological response. Vesicular exocytosis, as a representative process of intercellular signal exchange, is implemented in an membrane trafficking pathway. It expels those messenger contents such as hormones and neurotransmitters to the extracellular medium synchronously with the incorporation of membrane proteins and lipids to specific domains on plasma membrane. Due to its crucial standing in cell biology and pathological events, investigation of vesicular exocytosis has attracted tremendous attention during the last decades.

1.1.1 Principle of exocytosis

Exocytosis is the main mechanism for communication among secretory cells to deliver molecules out of cell by virtue of membranous containers. In general terms, an individual exocytotic event can be divided into four steps [1], as displayed in Fig. 1.1. At the beginning, the biochemical messengers responsible for signal transmission are synthesized and diverted into secretory vesicles suspended in the cytoplasm. Those mature vesicles are then trafficked towards the cellular membrane through microtubules and their lesser extent, actin filaments, which we interpret in 1.2.2.1. Following the access of vesicles to the secretory site, SNAREs (soluble N-ethylmaleimide sensitive fusion protein attachment receptors)-dependent docking process occurs [2]. Docking begins with the formation of a loose SNAREs complex by the attraction of two kinds of SNAREs: v-SNAREs embedded in vesicular membrane and t-SNAREs expressed on cellular membrane. The progressive tightening step of SNAREs complex overcomes the natural electrostatic repulsion between cellular and vesicular membranes and diminishes the inter-membrane distance to the scale of angstrom level prior to fusion [3, 4]. A small fusion pore ensues in the merged membrane through which biochemical messengers are capable of releasing to the extracellular medium. Eventually, the enlargement of the fusion pore driven by membrane surface tension induces the larger flow of messengers' expulsion.

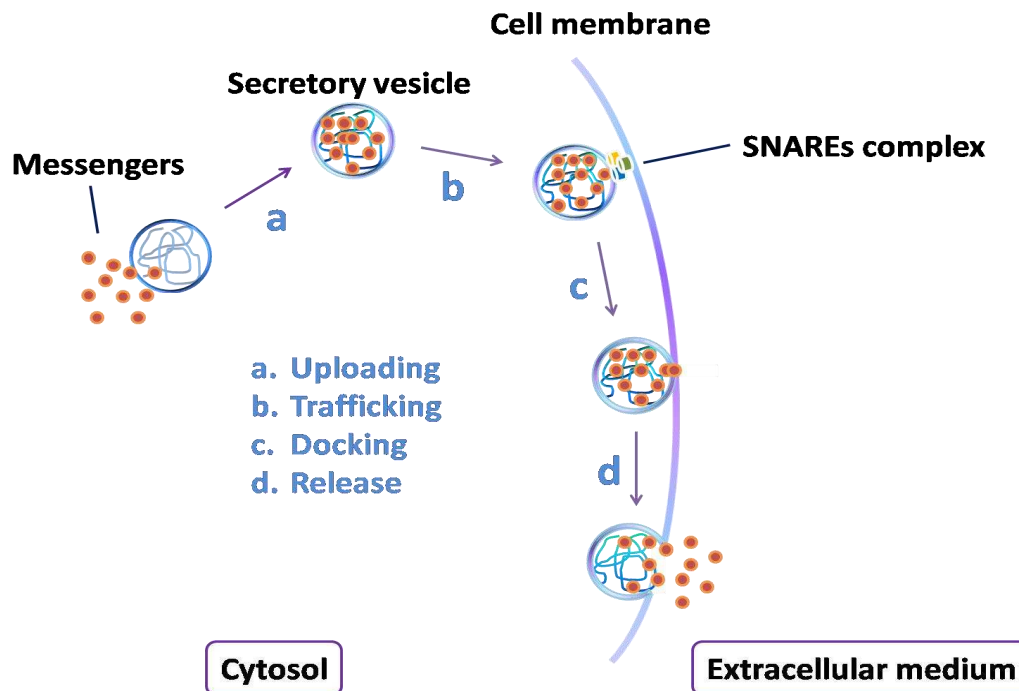


Fig. 1.1 Schematic representation of the main steps of exocytosis

1.1.2 Types of exocytosis

In eukaryotes, depending on different releasing mechanisms, classical exocytosis can be differentiated into two pathways: non-external stimulus triggered constitutive exocytosis and stimulus induced regulated exocytosis, as shown in Fig. 1.2. The constitutive exocytosis is a constant, on-going process that occurs in every cell type. Its presence is significant for the maintenance of plasma membrane and several basic cellular functions. Constitutive exocytosis describes a pathway of continuous vesicular trafficking and non-selective release of protein cargo outward immediately after synthesis. On the contrary, the regulated secretory release only occurred in some specialized secretory cells to satisfy specific physiological tasks, such as neurotransmission, respiration, digestion, reproduction, and the immune response. In this case, both acidic proteins and small cationized molecules are stored in preformed secretory vesicles for later release responding to extracellular signal stimulation. Unlike the diversion of newly produced proteins into vesicles from Golgi apparatus, these small molecules are actively transported from the cytosol. The ionic interaction between cationic molecules and the acidic proteins (e.g. Chromagranin A) inside vesicles allows the osmotic balance of vesicular interior to cell cytosol and thus ensuring the maintenance of vesicular contents with high concentration. In this thesis, we mainly focus on Ca^{2+} regulated exocytosis.

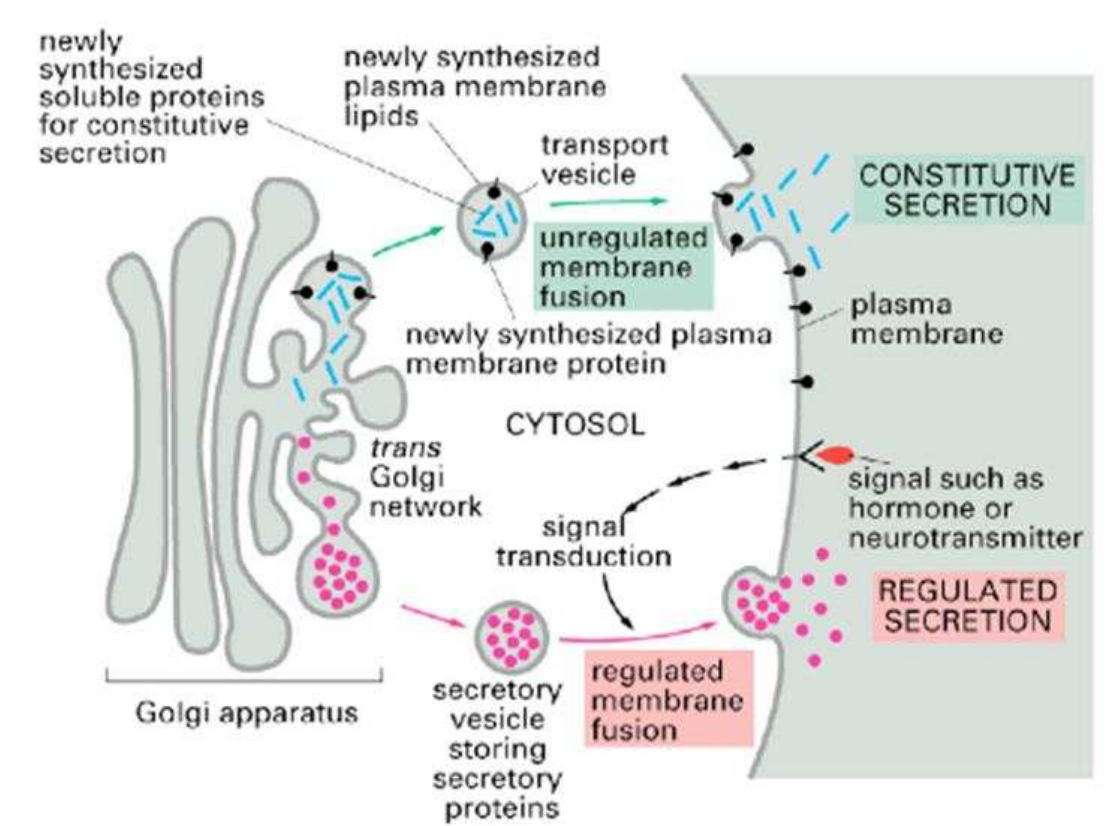


Fig. 1.2 The constitutive and regulated secretory pathways. Figure adopted from reference [5].

It's worth mentioning that for the regulated secretory release, the complete merging of the vesicular membrane to the plasma membranes, or so called "full fusion", is not always the case. Strong evidences demonstrate that vesicle fusion with partial release of transmitter content occupies a large proportion in the exocytosis [6]. The key difference between "full fusion" and "partial fusion" appears in whether the fusion pore expands or closes at the end of release. If the vesicle transiently fuse with plasma membrane with tiny amount of secretory release and then followed by the closure of the nanometric fusion pore, the process can be described as "kiss-and-run" [7]. While in the "full fusion" mode, all the vesicular content is discharged outward due to the expansion of fusion pore and the collapse of vesicle into cellular membrane. Also there is an evidence for transition behaviour in between this two extreme modes, which the fusion pore closes up again after massive release. The similar behavior of vesicles as that in "kiss-and-run" obtains an additional adjective before the name of the mode, that is "extended kiss-and-run".

1.1.3 Cell models for exocytosis study

Cellular models comprised of primary neurons or neuron-like cell lines are widely used to

study exocytosis. Neurons, the basic units of neuronal system, are indisputably employed as preferred cell model since vesicular exocytosis is the essential process for propagating nerve impulses in neuronal communication. However, as primary culture cells, experiments depending on neural cells are confronted with a series of restrictions. For instance, primary neurons have to be isolated from fresh nerve tissues each time. In order to guarantee the activity of neurons, the isolation step should be manipulated in few minutes and their cultures can only be maintained for up to two weeks. Compared to neurons, neuron-like cells represent eminent advantages such as easy access and stable proliferation. Various neuron-like cells have been employed as cell models providing insight into the molecular machinery during exocytosis, such as mast cells [8, 9], basophils [10, 11], neutrophils [12, 13], which are not emphasized here. In this section, we focus on introducing chromaffin cells and PC12 cells widely used as highly informative cell models for neurosecretion research. BON cell line successfully applied in coupling measurement for exocytosis study is also briefly referred to.

1.1.3.1 Chromaffin Cells

Chromaffin cells are neuroendocrine cells found mostly in the medulla of the adrenal glands in mammals. In terms of cells communication, they are in close proximity to pre-synaptic sympathetic ganglia of the sympathetic nervous system. While with respect to structure, they are more similar to post-synaptic sympathetic neurons. That's why adrenal chromaffin cells have been used as the prioritized model system for multidisciplinary investigation into the mechanisms of exocytosis [14]. In addition, the attractive properties such as relative large size of vesicles (~170nm radius) [15], fast response to external stimuli and initial storage of catecholamines inside vesicles, expand its applications in both visual and electrochemical detection. However, as a primary cell line, chromaffin cells can only be freshly derived from laboratory animals, mainly rats and mice, or from slaughterhouses in case of bovine chromaffin cells. The non-proliferation feature complicates the experimental operation and increases hazard of cell heterogeneity.

1.1.3.2 PC12 cells

The PC12 cell line was first derived from a transplantable rat pheochromocytoma, an adrenal medullary tumor in 1976 by Green and Tischler [16]. Rapidly, the ease of handling, consistency and extreme versatility for pharmacological manipulation make PC12 cells a popular cell model in cell biological study.

PC12 cells possess two categories of vesicles: large dense core vesicles (LDCVs) and small

synaptic-like vesicles (SSLVs) [17]. Like adrenal chromaffin cells, PC12 cells have been verified possessing the machinery to synthesize, store and take up catecholamines, the major of which is dopamine, in LDCVs. The expression of an ATP-dependent reserpine-sensitive vesicular monoamine transporter (VMAT) on the vesicular membrane assists the accumulation of monoamine neurotransmitters (e.g. dopamine) inside secretory vesicles. Upon depolarization in a Ca^{2+} -dependent way, these electroactive neurotransmitters can be released via exocytosis. This endogenerated electrochemical probe makes PC12 cell an attractive model for the investigation of secretory pathway using amperometry. Notably, although PC12 cells have similar monoamine storage as chromaffin cells, their LDCVs more closely resemble vesicles in neurons with smaller size (75-120nm, radius) [18]. Considering the adequate storage of natural synthesized electroactive probes inside vesicles, PC12 cells were chosen as our cell model for exocytosis inspection in this thesis.

In addition, PC12 cells can undergo differentiation under the help of nerve growth factor (NGF) treatment [19]. In response to NGF, PC12 cells are converted from chromaffin-like cells to sympathetic ganglion neurons like phenotype with extended axons. This specific feature of PC12 cells offers the opportunity to be used as a convenient model of neuron in vitro.

1.1.3.3 BON cells

BON cell line was derived from a metastatic human carcinoid tumor of the pancreas. Consistent with the enterochromaffin cells, BON cells possess comparable large secretory vesicles (100-150nm radius). It also secretes a variety of biochemical molecules (mainly serotonin) as well as peptide during exocytosis. Two stable clones of BON cell lines (named BC21 and N13) have been recently involved in investigation of exocytosis. BON BC21 cells stably express green fluorescent protein-tagged Neuropeptide-Y (NPY-GFP) in the lumen of vesicles, thus opening an opportunity for optical recording of exocytotic events [20]. While for BON N13 cells, there is neither electroactive nor fluorescent probe inside vesicles [21]. However, thanks to the monoamine transport mechanism of VMAT reserved on the membrane, uploading various probes into vesicles of BON N13 according to experimental requirements becomes possible and turns into one of its merits when applied as cell model for exocytosis investigation.

1.2 Actin cytoskeleton

Actin is a family of globular multi-functional proteins presented in all eukaryotic cells except nematode sperm. It exists as either a free monomer called G-actin (globular structure) or as

part of a linear polymer microfilament called F-actin (filamentous structure). Flexible morphological transition under the control of nucleotide hydrolysis, and abundant interactions with its binding proteins make actin cytoskeleton a complex but critical player in a multitude of cellular processes, ranging from cell motility, cell communication, cell division to the maintenance of cell junctions and cell shape.

1.2.1 Functions of actin in exocytosis

Regulated exocytosis, as the main mechanism utilized by specialized secretory cells to deliver signal molecules to the external surface, involves a series of highly coordinated and sequential steps. The whole exocytosis includes the biogenesis of the vesicles, their delivery to the cell periphery, their fusion with the plasma membrane and the release of their content into the extracellular space. Actin cytoskeleton has been demonstrated to participate nearly in the regulation of all these steps. In this section we will briefly elaborate the current knowledge regarding the involvement of actin during regulated exocytosis.

1.2.1.1 Facilitating the transport of secretory vesicles to fusion sites

A series of studies indicate that actin cytoskeleton could act as a track to deliver secretory vesicles to the fusion sites [22]. With the disruption of actin cytoskeleton by pharmacological agents, the freezing of secretion and vesicle movement is observed suggesting that actin network plays an active role in facilitating vesicle transmission [23, 24]. This movement of vesicles along actin filaments is advocated by actin associated motors such as members of the myosin V family, as mentioned above.

1.2.1.2 Anchoring site for the secretory vesicles or barrier function

Although current evidences show that actin cytoskeleton promotes the transport of secretory vesicles, varieties of experiments demonstrate that during pre-fusion step actin and other cytoskeletal elements also play a negative role on regulating exocytosis. So far, at least two models have been proposed to describe this obstruction effect. The first model depicts the actin cytoskeleton as a scaffold for anchoring secretory vesicles in close proximity to the plasma membrane with the help of anchoring factors. This model is based on the observation that upon stimulation the secretory vesicles initially associated with actin cytoskeleton underwent detachment with enhanced mobility. This phenomenon has been observed not only from live pre-synaptic terminal of rat neurons [25] but also from neuromuscular and cerebellar synapses [26]. While in the second model, actin and its associated proteins are regarded as a physical barrier between secretory carrier and plasma membrane for blocking the occurrence of exocytosis. This assumption is sustained by the

fact that popular release sites was compassed by actin filaments with low density observed under fluorescence microscopy [27]. In addition, time lapse microscopy in neuroendocrine cells also showed that stimulation of exocytosis results in the selective disruption of cortical actin that allowed the vesicles to dock and fuse to the plasma membrane [28].

1.2.1.3 Regulation of docking

Actin and its motors could interact or be functionally linked to some of the molecules involved in vesicle docking. For example, in primary rat β -cells and MIN6 β -cells, actin was observed to interplay with the first two N-terminal alpha helical coiled-coil domains of syntaxin 4 (one of SNAREs) [29]. With the impairment of this interaction, the stimulant-dependent secretory release could be enhanced. intersectin-1L, as an actin binding protein, has also been discovered in promoting docking of secretory vesicles via binding to SNAREs [30].

1.2.1.4 Mediating the development of fusion pore

Although it has been known for a few decades that cortical actin filaments coat large secretory vesicles in close proximity to the plasma membrane, the phenomenon that the recruitment of actomyosin complex occurs with a delay after the formation of fusion pore has been realized recently [31]. This observation proves the non-participation of actin cytoskeleton in the fusion step. Fusion between secretory vesicles and plasma membrane keeping ongoing with the pharmacological impairment of actin assembly further supports the conclusion [32]. The coating of vesicles with actin filaments then raise several other possibilities about their role in controlling the fusion pore evolution and kinetics of secretory release as a consequence.

Currently, two explanation of actin coating involved in post-fusion event are plausible. In one theory, the contractile activity of actin network surrounding the vesicle provides force to compress the vesicle membrane and facilitates the discharge of vesicular cargo [33, 34]. Clear evidence of such extrusion has been verified within endothelial cells by visualizing both vesicle luminal protein and actomyosin complex formed during exocytosis [32]. While in the alternative theory, the formation of actin filaments' shell instead regulates the maintenance and closure of the fusion pore. Evidences such as latrunculin B-mediated actin disruption help promote pore closure in pancreatic acinar cells have been proposed to support this assumption [22, 31].

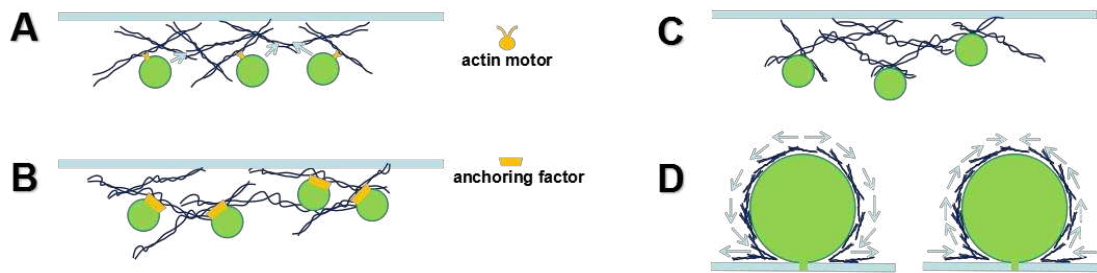


Fig. 1.3 The actin cytoskeleton in exocytosis: In the pre-fusion steps, the actin cytoskeleton may provide a track to transport the vesicles to the fusion site (A), provide a scaffold for anchoring secretory vesicles in close proximity to the plasma membrane (B), or act as a physical barrier (C). In the post-fusion step, the actin cytoskeleton may push the membranes of the secretory vesicles toward the plasma membrane by exerting a force tangential to the surface of the vesicles, or it may also take part in controlling the retrieval of the vesicular membranes to maintain plasma membrane homeostasis (D).

As a summary, cortical actin filaments have been shown by many researchers to possess multi-functions during the whole process of exocytosis. And it is essential to point out the emphasis that all the possible functions are not mutually exclusive. Instead, they are interlinked and represent an overall impact on exocytosis.

1.2.2 Actin associated proteins

Actin cytoskeleton in vivo is not merely composed of actin, several related proteins are also required for its formation, maintenance and function. Actin-binding proteins are demonstrated to be involved in actin's polymerization, depolymerization, relative movement and thus influence its construction, fragmentation and reorganization. Owing to the diversity of these proteins, actin shows high participation in protein-protein interactions and occupies a crucial position in mediating cell physiology. Here we would like to introduce some actin associated proteins that are responsible for modulating regulated exocytosis joint with cortical actin filaments.

1.2.2.1 Myosin

Myosin is an emblematic example of a molecular motor responsible for actin based motility. It represents a huge family of proteins which is capable of converting ATP chemical energy to mechanical energy, thus generating force and movement. Nearly all eukaryotic cells contain myosin isoforms, however, both the structure and function of these isoforms are specialized and strongly conserved across species. We concisely present two isoforms related with remodeling of actin network.

➤ **Myosin II**

Myosin II, a well-known myosin isoform responsible for actin's movement, especially in muscle contraction. The two head domains of myosin can "walk" along the actin filament and causes the relative displacement of two nearby filaments. The driving force of this movement is provided by a power stroke mechanism described as follows [35]. Myosin II is tightly bound to actin in the initial state. Then the fracture of high-energy phosphoanhydride bond in ATP attached on myosin II provides the energy for transforming myosin into its twisted conformation, which pulls against the actin like a bend "spring". Through the release of energy, this rigor state "spring" bounces back and promotes actin to move. With the release of ADP and new binding of ATP molecule, myosin II can be bound to actin again to restart the cycle.

The extensive evidence of F-actin involvement in all steps of secretion suggest that myosin II, who contributes to the reorganization of actin network, may also play a role. Indeed, participant status of myosin II in vesicular movement has been confirmed by inhibiting its motor activity and observing the following reduction of vesicular mobility in the cortical area [36]. Moreover, myosin II is involved in geometry variation of actin network from protrusion to contraction form and further drives the membrane merging [37]. More recently, it is proposed that myosin II could exert pressure on actin network that subsequently affect the vesicular membrane tension as well as fusion pore expansion [38]. So far, myosin II has been verified to take participation in regulating the secretory processes of a variety of cells, including: mast cells[39], hippocampal [40], sensory neurons [41], chromaffin cells [36], epithelial cells [42] and oocytes [43]. In this thesis, using PC12 cell line as our cell model, we mainly discuss the involvement of myosin II in the regulation of post fusion behaviour, specially fusion pore development.

➤ **Myosin V**

Unlike myosin II, myosin V is a less common myosin motor. This myosin also translocates along actin filaments towards the barbed end of the filaments. Myosin V has been reported to participate in the transport of cargo (e.g. RNA, vesicles, organelles) to the periphery of cell. It is further discovered acting as a dynamic tether for retaining vesicles and organelles in the actin rich peripheral region [44].

1.2.2.2 Actin-related protein 2/3 (Arp2/3) complex

Arp2/3 complex is a seven-subunit protein complex involved in the regulation of the actin cytoskeleton. As a catalyst of F-actin nucleation, the Arp2/3 complex is able to bind to the

sides of pre-existing filaments, activate this region, and trigger the growth of filaments as new branches on these binding sites[45].

1.2.3 Pharmacological drugs for arresting actin dynamics

As we elaborated above, actin dynamics are essential for steps in the whole exocytotic process. To precisely examine the role of actin dynamics, investigators commonly choose to interfere the movement of the actin cytoskeleton such as polymerization, depolymerization, and rearrangement by specific pharmacological agents or toxins. These actin drugs can be generally sorted into 3 classes based on their influence on actin assembly, actin disassembly and actin remodeling, respectively. Here we will concisely enumerate the most prevalent actin modulation drugs sorted by category.

1.2.3.1 actin assembly inhibitor

➤ Latrunculin

The latrunculins are a family of natural products and toxins produced by certain sponges. It belongs to the first class of actin drugs. By sequestering actin monomer pools near the nucleotide (Fig. 1.4), Latrunculin prevent them from assembly, thus resulting in the disruption of the actin filaments' movement and allowing the visualization of the corresponding changes on exocytosis pattern [46]. Latrunculin A and Latrunculin B are two of the most shining members in this family, which present 10 to 100-fold potent than cytochalasins in blocking actin's polymerization.

1.2.3.2 actin disassembly inhibitor

➤ Jasplakinolide

Jasplakinolide, a cyclo-depsipeptide, is commonly used for stabilizing actin construction. It's originally isolated from a marine sponge, and now can be artificially synthesized and become commercially available. The cell permeable characteristic makes Jasplakinolide outstanding among other actin stabilizers. In vivo, Jasplakinolide has been observed binding on the side of actin filaments, and the dissociation rate of barbed-end actin has been detected reducing to essentially zero at the same time [47]. Combined with these two phenomenons, the conclusion that Jasplakinolide could stabilize actin network by inhibiting the depolymerization is reasonably speculated.

1.2.3.3 actin remodeling inhibitor

➤ Y27632

Y27632 is a cell-permeable, highly potent and selective inhibitor of Rho-associated, coiled-coil containing protein kinase (ROCK). It inhibits both the Rho kinase-I (ROCK1) ($K_i = 220$ nM) and the Rho kinase-II (ROCK2) ($K_i = 300$ nM) by competing with ATP for binding to the catalytic site. The “blind” kinase arrests the signal cascade driving phosphorylation and activation of myosin II, thus inhibiting the relative motion of neighboring actin filaments associated with myosin II [47]. Owing to its characterized indirect interference on actin, Y27632 is employed as a gentle actin-myosin complex inhibitor that sets obstruction for the actin network remodeling.

➤ CK-666

CK-666 is a cell-permeable inhibitor of actin branching mediated by actin-related protein Arp2/3 complex. Binding to Arp2/3 complex, CK-666 stabilizes the inactive state of the complex and prevents its conversion into the active conformation. The inactive Arp2/3 complex thus losing its ability to bind with the pre-existing actin filaments as a nucleus for new branch formation [45].

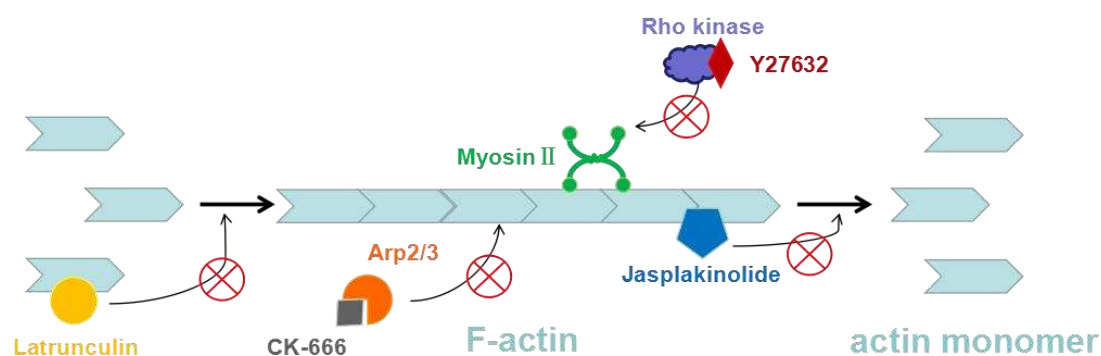


Fig. 1.4 Schematic diagram of actin inhibitors. Latrunculin prevents actin monomers' incorporation into actin polymer by binding to their active zone ; Jasplakinolide bundles on the side of actin polymer and inhibits its disassembly; Y27632 interferes with Rho kinase and further influences the activity of myosin II; CK-666 prevents the activation of Arp2/3 complex for actin branching inhibition.

1.3 Ultramicroelectrode in electrochemistry

Ultramicroelectrodes (UMEs) can be defined as an electrode with its diffusion layer comparable or even larger than the dimension of the electrode at the same time scale of

electrochemical detection. To fulfil this condition, at least one of the characteristic geometric dimension of the UME shall be confined to microns range. Compared to the conventional electrode which generally has millimetric or larger size, UME shows superior performances such as fast response time, relative less deviation of measurement by the ohmic drop and improved signal-to-noise ratio [48]. Over and above this, the small size of UME guarantees that the experiment will not disturb the object measured. All the merits mentioned above make UME a valuable electrochemical tool for biological investigation at single cell level.

1.3.1 Ultramicroelectrode geometry

UMEs have been designed with various geometries (cylinder, hemisphere, disk, band, ring, etc.) depending on the request of specific analysis. Among these, the planar disk is the most commonly used UME during experiments, as shown in Fig. 1.5. The fundamental planar disk electrode can be easily fabricated by encasing a metal wire or a carbon fiber in glass or plastic capillary and the flat surface at the end of the insulated wire serves as the detecting zone. In many experimental conditions where the larger surface area of UME is required, band or ring structure are always employed. The working area can be enlarged by prolonging the length of the band or widening the circumference of the ring without destroying electrode properties. The larger surface can also be obtained with the construction of electrode array or by forming the interdigitated structure. Following the basic features, each UME with specific morphology shows its own unique application. Here, we take the typical planar disk as an example to explicate the specific properties of UME compared with conventional electrode.

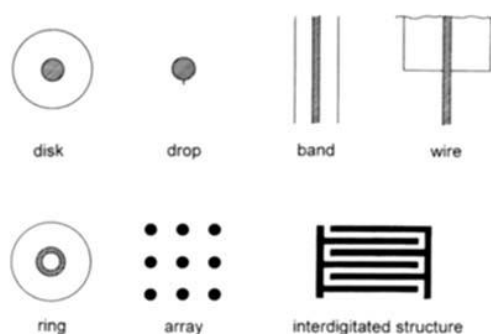


Fig. 1.5 Typical configurations of UMEs [49].

1.3.2 Specific properties of UME

1.3.2.1 Mass transport

Similar to the conventional electrodes, the electron transfer only occurs on the electrode interface during oxidation/reduction process. This heterogeneous charge transfer can cause

the change of electroactive substance's concentration at the electrode surface, while the bulk concentration of the electroactive specie remains. The concentration gradient between the electrode surface and the bulk solution then sets off the diffusive mass transport to the electrode. For the conventional electrode, the larger diameter of the electron transfer region compared to the micrometric thickness of diffusion layer weakens the edge effect. Hence, the diffusive mass transport can be regarded as a result of the linear diffusion orthogonal to the electrode surface. According to the Cottrell's law, the faradic current (i_f) decreases as time accumulated ($\sim t^{-1/2}$) and is proportional to the electrode surface ($\sim r_0^2$). When the size of the electrode shrinks to micrometer range, which is comparable to the diffusion layer thickness, the radial diffusive component parallel to the electrode surface can't be neglected. Within one millisecond, one dimension diffusion is rapidly transformed to the combination of linear and radial diffusion, or so called spherical diffusion, as illustrated in Fig. 1.6. This convergent regime of diffusion field leads to a steady state with a constant diffusion layer (a few r_0) and a constant faradic current only related to disk electrode radius (r_0).

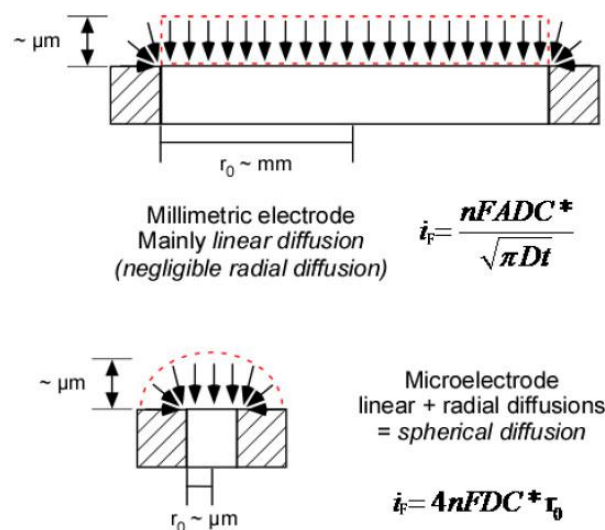


Fig. 1.6 Patterns of diffusion layer for conventional millimetric electrode and UME. (r_0 : disk radius, D : diffusion coefficient, F : faraday's constant, C^* : the bulk concentration of electroactive species) [50].

Additionally, the rapid transition to the stationary state on UME yield the steady-state current-voltage curve represented as a platform in the voltammogram instead of the characteristic redox peaks from conventional electrode. (Fig. 1.7)

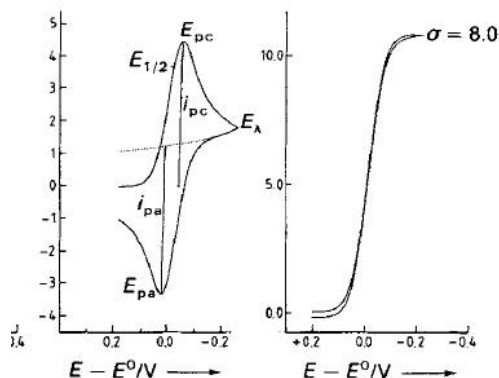


Fig. 1.7 Characteristic voltammogram. Left: for semi-infinite planar diffusion on conventional disk electrode; right: for semi-infinite hemispheric diffusion to a microdisk electrode. (E_{pa} = anodic peak potential, E_{pc} = cathodic peak potential, i_{pa} = anodic peak current, i_{pc} = cathodic peak current.) Image adapted from reference [49].

The electron transferred to UME surface undergoes the same pathway as that on conventional electrode, that is, the current recorded by UME is also proportional to the instant flow of electroactive species. Therefore, UME becomes an outstanding electrochemical detector to trace the variation of concentration with super low temporal distortion.

1.3.2.2 Fast double layer charging

An electrochemical double layer is formed at the electrode/solution interface acting as an electrolytic capacitor when applying a potential on the electrode. If the applied potential alters, the recharging of the electrolytic capacitor induces the capacitive current (i_c) and distorts the real potential applied on the electrode. Hence, the electrochemical measurement is not so precise until the charging process is accomplished. The capacitive current (i_c) represents an exponential decay whose duration is described as a time constant (τ), then the time scale of the capacitive distortion can be measured by the value of time constant. Taking disk electrode as an example, the time constant (τ) is proportional to the electrode radius (r_0). Based on this relation, by comparison with millimetric electrode, UME responds rapidly to potential variation. The fast response allows distortion-free detection within a short time, making UME more competitive in recording of high speed redox reaction.

1.3.2.3 Minimized ohmic iR drop

When the current flow (i) pass through the solution with resistance (R), the real working electrode potential is distorted by an ohmic drop iR compared to the applied potential. For the conventional electrode, the ohmic drop (scaled with electrode radius) is not negligible,

therefore three-electrode configuration is introduced to compensate the potential loss. While with UME, both the electrode radius and the detected current flow are relatively small which attributes to the minimized ohmic drop. In consequence, the counter-electrode is not so necessary in the experiment with UME and thus facilitating the manipulation.

1.3.2.4 High sensitivity

For UME, under the spherical diffusion regime, the faradic current is proportional to the electrode radius (r_0) and the intrinsic noise depends on the electrode area ($\sim r_0^2$). The signal to noise ratio is thus related to $1/r_0$. Small dimension of UME ensures high signal-to-noise ratio and makes it attractive in sensitive electroanalytical detection.

1.3.3 Types of UMEs applied in exocytosis study

Unraveling the dynamics of exocytosis is challenging due to its limited temporal and spatial domains. Usually, the volume of a synaptic vesicle is on the order of zeptoliters and contains detectable molecules within zeptomoles range. Moreover, since the duration of a typical fusion event ranges from 0.1 to 100 ms, such a short time scale thus requires measurement with high temporal resolution and high signal-to-noise ratio. Electrochemical measurements, thanks to its high temporal resolution as well as high sensitivity, attracts more and more attention in exocytosis investigation. It generally relies on the redox response of molecules released during exocytosis at the surface of an electrode. Considering that the intrinsic noise of electrode is dependent on the electrode area, whereas the desired signal due to faradic current (around picoampe) depends on the amount of neurotransmitter released that seems taking place randomly on the cellular surface. It is important to restrict the area of the electrode surface to the cell size in order to obtain superior S/N. In addition, the instant release with milliseconds scale also requires detector showing rapid response. By virtue of its unique features, microelectrode stands out as an appropriate electrochemical detection tool for exocytosis study.

1.3.3.1 Single ultramicroelectrode

The most widely used UMEs to perform electrochemical measurements aiming at recording exocytotic events at living cells are fabricated with carbon fibers. Generally, carbon fiber with diameter ranging from 1 to 10 μm is sealed and embedded into a glass capillary before or after insulation [51]. Such sealing procedure significantly reduces capacitive current, ensuring that all the faradic information comes from the tip of carbon fiber with a known and controlled active surface area. Insulation of the outer cylinder surface of carbon fiber can be implemented by electrodeposition of polymer (e.g., polyethylene [52],

polypropylene[53], poly(oxyphenylene) [54]) or by means of cathodic electrophoretic painting. The fibers are usually cut into sought dimension according to measurement requirements and polished to obtain the flat controlled conductive area at the tip. Every polishing operation on carbon fiber renovates the working surface of UME, making carbon fiber based UME a reproducible electrochemical detection tool. The restricted dimension of active surface allows its analysis at single cell level. Considering that most electroactive species released during exocytosis through fusion pore can easily undergo oxidation at bare carbon fiber surface and recorded as stable electrochemical signal, plus with low cost, flexibility owing to carbon fiber itself, numerous studies on secretion directly applied simple carbon fiber UMEs (CFE). The electrochemical measurement for exocytosis study carried out by placing a carbon fiber microelectrode on cell surface was first performed by Leszczyszyn et al. [55]. In this experiment, released chemicals from chromaffin cells through exocytosis were quantified with amperometry and identified as catecholamines with cyclic voltammetry. After that, amperometry at single CFE gradually developed as a routine analytical tool for the investigation of exocytosis mechanism and promoted to the inspect of various physio-chemical/biological factors related to secretory release. For instance, taking advantage of high sensitivity of amperometry with common CFE, Kozminski et al. successfully monitored single exocytotic event from dopaminergic nerve cell model with detailed information about the amount as well as kinetics of secretory release [56]. Relying on this amperometric detection scheme they further explored the possible distribution of catecholamines inside mature vesicle lumen [57].

On the basis of bare carbon fiber UME, surface modified UME with enhanced performance is also designed for exocytosis investigation. A thin film of the perfluorinated cation-exchange material Nafion was deposited on the electroactive surface of CFE. This modified CFE showed specific recognition to the cations. For example, the protonated catecholamines released from chromaffin cells can easily permeate the film, hence the unique detection of cationic catecholamines was able to be achieved [58]. CFE electrochemically coated with polynuclear ruthenium oxide/cyanoruthenate film was also applied in amperometry measurement for exocytosis detection at pancreatic β -cells through fast catalysis of insulin oxidation [59]. Apart from carbon fiber based UME, recently modified platinum electrode involving a thin layer of conducting diamond have shown effectiveness for monitoring secretion of serotonin from enterochromaffin cells of the intestinal mucosal layer [60].

In recent years, thanks to the blooming development on microfabrication, various electrically conductive materials (Pt [61], Au [62], ITO [63], conductive polymers [64], etc.) have been

employed to fabricate UMEs for exocytosis monitoring. Due to the flexibility in its fabrication, novel UMEs provides abundant geometry for fitting experiment requirements. For example, in our group, a microdevice composed of four independent ITO bands was fabricated and successfully applied for tracking exocytotic events from neurosecretory cell model with combined detection with TIRFM and chronoamperometry. Active surface of ITO were carefully carved by photolithography and acid etching process. ITO microchips with different lengths, shapes and configurations could be conveniently obtained by altering masks with various patterns during photolithography depending on research interest (Fig. 1.8). In particular, relying on the transparency as well as the semi-conductive property of ITO, exocytotic events occurring at the bottom of the cell can be synchronously recorded by fluorescent imaging and amperometry. Through optical monitor, the precise location of secretory release recorded by amperometry can be determined.

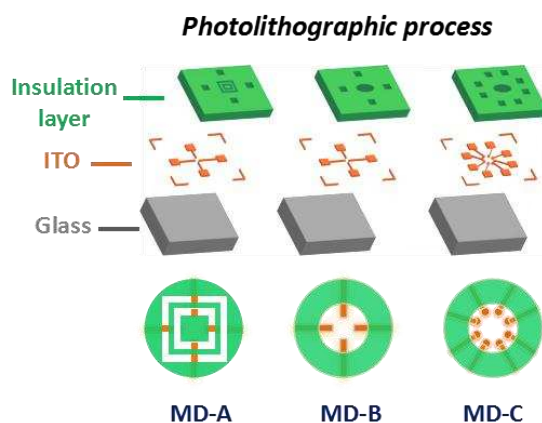


Fig. 1.8 Three microfabricated ITO devices with various defined working area: ITO are shown in orange and the isolation layers displayed in green are composed of a non-conductive layer of photoresist. Figure adapted from reference [21].

1.3.3.2 UME arrays

Exocytosis activity in a single cell has been proposed to show inhomogeneous behaviour and secretions are concentrated at active release sites termed as “hotspots”. Along with the propose of the concept “hotspots”, resolving the location of active release sites on secretory cells becomes a hot issue in neurosecretion analysis. Electrochemical detection can provide insight into release location together with the corresponding kinetic information by assembling UMEs into arrays (MEAs). Massive separated electrodes offset the vacancy of spatial resolution at the sub-cellular scale from single UME and allows the detection from multiple sites on a single cell. Classic MEA composed of a set of electrodes with few microns in dimension is illustrated in Fig. 1.9. The current traces from each of the individually addressed electrodes can be recorded in real-time. Hence, the heterogeneity of release

observed from various regions of the cell could be resolved by quantitative assessment of recorded amperogram, allowing the map of spatio-temporal vesicular release at single cell level. Similar as dealing with single UME, to further improve the properties of MEAs, one may concern about changing the original materials for electrode fabrication or attempting to modify the working surface by some novel nano-materials.

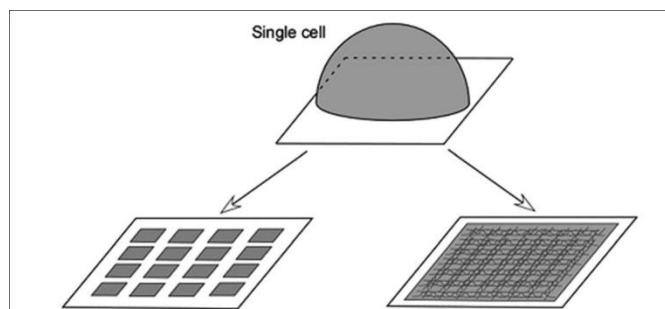


Fig. 1.9 Two strategies related to single cell analysis with MEAs. Left: MEAs with subcellular UME dimensions should help to perform the electrochemical mapping of the cell release. Right: MEAs with electrode material other than carbon and with surface modifications (CNT etc.) for improving the electrode sensitivity. Figure extracted from reference [65].

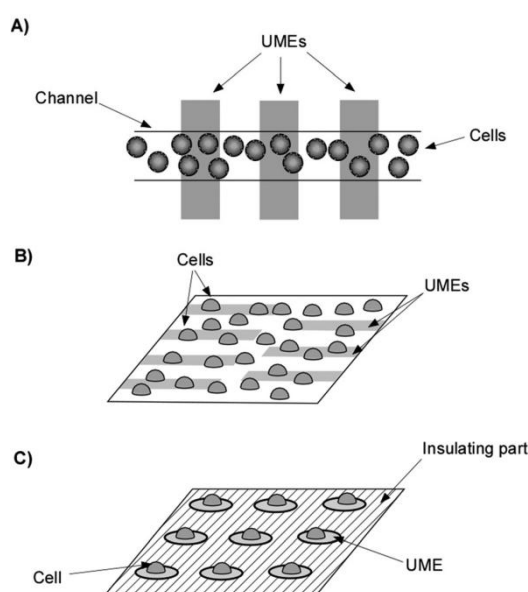


Fig. 1.10 Schematic views of the main strategies for the investigation of cell population using MEAs. (A) Within a microchannel. (B) With a cell population randomly adhered on the MEA. (C) With a cell population selectively adhered on the UME surfaces. Figure adapted from reference [65].

Besides resolving the spatial resolution at sub-cellular scale limited by UMEs, MEAs can also be applied to avoid numerous repetitive work performed by UMEs for data accumulation. Some novel microdevices with rapid and high through-put characteristics have been developed so as to augment the amount of events recorded during each performance. It's

worth noting that the high through-put property of microdevice are usually achieved by tracking amperometric signals from a cell population above the embedded microfabricated electrodes rather than a single cell. Three main strategies for the design of microchips suitable for “cell populations” investigation are displayed in Fig. 1.10.

In the above, we use UME as an example to present unique features as well as applications of electrodes with minute size. Notably, there has never been an absolute division between ultramicroelectrode and microelectrode. Indeed, electrodes’ behaviour not only relates to their dimensions but also depends on the time scale of experiment as well as the thickness of the convection-free layer [66]. In our experiments, either CFE or ITO band used as working electrode, their dimensions are not strictly in accordance with the ultramicroelectrode standard. According to the designed working surface area, our CFE within 10 μm in diameter can be sorted into microelectrode category, while our ITO band (200 μm \times 500 μm) is in between microelectrode and macroelectrode. Although capacitive current decline is associated with the electrode surface area, owing to chronic recording of amperometry applied in our detection, the relative slower decay of capacitance current within our CFE/ITO compared to true UME prior to stimulated exocytosis recording is insignificant. Whereas the faradic current we concerned is determined by the actual active regime on the electrode surface for the occurrence of electrochemical reaction. In our exocytosis detection, the effective working surface of electrode is determined by the minute secretory release through the tiny fusion pore within nanometric diameter. Moreover, the limited distance between our electrode and cellular membrane restrains the diffusion of the electroactive species accessed to the electrode. Hence, although in terms of size our electrodes cannot be divided into UMEs, their electrochemical behaviour appeared during exocytosis recording still abide by feature of UMEs.

1.4 Analytical techniques for exocytosis investigation

Advances in methodology over the past 30 years allow the chemical measurement to deal with decreasing amounts of analyte at tiny spatial dimensions. It drives detailed investigations presenting unique chemical and biological insights at single cell level. As described in section 1.1, in the central nervous system cells communication is mainly achieved by the transmission of chemical/biochemical molecules (neurotransmitters, peptide, hormones, etc.) with secretory vesicles from the emitting cell to induce the corresponding physiological responses of target cells. Mechanistic studies of exocytosis are focusing on exploring regulated neurotransmission. Thereby, various analytical methods have

been developed to measure and characterize membrane fusion as well as the subsequent minute release of molecules. These methods generally depend on three powerful routes: optical technique such as total internal reflection fluorescence microscopy (TIRFM) and electrical techniques including patch-clamp and amperometry. In this section, we will present these routinely used techniques and compare their merits as well as shortcomings.

1.4.1 Electrical methodology

During cell communication, an infinitely minute number of molecules are released through nanometer-sized fusion pore within a brief fraction of time from a living cell to its surroundings. According to distinct target or the scope of transmission, these signal messengers are released into biological fluids such as blood flow, the strait interspace (e.g. synapse), or extra-body environment. Such small dimension of fusion pore (usually tens of nanometers depending on cell type), the relative low amount of release, and the extreme short time of completion of the whole secretion event propose the challenge for the actual analytical standards. Electrical methods, especially microelectrode systems, owing to their unique high sensitivity, high time resolution, have emerged as the most attractive technique for fundamental study of exocytosis taking place in ultra miniature environment.

1.4.1.1 Patch-clamp

Patch-clamp was first developed by Erwin Neher and Bert Sakmann in the late 1970s for recording the current of single ion channel molecules across the membrane patch of a frog skeletal muscle [67]. It's an electrophysiological technique based on measuring the variation of electrical conductivity and capacitance of cell membrane leaded by exocytosis. The emergence of powerful software packages blossomed in the 1990s resolve the time resolution as well as increase the sensitivity of patch-clamp. The amelioration greatly promotes patch-clamp's application in monitoring membrane associated processes in millisecond time scale such as vesicular exocytosis [68].

➤ Configurations for detection

During a patch clamp recording, a hollow glass micropipette known as patch pipette is employed as a recording electrode contacting the membrane of an isolated cell. While a reference electrode is placed nearby in the buffer surrounding the cell. The diameter of the pipette tip may vary according to the experimental request, but it is usually in the micrometer range [69]. The small size of microelectrode is allowed to capture a tiny membrane surface area containing just one or a few ion channel molecules, thereby enhancing the sensitivity. Distinct from microelectrodes with sharp tip used to puncture cells

in traditional intracellular recordings, the recording electrode applied in patch-clamp is sealed onto the surface of the cell membrane for signal collection. Depending on the research interest, four main configurations have been explored to date. They are “cell-attached mode”, “whole-cell mode”, “inside-out mode” and “outside-out mode”, as displayed in Fig. 1.11. Apart from these four configurations, more modifications derived from the fundamental configuration are also developed, such as “loose patch mode” and “perforated patch mode”.

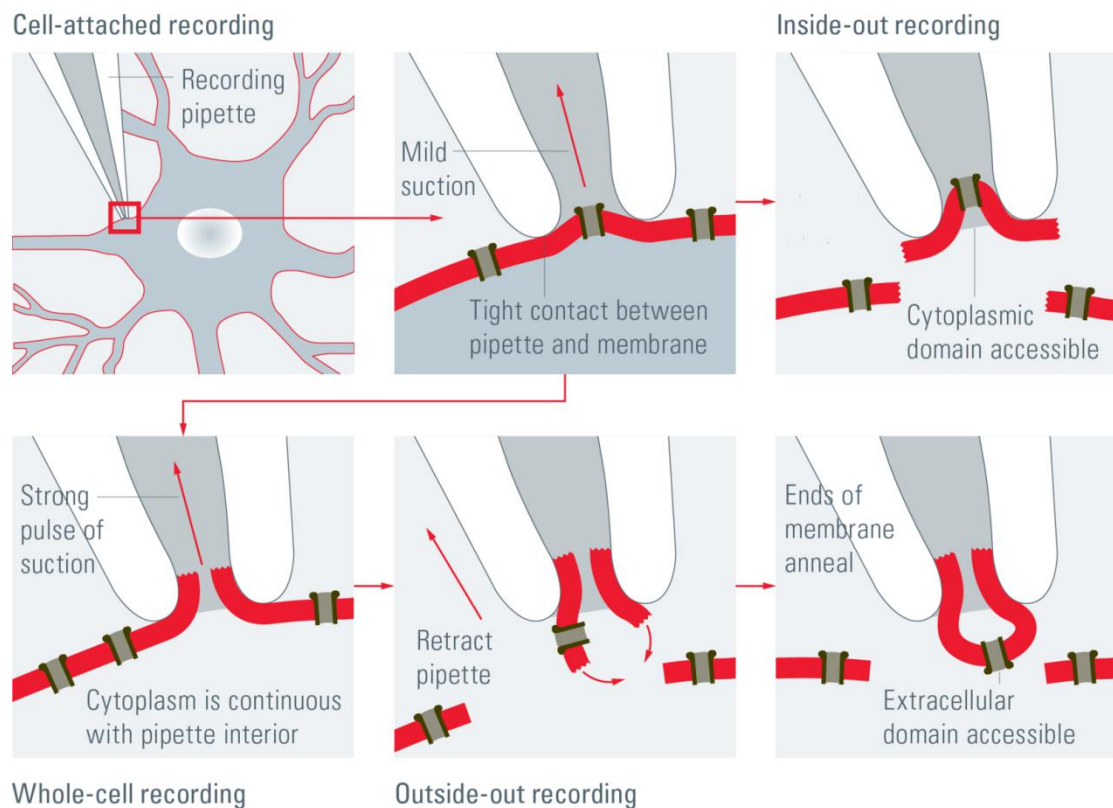


Fig. 1.11 The four recording methods for patch-clamp: Cell-attached: When the pipette is in closest proximity to the cell membrane, mild suction is applied to gain a tight seal between the pipette and the membrane. Whole-cell: By applying brief but strong suction, the cell membrane is ruptured and the pipette gains access to the cytoplasm. Inside-out: In cell-attached mode, the pipette is retracted and the patch is separated from the rest of the membrane. The cytosolic surface of the membrane is exposed. Outside-out: In the whole-cell mode, the pipette is retracted resulting in two small pieces of membrane that reconnect and form a small vesicular structure with the cytosolic side facing the pipette solution. Image adapted from: <http://www.leica-microsystems.com/science-lab/the-patch-clamp-technique/>.

In “cell-attached mode”, the pipette is sealed onto the cell membrane with mild suction to obtain a gigaseal, while maintaining the integrity of cell membrane. The patch of membrane enclosed by micropipette allows the recording of currents through single, or a few, ion channels located in this isolated portion. The gentle attaching to the exterior of the cell membrane greatly weakens the disturbance on the cell structure [70]. Without disrupting the interior of the cell, intracellular mechanisms commonly influencing the channel is still able to function.

The most commonly used patch-clamp mode is the “whole-cell mode”. Unlike “cell-attached mode”, to achieve whole-cell recordings, the membrane patch is ruptured by applying briefly but strong suction. As a consequence, the pipette is gigasealed with cell membrane and connect interior of the pipette to the intracellular space of the cell. This method is usually used to record the electrical potentials and currents through multiple channels simultaneously, over the membrane of the entire cell.

Both “cell-attached mode” and “whole-cell mode” configurations are used for recording electrophysiological signals at a single cell level. However, It is also possible to record signals from a small patch instead of the whole cell. The restricted regime detection can eminently raise the chance of recording single channels. The patch can be orientated in two different directions inside the patch pipette. To achieve the inside-out configuration the patch pipette is attached to the cell membrane and then retracted to break off a patch of membrane. In this case the cytosolic surface of the membrane is exposed [71]. This is often used to investigate single channel activity with free alternation of medium exposed to the intracellular surface. If the aim is to study the influence of extracellular influence factors such as neurotransmitters, the outside-out configuration should be chosen. In this case the pipette is retracted during the whole-cell configuration, causing a rupture and rearrangement of the membrane. This configuration provides the opportunity to examine the properties of an ion channel isolated from the cell and exposed successively to different solutions on the extracellular surface of the membrane.

➤ **Patch-clamp capacitance measurements as an assay of exocytosis**

Exocytosis in neurons and neuroendocrine cells occurs through fusion of vesicular membrane with the plasma membrane. After fusion pore formation and release of secretory cargo, secretory membrane can either be retrieved or can fully collapsed driving swelling of the plasma membrane. The temporal resolution of patch-clamp technique is exactly comparable to the time course of this rapid process. In addition, with its precise detection at single cell level, patch-clamp has been applied for the investigation of vesicular secretion in

various cell type such as mast cells, neutrophils and chromaffin cells [72].

In patch clamp measurement, the cell membrane serves as an electrical capacitor with capacitance proportioned to the surface area. The capacitance is closely related to membrane surface enrichment caused by formation of fusion pore that coalesces vesicular membrane with cellular membrane. Conversely, fission of vesicle from cellular membrane results in a decrease of membrane surface. The sudden variation of cellular membrane surface are thus expected to be depicted as an instant capacitance transition recorded by patch clamp. Therefore, the moment of fusion and fission can be presented honestly. Following this viewpoint, patch-clamp in “whole-cell” configuration has fulfilled monitoring exocytotic response upon extensive stimulation on chromaffin cells [73]. For mast cells with bigger secretory granules (~2.5 μm diameter), individual exocytotic secretions caused relative larger membrane surface expansion. Hence, each exocytosis from mast cell was appeared as more apparent “stepwise” increases in capacitance at the same detection configuration[8]. In the meanwhile, the reversibility of the fusion event can also be demonstrated by step-like decreases of the same size as immediately preceding step increases. Therefore, the kinetics of rapid fusion/fission events (“kiss and run mode”) can be captured [74]. In addition, with offline signal conversion relying on the original current varied as a function of time recorded by patch clamp, the conductivity revision at single exocytotic event can be realized. Based on rational assumption of both resistance and length of the tubular channel connecting vesicle and cellular membrane, the cross-section area then is able to be figured out and thus drives the accomplishment of fusion pore size tracking. Moreover, patch-clamp allows easy manipulation of the intracellular environment of the cell. In particular, loading of fluorescent indicators, drugs, peptide and additional messengers into cells can be implemented by diffusion from the pipette solution without disrupting capacitance measurement [72]. This positive feature offers the opportunity for investigating exocytosis combining patch-clamp with other optical measurement.

Although patch-clamp has been demonstrated efficient of characterizing exocytotic fusion pores and synaptic membrane events, however, this method still possesses several weaknesses. In general, for capacitance techniques to be truly useful, they must be embedded within a powerful, flexible software package capable of executing complex stimulus protocols while recording and displaying multiple data streams in real time[68]. Beyond software requirements, another shortcoming of patch-clamp is that when exocytosis and endocytosis are simultaneously triggered representing an overlapping of signals, the real contribution of exocytosis will then be concealed [75]. In addition, the application of

patch-clamp is also limited by lacking the spatial information of the locations where exocytosis occurs.

To set up more powerful tool for scientific research, patch-clamp has been coupled to several measurements such as amperometry or fluorescent microscopy. For instance, combined with amperometry, the kinetic information of exocytotic release is able to be known. While combined with fluorescence microscopy, it accomplishes distinguishing locations of different granular populations undergo secretory release at similar times. The coupling measurements for exocytosis investigation will be elaborated later in section.

1.4.1.2 Amperometry

As mentioned above, the most common ways for intercellular communication is mainly achieved by the release of endogenous chemical/biochemical messengers through exocytosis. Monoamine neurotransmitter is one of signaling molecules undertaken the mission of neurotransmission. The attractive feature of some well-known monoamine neurotransmitters (e.g. dopamine, serotonin) is their electroactive property owing to the hydroxyl group in molecular structure. The natural construction promises their possibility of to be quantitatively detected with electrochemical technique. In the 1990s, catecholamines' quantal secretion was electrochemically monitored for the first time with a CFE placed adjacent to a single chromaffin cell by Wightman and his colleagues [55]. Along with decades of development, amperometry gradually becomes the most widely applied electrochemical technique for exocytosis investigation because of its remarkable advantages such as facility to control, low cost, high temporal resolution as well as high sensitivity [76, 77].

➤ Basic principle

Electrochemical recording of exocytotic secretion generally relies on the instantaneous oxidation of electroactive molecules diffused to the electrode surface located close to the cell membrane. The recorded currents thus reflect quantities of molecules as well as the dynamics of release itself.

To perform the amperometric measurement, a microelectrode with comparable size is positioned at micrometric or submicrometric distances from a living cell, thus allowing the restriction of the extracellular volume in which the molecules generated by the cell are spreading. A constant potential ensuring adequate oxidation of electroactive molecules expelled during exocytosis is then applied to the microelectrode and the resulting electrochemical current is monitored as time accumulated. In this configuration, a small number of molecules released from fusion pore is diffused to the local area of the electrode

in the close vicinity to give a large concentration gradient [78]. As a consequence, the signal-to-noise constraint can be overcome for kinetic detection of secretion with zepto- to attomoles of chemical messengers released during a millisecond time scale. This microelectrode/living cell assembly is inspired by nature to constitute a semi-artificial synapse with working electrode as the function of receiving neuron [76].

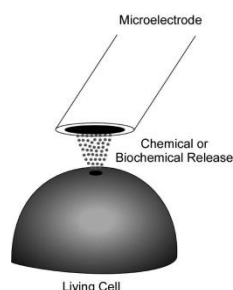


Fig. 1.12 Principle of the semi-artificial synapse configuration. Figure adapted from reference [78].

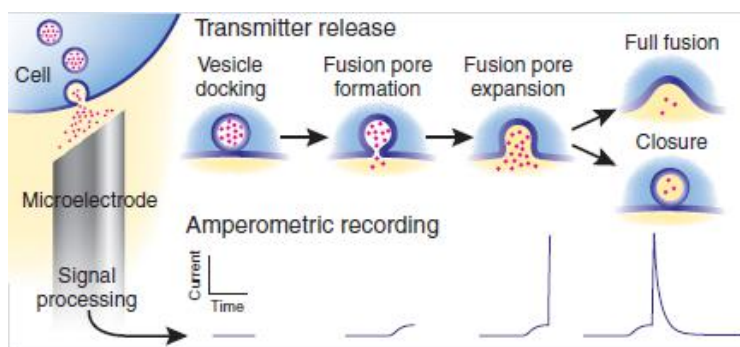


Fig. 1.13 Illustration of a typical amperometric spike representing a single exocytotic event. The initial phase of fusion pore opening and the volume release can be respectively revealed by pre-spike feature (PSF) and the main current spikes resulting from oxidation of the discharged transmitters at electrode surface positioned against to the cell membrane. Major quantitative and kinetic information of release can be extracted from parameters of amperometric spike. Image adapted from reference [79].

Fig. 1.13 concisely displays how an amperometric spike records the independent exocytotic event. In response to an appropriate stimulation, a nanometric fusion pore is firstly formed at the beginning for the leakage of small neurotransmitters to the extracellular space (tightly contacting electrode surface). The small amount of release during initial opening of fusion pore sometimes can be revealed as a small foot (either with a “ramp” shape or a “plateau” shape) appearing before the main spike [80]. Later due to the expansion of the fusion pore, a rapid flux of transmitter rushes onto the electrode surface, leading to a sharp increase of current to a peak amplitude. Along with either the depletion of neurotransmitters stored in secretory vesicles or the closure of fusion pore, less electroactive molecules can reach to the

microelectrode, forming a gradual decay of current to baseline [81]. Each stimulation may trigger hundreds of exocytotic events occurred successively, recording as an amperometric trace composed with a series of such amperometric spikes (Fig. 1.14A).

➤ **Typical parameters for analysis**

For each amperometric spike, several kinetic parameters such as full width at half maximum $t_{1/2}$, maximal current I_{max} can be deduced by examination of each individual event. All these parameters are all applied to describe the morphology of a spike, acting as an evidence for judging the pattern of secretory release. The electrical charge Q (fC or pC) from each amperometric spike reflects the amount of molecules collected during one individual event by the mean of Faraday's law:

$$Q = nFN ;$$

where n is the number of electrons transferred in the electrode surface oxidation ($n = 2$ for catecholamines) and F is Faraday's constant (96,485 C/mole). The charge can be easily obtained by the integral of current with respect to time. Thanks to the high signal/noise ratio accomplished by artificial synapse, the electroactive messenger fluxes can be amperometrically measured with a sensitivity in the range of 1000 molecules per ms. Rapid data collection as well as low detection limit from amperometry allows it to be a statistical and comprehensive analysis tool of the exocytosis.

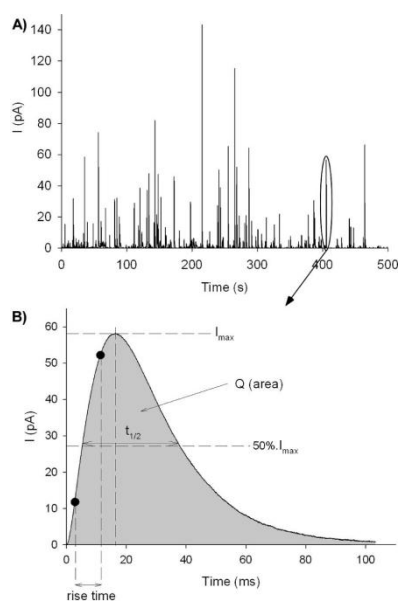


Fig. 1.14 (A) Representative amperometric trace obtained during exocytosis of a single chromaffin cell (the potential of the carbon fiber microelectrode is held at 650 mV vs Ag/AgCl; at this value, all of the catecholamines released during an exocytotic event are oxidized). (B) Usual amperometric analysis of an exocytotic event: major relevant quantitative and kinetic parameters extracted from an amperometric spike. Image adapted from reference [78].

➤ **Applications in exocytosis investigation**

● **Evidences of multiple vesicular populations**

The existence of different types of vesicular populations have been implied by statistic analysis of distribution of electrical charges [82]. The released charge (Q) per amperometric spike, which represents the number of molecules released per exocytotic event is related to the vesicular radius, By combining the Faraday's law and the formula of the spherical volume, one would obtain:

$$r = \left(\frac{3Q}{8\pi F C_{ves}} \right)^{1/3}$$

Assuming that the intravesicular detectable molecule concentration C_{ves} is a constant value in all the secretory vesicles, then the vesicle size (r) becomes the only decisive factor in regulating the electrical charge (Q) detected on the electrode surface.

$$r \propto Q^{1/3}$$

Whenever this basic equation holds, it shows that the amperometric charge is proportional to cube root tantamount of the vesicular size. Grabner et al. reported a dual size-differentiated population of vesicles in chromaffin cells estimated by the mean of describing the quantal size distribution into the sum of two Gaussian distributions. This result was further confirmed by optical microscopy [83]. Similar amperometric results were also recorded on the cell body of the dopamine-containing neuron of *Planorbis corneus* [84], undifferentiated rat PC12 cells [85], and Retzius cells [86, 87]. With deep analysis of the charge from amperometric data, Tang et al. even found that the volumes of vesicles from chromaffin cells could be reasonably divided into at least three Gaussian distributed populations [88].

● **Mapping cell surface**

The lack of spatial resolution is usually encountered when common microelectrode is applied for single cell detection. On account of improving its property, efforts were mainly made on minimization of the dimension of individual microelectrodes by etching [54] and recombination of these surface-reduced electrode into array. To obtain the spatial information as much as possible, researchers bundled up a set of etched microelectrodes to fabricate MEAs with subcellular size to collect information regarding to exocytotic zones on the surface of individual cells. By positioning two independent CFE (5 μm in diameter) on the single cell surface, Wightman and his coworkers discovered for the first time that exocytosis behaviour was inhomogeneous at the cell membrane of chromaffin cells [89]. Similar

configuration has also been applied on endocrine cells revealing the existence of different release sites. Notably, in this experiment the correlation between the active zones and a high local intracellular calcium concentration was evidenced. Thereby calcium pumps spatially close to fusing points equipped with SNAREs machineries was clearly revealed [90].

- **Investigation of controlling factors in regulation of exocytosis**

Owing to the excellent temporal resolution as well as the comprehensive dynamic data provided by amperometry, electrochemical studies allow a fine understanding at a quantitative level. With the help of amperometry, we are able to trace detailed kinetics of each exocytotic secretion in real-time. Hence, amperometry becomes a powerful tool for the study of those controlling factors taking part in the regulation of secretory release. To date, the biological parameters, such as the enzymatic systems, SNAREs proteins, intracellular calcium concentration, actin cytoskeleton, the nature of the secretagogues, and the biosynthesis of the secretory vesicles, have all been evidenced to have a crucial influence on vesicular exocytosis monitored by amperometry [91, 92]. In addition to biological controlling factors, physical and chemical properties of the systems have also been shown to play an important role during the exocytotic mechanism. On a physico-chemical point of view, these parameters such as pH value [93, 94], temperature [95, 96], and osmolarity [97, 98] regulate the exocytotic frequency and dynamics through modulating the membrane properties concomitantly to the vesicular matrix role [78].

1.4.2 Optical methodology

Exocytosis from living cells is achieved through the transport of signaling messengers within nano-scale vesicles to the extracellular environment in a few milliseconds. Such a small dimension as well as the random occurrence location pose great challenges to analytical methods. Optical microscopy with inherent spatial resolution provides reliable tools for visualization of dynamic process of exocytosis. So far, optical observation of exocytotic secretion has been achieved by several microscopy techniques such as confocal microscopy and TIRFM. Notably, TIRFM with its outstanding temporal resolution compared to the other optical techniques has attracted more attention and obtained broader application in the study of exocytosis.

1.4.2.1 Total internal reflection fluorescence microscopy

TIRFM is an application of fluorescence microscopy with its illumination restricted to the glass-water interface instead of penetrating through the specimen. By selectively imaging the basal surface of the sample, TIRFM overcomes the loss of resolution occurring in standard

epi-fluorescence microscopy ascribed to the noise from the bulk of the cell. Moreover, unlike confocal techniques, no pinhole is required to produce thin optical sections (500 nm) [99]. The wide scope illumination of TIRFM allows its instant collection of all excited signals by camera, providing a relative high time resolution. Therefore, it is well suited for studying the localization and dynamics of events occurring within or near the cell membrane in living cells, such as exocytosis [100, 101].

➤ **Physical principle**

According to Snell's law, when light passes a boundary between two different isotropic media, such as water, glass, or air, refraction occurs on the interface between the different phase. The ratio of the sines of the angles of incidence and refraction is equal to the reciprocal of the ratio of the two refraction indexes. When light goes from optically denser medium to the interface with the less dense medium, such as from glass to aqueous sample, there must be a critical state that exactly all the light beam can be completely reflected and does not propagate into the sample. In this critical state, the incidence angle, or namely critical angle (θ_c), is given by Snell's law:

$$\theta_c = \sin^{-1}(n_1 / n_2),$$

where n_1 and n_2 represent the refraction indexes of optically low dense medium and optically denser medium, respectively.

If the incidence angle (θ) of light beam is lower than θ_c , part of the excitation light propagates through the sample, similar as what occurs in epifluorescence. However, if θ is equal to or higher than θ_c , the total internal reflection (TIR) takes place. The excitation light is reflected-off from the interface and some of the incident energy propagate along the interface, creating an evanescent electromagnetic field with restricted thickness (Fig. 1.15). The intensity of the evanescent field (I_z) decays exponentially with the perpendicular distance from the interface (z). The intensity at any position z is described by:

$$I_z = I_0^{-z/d},$$

where I_0 is the intensity of evanescent field on the interface. The depth of evanescent field, d , referring to the distance from the interface where the excitation intensity decays to $1/e$ of I_0 , depends on several parameters including the wavelength of excitation light beam (λ_0), the incidence angle (θ) as well as the refraction indexes of the two medium n_1, n_2 . Depth d can be defined by:

$$d = (\lambda_0/4\pi) * (n_2^2 \sin^2\theta - n_1^2)^{1/2}.$$

For a given system, the wavelength of incidence light and the refraction indexes of the two medium are fixed, so the depth d only depends on the incidence angle: the higher the

incidence angle, the thinner the evanescent field. In total internal reflection fluorescence microscopy (TIRFM), this evanescent field can act as excitation field. With the typical value of depth d in around 100-500 nm, the visual thickness of TIRFM is limited to hundreds of nanometers. Therefore, only fluorophores located within this region could be illuminated while those far away from the interface remain dim, leading to the enhanced high spatial resolution of TIRFM.

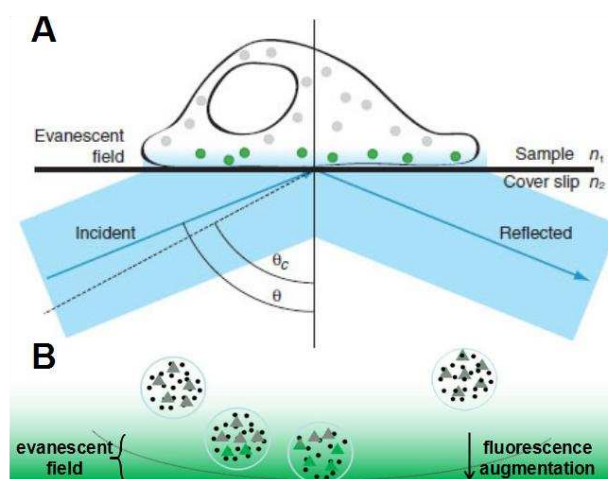


Fig. 1.15 The physical basis of TIRF illumination

➤ **Applications in exocytosis investigation**

● **Mapping vesicle movement and secretory release**

Studies based on fluorescently-tagged proteins using TIRFM have contributed a wealth of new information on the *in vivo* exocytotic process. Exocytosis begins with the transport of cargo-enriched vesicles to a site where exocytosis will be completed. This first step of exocytotic behaviour has readily identified by TIRFM. Taking advantage of high spatial resolution of TIRFM, Lang's group has implemented the identification of secretory carriers along the membrane [102]. The small motions of individual fluorescence-marked secretory carriers in the direction towards plasma membrane (the axial or z-direction) has also been traced by Allersma et al. through following intensity changes. They pointed out that owing to the evanescent excitation field of TIRF, the precision of tracking such axial movements can be as small as 2 nm [103]. After access to the target membrane, granules or vesicles may undergo attachment that well within the TIRF detection zone. The attachment is likely to encompass the biochemically identified processes described as tethering and docking. Chen et al. observed that the movement of vesicles was highly restricted in a small region related to attachment process during exocytosis by tracking fluorescence from fluorescent proteins labeled vesicle under TIRFM [104]. In the ultimate state of exocytosis, the attachment

process facilitates targeting of vesicles on the cellular membrane through direct protein-protein interactions preparing the vesicles for the final delivery of cargo in a process known as fusion. The secretory release occurs by discharging cargo from vesicle to the extracellular space through the formed fusion pore. Single vesicle fused with cellular membrane was identified as a diffusion process of optical probe to the surroundings around releasing site under TIRFM. By quantitative analysis of fluorescence intensity as well as its spreading with respect to time, it was found that many of the vesicles did not exhaust in a single fusion step, but required two or more fusions to fully discharge their cargo [105, 106].

- **Examples of biological parameters revealed by TIRFM**

Before fusing with cell membrane, secretory vesicles have been shown linking to the plasma membrane under the help of SNAREs complex. SNAREs proteins then are assumed to take part in different stages (docking and fusion) of secretory cycle. Some of these roles have already been verified by TIRFM. Johns and his colleagues examined exocytotic process in chromaffin cells with SNAREs proteins cleaved by TIRFM and confirmed that SNAREs proteins were not necessary for the decreased mobility at the docking sites. However, SNAREs may play a role in regulating the interaction between the secretory vesicles with corresponding docking sites as the damage of SNAREs leading to the decreased time for some vesicles move close to the cell membrane [107]. In pancreas β cells, it was also observed by TIRFM that SNAREs proteins were essential for the docking and fusion of insulin granules, in accordance with the results obtained from chromaffin cells [108]. Besides, in PC-12 cells, all three components of the SNAREs complex (synaptobrevin, syntaxin and SNAP-25) contributed to promote secretory vesicle docking according to the TIRFM tracking [109]. The dynamics of the cytoskeleton near the plasma membrane have also been studied with TIRFM, leading to new insights in its contribution to exocytosis. Schmoranzler and Simon observed a cortical microtubule network extended immediately adjacent to the plasma membrane with secretory vesicles attached until the moment of vesicle fusion [110]. Moreover, the quantification of microtubule motility in the axial direction revealing microtubules' target to focal adhesion was accomplished by Krylyshkina et al. [111] In addition, TIRFM with its unique spatial and temporal resolution also provides a powerful tool to study the dynamics of actin and actin associated proteins near the plasma membrane in several endocytosis studies [112, 113].

1.4.3 Coupling of optical and electrochemical methods

All the analytical techniques elaborated above give access to practical information of

exocytotic secretion in their respective fields. However, due to the various shortcomings of each technique, the employment of single analytical methods seems not adequate to fully analyze the complicated exocytotic process. For example, patch clamp traces the formation of fusion pore while the secretory release dynamic is completely lost. Amperometry efficiently records the cargo discharge from exocytotic vesicle in real-time but it is blind about the occurrence site of exocytosis. Although TIRFM offers prominent spatial resolution, its acquisition time restricted by set-up is not sufficient for exocytotic investigation. In order to improve the performance of analytical technique, detection combining two analytical methods for mutual complementation are implemented.

1.4.3.1 Coupling between amperometry and capacitance measurements

Patch-clamp measurements allow the recording of the cell membrane surface variation based on the principle that the cell membrane capacitance is directly proportional to its surface. As a consequence, each exocytotic event can be depicted as a capacitance step during the time course of exocytotic release. The capacitance measurements afford the signal of fusion pore formation. However, no data related to the vesicular content may be provided. The big challenge for capacitance detection happens to be the most attractive merit of amperometric detection. Combining this two electrical methods, both electrophysiological (electrical capacitance) and amperometric (oxidation current) signals are able to be simultaneously recorded at single cell level, giving access to details about fusion pore variation as well as dynamics of secretory release from individual vesicles.

The first combination between capacitance measurements and amperometry was developed two decades ago for investigating exocytosis at chromaffin and beige mouse mast cells [114, 115]. In these studies, the patch-clamp measurements were performed in the whole-cell configuration with a microelectrode placed outside the micropipette (Fig. 1.16B), providing comprehensive information (frequency, kinetics, and cell membrane variation) on the release process. Henceforth, the combination idea became popular in exocytosis investigation [116, 117]. Nevertheless, due to the inconsistency of detection targets from “whole-cell” configuration of capacitance measurements (surface changes on whole cell membrane) and amperometric tracking (secretion limited to an electrode surface), signal matching is not so ideal as imagined. For the sake of improving the coupling performance, two other configurations: “inside-out” and “cell-attached” modes came to being, upon which microelectrode is inserted into the patch pipette [118, 119] (Fig. 1.16A). Both configurations enhance the capacitance measurements resolution, thus allowing studies of “kiss-and-run” events [120], the refinement of the fusion pore analysis [121], and investigations on the

release process regulated by fusion pore size [122]. Despite its distinct advantages, patch-amperometry has some intrinsic shortcomings. Indeed, there is still a possible delay between the amperometric and the capacitance recordings [123, 124], and the distortion of the amperometric spikes shape result from broaden diffusion caused by relatively large distance of the carbon electrode from the patch can't be avoided sometimes [118, 125].

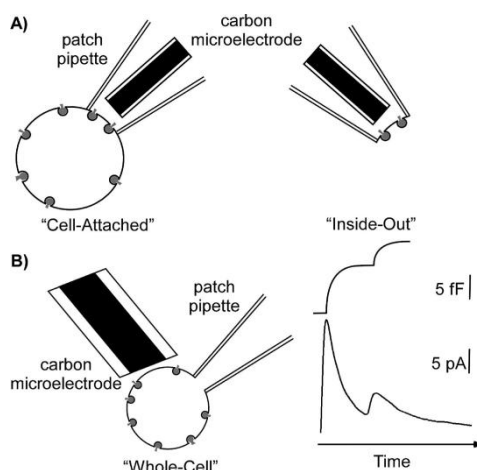


Fig. 1.16 Schematic representation of the three main patch-clamp/amperometry combinations. (A) Left, picture of the cell-attached configuration/amperometry device; right, picture of the inside-out configuration/amperometry device. In both cases, the carbon fiber microelectrode that allows the amperometric detection is located inside the patch pipet. (B) Left, picture of the whole-cell configuration/amperometry device; right, schematic example of temporal correlation between capacitance and amperometric recordings. Figure adapted from reference [78].

1.4.3.2 Coupling patch-clamp with TIRFM

Patch-clamp is a membrane surface variation detection technique, similar as the other electrical method, lacking of spatial resolution becomes its main weakness for exocytosis investigation. To offset this blind zone of detection, optical measurement, especially TIRFM was combined with patch-clamp to pursue inspection with high temporal and spatial resolution.

Taking advantage of coupling detection, Becherer and his colleagues investigated the secretion occurring on the whole surface of cellular membrane (capacitance measurement) and at the bottom of the cell (TIRFM), and realized that PMA treatment (a drug that promotes exocytotic secretion) resulted in a similar increase of global secretion and basal secretion [126]. Besides, investigation of adiponectin effect on insulin secretion in pancreatic β cells were achieved by employing this coupling method [127]. In addition, the fact that

docking stage of secretory vesicles was more sensitive to low intracellular Ca^{2+} than priming in chromaffin cells was revealed by this novel technique [128].

1.4.3.3 Coupling amperometry with TIRFM

Optical techniques based on TIRFM allow highlighted visualizing the different stages of vesicles (transport, docking and fusion) during the exocytotic process. Thanks to the supermolecular binding properties of fluorescent probe, the track of secretory vesicles may be performed in real-time. Nevertheless, this technique is generally applied in order to interrogating the status of the vesicles instead of the exocytotic event itself. Moreover, since the intensity of fluorescence is affected by various factors such as pH value, light refraction and the distance to the interface in terms of TIRFM, the quantitative analysis through optical measurement still encounters heavy obstacles. Besides, due to the restriction of acquisition time of camera, full illustration of exocytosis is hard to achieve solely by fluorescence tracing. Conversely, amperometry with its inherent high temporal resolution (\sim ms) attracts numerous attention in the investigation of exocytosis. In particular, the dynamics of secretory release can be quantitatively recorded, thus offering the opportunity for glimpse at the process of fusion pore expansion. Aiming at integrating the complementary advantages of these two techniques for exocytosis detection, a novel coupled method combining TIRFM with amperometry was established in our group [129]. This set-up enabled the simultaneous monitoring of both optical and electrochemical signals resulting from exocytotic secretions at the bottom of a single cell. Such TIRFM/amperometry coupling test was based on an microchip embedded with four ITO bands as microelectrode for amperometric recording, as displayed in Fig. 1.17. In the meanwhile, the transparency property of ITO allowed fluorescent signal to penetrate, thus guarantee the TIRFM observation. Later in the thesis work of Xiaoqing Liu (a former PhD in our group, 2013-2016), this coupling set-up was optimized and combined with a dual-signal probe to achieve various exocytosis recording [130]. In this thesis, the coupling set-up is further applied for inspecting the lifetime difference between fusion pore opening and monoamine release, as well as the quantitative characterization of various exocytotic mode in PC12 cells. This work will be elaborated in Chapter 4. Similar investigation have been conducted in chromaffin cells by Kisler and his colleagues by using microsystems with transparent/semi-transparent ITO or Au microelectrodes [131].

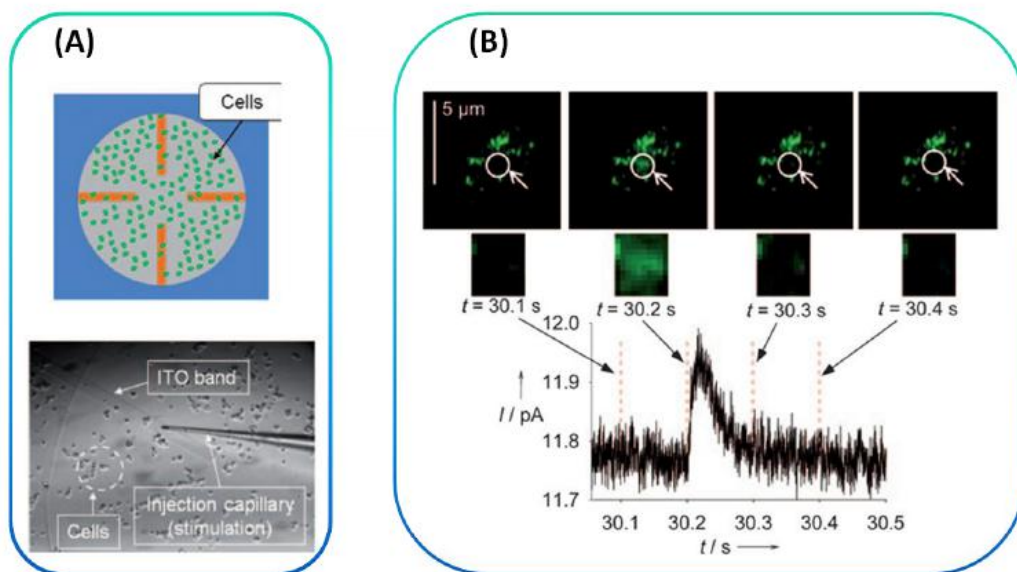


Fig. 1.17 (A) Top: scheme of cells adhered on the microdevice with four independent ITO electrodes (in orange); bottom: inverted microscopy image of BC21 BON cells adhering to the well containing the ITO microelectrodes; (B) A representative examples of combined analyses of an exocytotic event (top: TIRFM; bottom: amperometry) obtained with the ITO microdevice. Images adapted from reference [130].

Amperometric detection of secretory release relies on the oxidation of electroactive molecules discharged from vesicle lumen, while TIRFM requests optical probes labeled either on vesicular membrane or as vesicle luminal cargo. To perform detection combining TIRFM and amperometry on exocytosis study, secretory vesicles labeling with two signal sources is also a crucial issue. This topic will be discussed in the next section.

1.5 Single vesicles' labeling for tracking exocytosis

Exocytosis, one of the fundamental molecular mechanisms of cell communication, has attracted a tremendous amount of attention throughout the last few decades. In particular, measuring individual exocytotic events at single cells under in vitro experimental conditions is highlighted recently and the analytical investigation of exocytosis is prompted from tissue in vivo to single cell level. Identified as the primary intracellular unit for highly efficient storage and release of chemical messengers, the secretory vesicle is served as the research object to discover the contributing factors in regulation of neurotransmission. However, the millisecond time scale of exocytotic event as well as the tiny proportions of messengers release varying from zeptomole to femtomole amounts per vesicle make individual exocytosis experimentally challenging to monitor. The specific labeling of secretory vesicles

can significantly increase both sensitivity and selectivity of traditional analytical measurements and therefore settle the foundation for precise recording of exocytosis process. For different bioanalytical techniques, common vesicle marking can be simply divided into two categories: optical visualization and electrochemical signal generation. In this section, we will elucidate the mechanisms of both and proliferate their applications in coordination with respective analytical methods.

1.5.1 Optical probe for visualization

Imaging exocytosis has been a commonly used research method since the early stage of neurotransmission study. With the rapid development of novel fluorescence microscopy methods, the visualization of unique secretory vesicles attracts more and more attention for yielding the information about real-time dynamics of exocytosis. Continuous efforts have been directed toward the exploration of innovative vesicle labeling method with the core concept of introduction of fluorescent tracer molecules specifically recognized on active vesicles. Depending on different marking principles, main labeling methods can be divided into four categories: fluorescent probe integrated into lipid membrane (Fig. 1.18a), attached to various membrane proteins (Fig. 1.18b), entrapped within acidic compartments (Fig. 1.18c), or replaced peptide vesicle cargo (Fig. 1.18d).

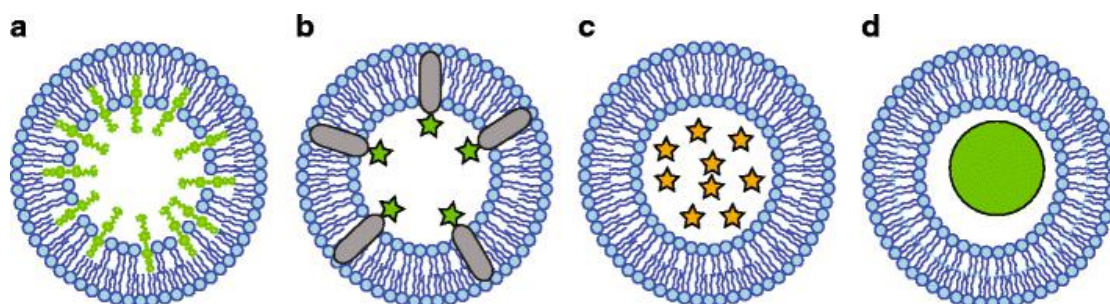


Fig. 1.18 Fluorescent probe used in labeling secretory vesicles. A) Styryl dye molecules as optical probe are encapsulated to the inner leaflet of membrane vesicles via endocytosis. B) Vesicular proteins are labeled with pH-sensitive fluorescent proteins that are temporally quenched in the lower-pH environment inside vesicle cavity while recovering fluorescence when faced to the higher pH value, i.e. extracellular media. C) Acidotropic dyes penetrate through membranes and become charged in the low-pH environment vesicle cavity, thereby concentrating and labeling the vesicle compartment. D) Vesicular peptide linked with green fluorescent protein are introduced into the lumen via transfection. Image adapted from reference [132].

Fluorescent styryl dye, bearing both lipophilic and cationic charges located in their headgroup, can reversibly partition into the outer leaflet of surface membrane without permeating. When exocytosis is evoked by cell stimulation in the presence of styryl dye, the

dye molecules can be inserted into the membrane by internalization during compensatory endocytosis and forming newly stained secretory vesicles [133, 134]. The integration of styryl dye into the vesicular domain significantly enhance the fluorescence intensity compared with fluorophore in the bulk, forming it as a powerful tool for investigating the recycling of secretory vesicles. However, due to the similar composition of vesicular and cellular membranes, portion of styryl dye remains on the cellular membrane during staining, thus increasing the background fluorescence and weakening the contrast of vesicle imaging. Also, in some extent the constant fluorescence from styryl dye brings the identification of exocytosis mode into dilemma. For example, the fast full fusion of vesicular membrane and cellular membrane shares the same visual effect as the kiss and run mode, both representing the sudden disappearance of bright dot under fluorescent microscopy. Monitoring alterations in pH associated with exocytosis opens another avenue for measuring vesicular release in real time. It has been accomplished through the introduction of pH-sensitive fluorescent proteins on the vesicular membrane. By attaching pH-luorin to the membrane protein, one can monitor the significant enhancement of fluorescence signal induced when the vesicle lumen (pH ~5.5) encounters the extracellular medium (pH~7.4) owing to the fact that fluorescence of pH-luorin is quenched at low pH environment while recovered when contact with the medium at higher pH lever, thus rescuing the defect of styryl dye [135]. The pH-sensitive proteins have been applied in the investigation of several aspects of exocytosis such as the determination of secretory mode, the recycling of vesicular membrane proteins after exocytosis, and pH effect on the kinetics of exocytosis.

Unlike the staining of vesicular membrane, Almers' group visualized the secretory release process by accumulating acidotropic dyes inside vesicles [136]. The neutral charge of this dye at neutral pH offers its opportunity to permeate through membranes, while in turn, it becomes protonated encountering the lower pH environment inside the vesicle lumen, thereby labeling the vesicle compartment. Accompanying with total internal reflection microscopy, the whole release process can be perfectly recorded for the intracellular regulatory mechanism study. Similarly, pH-modulated fluorescent proteins are also applied to the labeling of vesicular content. By linking with neuro-peptide, fluorescent proteins are easily expressed in the vesicular cavity, thus providing the mean of tracking source for exocytosis [1].

1.5.2 electroactive probe for electrochemical recording

Electrochemical detection of neurosecretion has been the most quantitative dynamic assessment of the chemical messengers released during the secretory exocytosis. Compared

to optical tracing, it represents excellent accuracy for details recording owing to its high temporal resolution and precisely quantification according to Faraday's law. The utility of electrochemical measurement to investigate neurobiological phenomena is relying on the principle that messengers triggered during signal transmission are electroactive, and thus can be easily captured and reacted at a polarized electrode surface, presenting consequent secretory releases as a series of electrochemical signal. Some of vesicles can spontaneously store those molecules with electrochemical activity (e.g. dopamine, epinephrine, norepinephrine, serotonin, histamine, and various neuropeptide). While the other vesicles are almost invisible for the electrochemical detection since none of the content is able to undergo the oxidation or reduction process with applied potential. Even for these endogenous electroactive messengers contained vesicles, insufficient storage also makes trouble for signal recording. Therefore, the efficient loading of electroactive probe inside vesicles may determine the success of electrochemical monitoring. Dopamine, one of the typical vesicle garnered catecholamine, can undergo the irreversible oxidation process in around 600mV (vs. Ag/AgCl). The filling of vesicle cavity has been achieved by exposing to L-DOPA solution [57]. As the precursor of dopamine, L-DOPA can penetrate through cellular membrane and is further transported into vesicle by physiological synthesis. In PC12 cells, the pharmacological treatment with L-DOPA has been reported to significantly alter intravesicular dopamine storage. Serotonin, another common catecholamine, is also used to enhance the storage of neurotransmitters. Vesicular monoamine transporter protein (VMAT) on the vesicular membrane ships this small molecules into vesicle lumen through the recognition of monoamine group. This uploading of serotonin has been applied for the so called "empty" vesicles in BON N13 cells [1].

1.5.3 Collaborative marker for optical and electrochemical detection

Along with the technique progress, the pursuit of spatio-temporal resolution for exocytosis tracing makes the discovery of dual-signal probe imminently. Inspired by the transmission mechanism of VMAT, researchers dedicate to the synthesis of new artificial neurotransmitters for vesicle labeling. Fluorescent false neurotransmitters, abbreviated as FFNs, is a series of fluorescent compounds possessing similar structure as those monoamine neurotransmitters accumulated in synaptic vesicles [137, 138]. They directly mimic the molecular characteristics of chemical messengers stored in vesicle, in terms of their specificity and size. Therefore, FFNs can be selectively translocated from cytosol to the lumen of vesicles by the erroneous recognition of vesicular monoamine transporter [139]. Among them, 4-(2-aminoethyl)-6-chloro-7-hydroxy-2H-1-benzopyran-2-one hydrochloride is

one of the most attractive ratiometric pH-sensing probe for its bifunctional property. It was first synthesized by Sames and co-workers and briefly named FFN102. The molecular formula of FFN102 is presented as in Fig. 1.19. The ethylamino group offers the opportunity of vesicle addressing while the equilibrium between the protonated phenol and the deprotonated phenolate forms provides pH-dependent photophysical properties. Furthermore, thanks to the electron-withdrawing group (-Cl) on the 6-position of coumarin, the pK_a value of the phenolic hydroxyl group is decreased to around 6, landing in the acidic environment of secretory vesicles (c.a. 5~6). Thus a fluorescence augmentation should be observed when FFN102 diffuses out from the cellular vesicle lumen (pH=5~6) to the extracellular medium (pH=7). In particular, recently FFN102 has been reported displaying electroactive property owing to the phenolic hydroxyl group at the 7-position of coumarin, predicting it a promising application as a potential difunctional probe (i.e. optical and electrochemical) for dynamic vesicle tracking. In Chapter2, we will mainly discuss the mechanism of vesicle lumen enrichment with FFN102.

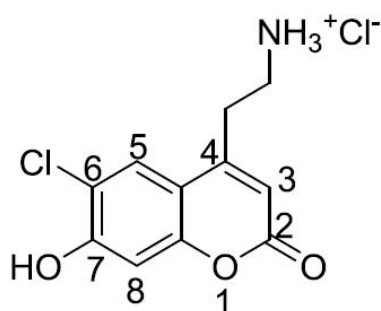


Fig. 1.19 Molecular formula of fluorescent false neurotransmitter (FFN102): 4-(2-aminoethyl)-6-chloro-7-hydroxy-2H-1-benzopyran-2-one hydrochloride.

1.6 Research objectives

The importance of vesicular exocytosis in biology and physiology has been sufficiently embodied in recent decades. Aiming at deeply deciphering the exocytosis process, my PhD work sequentially explored the kinetics of secretory release, its impact factor: fusion pore dimension expanded against time, the original constraint of fusion pore evolution: membrane tension regulated by associated protein, and the multiple types of exocytosis representing distinct vesicle behaviour. Owing to the fast acquisition time as well as accurate quantification properties of amperometry, the massive flux of neurotransmitters released from submicrometer sized vesicles can be precisely recorded. The wealth of information of secretory release obtained from amperogram offers the chance for further casting the light

on the process of fusion pore expansion as well as the participation of exocytosis related protein with additional help of inhibitor treatment. Whereas taking advantage of real-time optical observation from TIRFM with prominent spatial resolution, the whole process of exocytosis including but not limited to vesicular and cellular membrane fusion was fully rendered. Specifically, our research objectives in this thesis can be sorted into three aspects narrated as follows:

Firstly, we inspected the availability of FFN102 as a electroactive and optical probe for secretory release recording in PC12 cells with respect to its vesicular storage mechanism and performance during stimulated exocytosis. (Chapter 2) Secondly, we restored the actual fusion pore dimension from single current spike recorded relying on analytical simulation. This reconstruction enabled us to investigate the role of molecular motor myosin II in regulating fusion pore expansion by intuitive monitoring its impact on fusion pore size. (Chapter 3) Finally, monitoring vesicle behaviour during exocytosis was allowed by the introduction of measurement combined TIRFM with amperometry. In view of analysis of membrane protein spreading, exocytosis recorded was identified into two major modes with divergent performance and supported by amperometric data. The regular pattern of fusion pore enlargement in each mode was further summarized. (Chapter 4)

1.7 Reference

1. A. Meunier, M. Bretou, F. Darchen, M. Guille-Collignon, F. Lemaître, C. Amatore, *Amperometric detection of vesicular exocytosis from BON cells at carbon fiber microelectrodes*. *Electrochimica Acta*, 2014. **126**: p. 74-80.
2. D. Fasshauer, H. Otto, W. Eliason, R. Jahn, A. T. Brünger, *Structural changes are associated with soluble N-ethylmaleimide-sensitive fusion protein attachment protein receptor complex formation*. *Journal of Biological Chemistry*, 1997. **272**(44): p. 28036-28041.
3. T. Xu, B. Rammner, M. Margittai, A. R. Artalejo, E. Neher, R. Jahn, *Inhibition of SNARE complex assembly differentially affects kinetic components of exocytosis*. *Cell*, 1999. **99**(7): p. 713-722.
4. R. B. Sutton, D. Fasshauer, R. Jahn, A. T. Brünger, *Crystal structure of a SNARE complex involved in synaptic exocytosis at 2.4 Å resolution*. *Nature*, 1998. **395**(6700): p. 347.
5. B. Alberts, D. Bray, K. Hopkin, A. D. Johnson, J. Lewis, M. Raff, K. Roberts, P. Walter, *Essential cell biology*. Garland Science, 2004.
6. D. M. Omiattek, Y. Dong, M. L. Heien, A. G. Ewing, *Only a fraction of quantal content is released during exocytosis as revealed by electrochemical cytometry of secretory vesicles*. *ACS chemical neuroscience*, 2010. **1**(3): p. 234-245.
7. A. A. Alabi, R. W. Tsien, *Perspectives on kiss-and-run: role in exocytosis, endocytosis, and neurotransmission*. *Annual review of physiology*, 2013. **75**: p. 393-422.
8. J. Zimmerberg, M. Curran, F. S. Cohen, M. Brodwick, *Simultaneous electrical and optical measurements show that membrane fusion precedes secretory granule swelling during*

- exocytosis of beige mouse mast cells*. Proceedings of the National Academy of Sciences, 1987. **84**(6): p. 1585-1589.
9. D. Lawson, M. C. Raff, B. Gomperts, C. Fewtrell, N. B. Gilula, *Molecular events during membrane fusion. A study of exocytosis in rat peritoneal mast cells*. The Journal of cell biology, 1977. **72**(2): p. 242-259.
 10. K. Ozawa, Z Szallasi, M. G. Kazanietz, P. M. Blumberg, H. Mischak, J. F. Mushinski, M. A. Beaven, *Ca (2+)-dependent and Ca (2+)-independent isozymes of protein kinase C mediate exocytosis in antigen-stimulated rat basophilic RBL-2H3 cells. Reconstitution of secretory responses with Ca²⁺ and purified isozymes in washed permeabilized cells*. Journal of Biological Chemistry, 1993. **268**(3): p. 1749-1756.
 11. F. C. Mohr, C. Fewtrell, *Depolarization of rat basophilic leukemia cells inhibits calcium uptake and exocytosis*. The Journal of cell biology, 1987. **104**(3): p. 783-792.
 12. J. L. Johnson, H. Hong, J. Monfregola, W. B. Kiosses, S. D. Catz, *Munc13-4 restricts motility of Rab27a-expressing vesicles to facilitate lipopolysaccharide-induced priming of exocytosis in neutrophils*. Journal of Biological Chemistry, 2011. **286**(7): p. 5647-5656.
 13. A. A. Brzezinska, J. L. Johnson, D. B. Munafo, B. A. Ellis, S. D. Catz, *Signalling mechanisms for Toll-like receptor-activated neutrophil exocytosis: key roles for interleukin-1-receptor-associated kinase-4 and phosphatidylinositol 3-kinase but not Toll/IL-1 receptor (TIR) domain-containing adaptor inducing IFN- β (TRIF)*. Immunology, 2009. **127**(3): p. 386-397.
 14. M. Bader, R. W. Holz, K. Kumakura, N. Vitale, *Exocytosis: the chromaffin cell as a model system*. Annals of the New York Academy of Sciences, 2002. **971**(1): p. 178-183.
 15. R. E. Coupland, *Determining sizes and distribution of sizes of spherical bodies such as chromaffin granules in tissue sections*. Nature, 1968. **217**(5126): p. 384.
 16. L. A. Greene, A. S. Tischler, *Establishment of a noradrenergic clonal line of rat adrenal pheochromocytoma cells which respond to nerve growth factor*. Proceedings of the National Academy of Sciences, 1976. **73**(7): p. 2424-2428.
 17. Y. Liu, E. S. Schweitzer, M. J. Nirenberg, V. M. Pickel, C. J. Evans, R. H. Edwards, *Preferential localization of a vesicular monoamine transporter to dense core vesicles in PC12 cells*. The Journal of Cell Biology, 1994. **127**(5): p. 1419-1433.
 18. R. H. S. Westerink, A. Ewing, *The PC12 cell as model for neurosecretion*. Acta Physiologica, 2008. **192**(2): p. 273-285.
 19. C. M. Grau, L. A. Greene, *Use of PC12 cells and rat superior cervical ganglion sympathetic neurons as models for neuroprotective assays relevant to Parkinson's disease*, in *Neurotrophic Factors*. 2012, Springer. p. 201-211.
 20. V. S. Tran, A. Marion-Audibert, E. Karatekin, S. Huet, S. Cribier, K. Guillaumie, C. Chapuis, C. Desnos, F. Darchen, J. Henry, *Serotonin secretion by human carcinoid BON cells*. Annals of the New York Academy of Sciences, 2004. **1014**(1): p. 179-188.
 21. X. Liu, *More transparency in bioanalysis of exocytosis: application of fluorescent false neurotransmitters in coupling methodology of electrochemistry with fluorescence microscopy at ITO microelectrodes*. 2016, Paris 6.
 22. N. Porat-Shliom, O. Milberg, A. Masedunskas, R. Weigert, *Multiple roles for the actin cytoskeleton during regulated exocytosis*. Cellular and Molecular Life Sciences, 2013. **70**(12): p. 2099-2121.

23. L. Lanzetti, *Actin in membrane trafficking*. Current opinion in cell biology, 2007. **19**(4): p. 453-458.
24. M. Anitei, B. Hoflack, *Bridging membrane and cytoskeleton dynamics in the secretory and endocytic pathways*. Nature cell biology, 2012. **14**(1): p. 11.
25. S. Sankaranarayanan, P. P. Atluri, T. A. Ryan, *Actin has a molecular scaffolding, not propulsive, role in presynaptic function*. Nature neuroscience, 2003. **6**(2): p. 127.
26. T. Gotow, K. Miyaguchi, P. Hashimoto, *Cytoplasmic architecture of the axon terminal: filamentous strands specifically associated with synaptic vesicles*. Neuroscience, 1991. **40**(2): p. 587-598.
27. D. Giner, P. Neco, M. M. Francés, I. López, S. Viniegra, L. M. Gutiérrez, *Real-time dynamics of the F-actin cytoskeleton during secretion from chromaffin cells*. Journal of cell science, 2005. **118**(13): p. 2871-2880.
28. D. Giner, I. López, P. Neco, O. Rossetto, C. Montecucco, L. M. Gutiérrez, *Glycogen synthase kinase 3 activation is essential for the snake phospholipase A2 neurotoxin-induced secretion in chromaffin cells*. European Journal of Neuroscience, 2007. **25**(8): p. 2341-2348.
29. J. L. Jewell, W. Luo, E. Oh, Z. Wang, D. C. Thurmond, *Filamentous actin regulates insulin exocytosis through direct interaction with Syntaxin 4*. Journal of Biological Chemistry, 2008. **283**(16): p. 10716-10726.
30. F. Momboisse, S. Ory, V. Calco, M. Malacombe, M. Bader, S. Gasman, *Calcium-regulated exocytosis in neuroendocrine cells: intersectin-1L stimulates actin polymerization and exocytosis by activating Cdc42*. Annals of the New York Academy of Sciences, 2009. **1152**(1): p. 209-214.
31. A. Masedunskas, M. Sramkova, L. Parente, K. U. Sales, P. Amornphimoltham, T. H. Bugge, R. Weigert, *Role for the actomyosin complex in regulated exocytosis revealed by intravital microscopy*. Proceedings of the National Academy of Sciences, 2011. **108**(33): p. 13552-13557.
32. T. D. Nightingale, I. J. White, E. L. Doyle, M. Turmaine, K. J. Harrison-Lavoie, K. F. Webb, L. P. Cramer, D. F. Cutler, *Actomyosin II contractility expels von Willebrand factor from Weibel–Palade bodies during exocytosis*. The Journal of cell biology, 2011. **194**(4): p. 613-629.
33. A. M. Sokac, W. M. Bement, *Kiss-and-coat and compartment mixing: coupling exocytosis to signal generation and local actin assembly*. Molecular biology of the cell, 2006. **17**(4): p. 1495-1502.
34. T. D. Nightingale, D. F. Cutler, L. P. Cramer, *Actin coats and rings promote regulated exocytosis*. Trends in cell biology, 2012. **22**(6): p. 329-337.
35. H. N. Aguilar, B. Mitchell, *Physiological pathways and molecular mechanisms regulating uterine contractility*. Human reproduction update, 2010. **16**(6): p. 725-744.
36. P. Neco, C. Fernández-Peruchena, S. Navas, M. Lindau, L. M. Gutiérrez, G. Álvarez de Toledo, E. Alés, *Myosin II contributes to fusion pore expansion during exocytosis*. Journal of Biological Chemistry, 2008.
37. A. B. Verkhovskiy, T. M. Svitkina, G.G. Borisy, *Self-polarization and directional motility of cytoplasm*. Current Biology, 1999. **9**(1): p. 11-S1.
38. P. Neco, D. Giner, S. Viniegra, R. Borges, A. Villarroel, L. M. Gutiérrez, *New roles of myosin II during the vesicle transport and fusion in chromaffin cells*. Journal of Biological Chemistry, 2004.

39. R. I. Ludowyke, Z. Elgundi, T. Kranenburg, J. R. Stehn, C. Schmitz-Peiffer, W. E. Hughes, T. J. Biden, *Phosphorylation of nonmuscle myosin heavy chain IIA on Ser1917 is mediated by protein kinase C β II and coincides with the onset of stimulated degranulation of RBL-2H3 mast cells*. *The Journal of Immunology*, 2006. **177**(3): p. 1492-1499.
40. T. A. Ryan, *Inhibitors of myosin light chain kinase block synaptic vesicle pool mobilization during action potential firing*. *Journal of Neuroscience*, 1999. **19**(4): p. 1317-1323.
41. S. Mochida, H. Kobayashi, Y. Matsuda, Y. Yuda, K. Muramoto, Y. Nonomura, *Myosin II is involved in transmitter release at synapses formed between rat sympathetic neurons in culture*. *Neuron*, 1994. **13**(5): p. 1131-1142.
42. P. Bhat, P. Thorn, *Myosin 2 maintains an open exocytic fusion pore in secretory epithelial cells*. *Molecular biology of the cell*, 2009. **20**(6): p. 1795-1803.
43. K. A. Becker, N. H. Hart, *Reorganization of filamentous actin and myosin-II in zebrafish eggs correlates temporally and spatially with cortical granule exocytosis*. *Journal of cell science*, 1999. **112**(1): p. 97-110.
44. J. A. Hammer III, J. R. Sellers, *Walking to work: roles for class V myosins as cargo transporters*. *Nature Reviews Molecular Cell Biology*, 2012. **13**(1): p. 13.
45. B. Hetrick, M. S. Han, L. A. Helgeson, B. J. Nolen, *Small molecules CK-666 and CK-869 inhibit actin-related protein 2/3 complex by blocking an activating conformational change*. *Chemistry & biology*, 2013. **20**(5): p. 701-712.
46. R. I. Trouillon, A. G. Ewing, *Actin controls the vesicular fraction of dopamine released during extended kiss and run exocytosis*. *ACS chemical biology*, 2014. **9**(3): p. 812-820.
47. G. E. Peng, S. R. Wilson, O. D. Weiner, *A pharmacological cocktail for arresting actin dynamics in living cells*. *Molecular biology of the cell*, 2011. **22**(21): p. 3986-3994.
48. R. J. Forster, *Microelectrodes: new dimensions in electrochemistry*. *Chemical Society Reviews*, 1994. **23**(4): p. 289-297.
49. J. Heinze, *Ultramicroelectrodes in Electrochemistry*. *Angewandte Chemie International Edition in English*, 1993. **32**(9): p. 1268-1288.
50. S. Cosnier, *Electrochemical Detection of Exocytosis: A Survey from the Earliest Amperometry at Carbon Fiber Ultramicroelectrodes to Recent Integrated Systems*, in *Electrochemical Biosensors*. 2015, Pan Stanford. p. 14-65.
51. D. J. Leszczyszyn, J. A. Jankowski, O. H. Viveros, E. J. Diliberto Jr, J. A. Near R. M. Wightman, *Secretion of Catecholamines from Individual Adrenal Medullary Chromaffin Cells*. *Journal of Neurochemistry*, 1991. **56**(6): p. 1855-1863.
52. R. H. Chow, L. von Rüden, E. Neher, *Delay in vesicle fusion revealed by electrochemical monitoring of single secretory events in adrenal chromaffin cells*. *Nature*, 1992. **356**: p. 60.
53. Z. Zhou, S. Mislser, *Amperometric Detection of Quantal Secretion from Patch-clamped Rat Pancreatic -Cells*. *Journal of Biological Chemistry*, 1996. **271**(1): p. 270-277.
54. K. T. Kawagoe, J. A. Jankowski, R. M. Wightman, *Etched carbon-fiber electrodes as amperometric detectors of catecholamine secretion from isolated biological cells*. *Analytical Chemistry*, 1991. **63**(15): p. 1589-1594.
55. D. J. Leszczyszyn, J. A. Jankowski, O. H. Viveros, E. J. Diliberto Jr, J. A. Near, R. M. Wightman, *Nicotinic receptor-mediated catecholamine secretion from individual chromaffin cells. Chemical evidence for exocytosis*. *Journal of Biological Chemistry*, 1990. **265**(25): p. 14736-14737.

56. K. D. Kozminski, D. A. Gutman, V. Davila, D. Sulzer, A. G. Ewing, *Voltammetric and Pharmacological Characterization of Dopamine Release from Single Exocytotic Events at Rat Pheochromocytoma (PC12) Cells*. Analytical Chemistry, 1998. **70**(15): p. 3123-3130.
57. L. A. Sombers, M. M. Maxson, A. G. Ewing, *Loaded dopamine is preferentially stored in the halo portion of PC12 cell dense core vesicles*. Journal of Neurochemistry, 2005. **93**(5): p. 1122-1131.
58. R. M. Wightman, J. A. Jankowski, R. T. Kennedy, K. T. Kawagoe, T. J. Schroeder, D. J. Leszczyszyn, J. A. Near, E. J. Diliberto Jr, O. H. Viveros, *Temporally resolved catecholamine spikes correspond to single vesicle release from individual chromaffin cells*. Proceedings of the National Academy of Sciences, 1991. **88**(23): p. 10754-10758.
59. L. Huang, H. Shen, M. A. Atkinson, R. T. Kennedy., *Detection of exocytosis at individual pancreatic beta cells by amperometry at a chemically modified microelectrode*. Proceedings of the National Academy of Sciences, 1995. **92**(21): p. 9608-9612.
60. H. Zhao, X. Bian, J. J. Galliganb, G. M. Swaina, *Electrochemical measurements of serotonin (5-HT) release from the guinea pig mucosa using continuous amperometry with a boron-doped diamond microelectrode*. Diamond and Related Materials, 2010. **19**(2): p. 182-185.
61. H. Cui, J. Ye, Y. Chen, S. Chong, X. Liu, T. Lim, F. Sheu, *In situ temporal detection of dopamine exocytosis from l-dopa-incubated MN9D cells using microelectrode array-integrated biochip*. Sensors and Actuators B: Chemical, 2006. **115**(2): p. 634-641.
62. A. F. Dias, G. Dernick, V. Valero, M. G. Yong, C. D. James, H. G. Craighead, M. Lindau, *An electrochemical detector array to study cell biology on the nanoscale*. Nanotechnology, 2002. **13**(3): p. 285.
63. A. Meunier, R. Fulcrand, F. Darchen, M. Guille Collignon, F. Lemaître, C. Amatore, *Indium Tin Oxide devices for amperometric detection of vesicular release by single cells*. Biophysical Chemistry, 2012. **162**: p. 14-21.
64. S. Y. Yang, B. N. Kim, A. A. Zakhidov, P. G. Taylor, J. Lee, C. K. Ober, M. Lindau, G. G. Malliaras, *Detection of transmitter release from single living cells using conducting polymer microelectrodes*. Advanced Materials, 2011. **23**(24): p. H184-H188.
65. C. Amatore, J. Delacotte, M. Guille-Collignon, F. Lemaître, *Vesicular exocytosis and microdevices—microelectrode arrays*. Analyst, 2015. **140**(11): p. 3687-3695.
66. C. Amatore, C. Pebay, L. Thouin, A. Wang, J. S. Warkocz, *Difference between ultramicroelectrodes and microelectrodes: influence of natural convection*. Analytical chemistry, 2010. **82**(16): p. 6933-6939.
67. E. Neher, B. Sakmann, *Single-channel currents recorded from membrane of denervated frog muscle fibres*. Nature, 1976. **260**(5554): p. 799.
68. R. Borges, M. Camacho, K. Gillis, *Measuring secretion in chromaffin cells using electrophysiological and electrochemical methods*. Acta Physiologica, 2008. **192**(2): p. 173-184.
69. B. Sakmann, E. Neher, *Patch clamp techniques for studying ionic channels in excitable membranes*. Annual review of physiology, 1984. **46**(1): p. 455-472.
70. O. P. Hamill, A. Marty, E. Neher, B. Sakmann, F. J. Sigworth, *Improved patch-clamp techniques for high-resolution current recording from cells and cell-free membrane patches*. Pflügers Archiv, 1981. **391**(2): p. 85-100.

71. E. Neher, B. Sakmann, *The patch clamp technique*. Scientific American, 1992. **266**(3): p. 44-51.
72. G. Kilic, *Exocytosis in bovine chromaffin cells: studies with patch-clamp capacitance and FM1-43 fluorescence*. Biophysical journal, 2002. **83**(2): p. 849-857.
73. E. Neher, A. Marty, *Discrete changes of cell membrane capacitance observed under conditions of enhanced secretion in bovine adrenal chromaffin cells*. Proceedings of the National Academy of Sciences, 1982. **79**(21): p. 6712-6716.
74. L. Breckenridge, W. Almers, *Currents through the fusion pore that forms during exocytosis of a secretory vesicle*. Nature, 1987. **328**(6133): p. 814.
75. C. Smith, T. Moser, T. Xu, E. Neher, *Cytosolic Ca²⁺ acts by two separate pathways to modulate the supply of release-competent vesicles in chromaffin cells*. Neuron, 1998. **20**(6): p. 1243-1253.
76. A. S. Cans, A. G. Ewing, *Highlights of 20 years of electrochemical measurements of exocytosis at cells and artificial cells*. Journal of Solid State Electrochemistry, 2011. **15**(7-8): p. 1437-1450.
77. F., Lemaître, M. G. Collignon, C. Amatore, *Recent advances in electrochemical detection of exocytosis*. Electrochimica Acta, 2014. **140**: p. 457-466.
78. C. Amatore, S. Arbault, M. Guille, F. Lemaître, *Electrochemical monitoring of single cell secretion: vesicular exocytosis and oxidative stress*. Chemical reviews, 2008. **108**(7): p. 2585-2621.
79. D. Evanko, *Primer: spying on exocytosis with amperometry*. Nature methods, 2005. **2**(9): p. 650.
80. L. J. Mellander, R. Trouillon, M. I. Svensson, A. G. Ewing, *Amperometric post spike feet reveal most exocytosis is via extended kiss-and-run fusion*. Scientific reports, 2012. **2**: p. 907.
81. I. M. Robinson, M. Yamada, M. Carrion-Vazquez, V. A. Lennon, J. M. Fernandez, *Specialized release zones in chromaffin cells examined with pulsed-laser imaging*. Cell calcium, 1996. **20**(2): p. 181-201.
82. B. B. Anderson, S. E. Zerby, A. G. Ewing, *Calculation of transmitter concentration in individual PC12 cell vesicles with electrochemical data and a distribution of vesicle size obtained by electron microscopy*. Journal of neuroscience Methods, 1999. **88**(2): p. 163-170.
83. C. P. Grabner, S. D. Price, A. Lysakowski, A. P. Fox, *Mouse chromaffin cells have two populations of dense core vesicles*. Journal of neurophysiology, 2005. **94**(3): p. 2093-2104.
84. B. B. Anderson, G. Chen, D. A. Gutman, A. G. Ewing, *Dopamine levels of two classes of vesicles are differentially depleted by amphetamine*. Brain research, 1998. **788**(1-2): p. 294-301.
85. R. H. Westerink, A. de Groot, H. P. Vijverberg, *Heterogeneity of catecholamine-containing vesicles in PC12 cells*. Biochemical and biophysical research communications, 2000. **270**(2): p. 625-630.
86. D. Bruns, R. Jahn, *Real-time measurement of transmitter release from single synaptic vesicles*. Nature, 1995. **377**(6544): p. 62.
87. D. Bruns, D. Riedel, J. Klingauf, R. Jahn, *Quantal release of serotonin*. Neuron, 2000. **28**(1): p. 205-220.
88. K. S. Tang, A. Tse, F. W. Tse, *Differential regulation of multiple populations of granules in rat adrenal chromaffin cells by culture duration and cyclic AMP*. Journal of neurochemistry, 2005. **92**(5): p. 1126-1139.

89. T. J. Schroeder, J. A. Jankowski, J. Senyshyn, R. W. Holz, R. M. Wightman, *Zones of exocytotic release on bovine adrenal medullary cells in culture*. Journal of Biological Chemistry, 1994. **269**(25): p. 17215-17220.
90. I. M. Robinson, J. M. Finnegan, J. R. Monck, R. M. Wightman, J. M. Fernandez, *Colocalization of calcium entry and exocytotic release sites in adrenal chromaffin cells*. Proceedings of the National Academy of Sciences, 1995. **92**(7): p. 2474-2478.
91. P. Ñeco, O. Rossetto, A. Gil, C. Montecucco, L. M. Gutiérrez, *Taipoxin induces F-actin fragmentation and enhances release of catecholamines in bovine chromaffin cells*. Journal of neurochemistry, 2003. **85**(2): p. 329-337.
92. M. E. Graham, R. J. Fisher, R. D. Burgoyne, *Measurement of exocytosis by amperometry in adrenal chromaffin cells: effects of clostridial neurotoxins and activation of protein kinase C on fusion pore kinetics*. Biochimie, 2000. **82**(5): p. 469-479.
93. R. Borges, D. Pereda, B. Beltrán, M. Prunell, M. Rodríguez, J. D. Machado, *Intravesicular factors controlling exocytosis in chromaffin cells*. Cellular and molecular neurobiology, 2010. **30**(8): p. 1359-1364.
94. M. Camacho, J. D. Machado, M. S. Montesinos, M. Criado, R. Borges, *Intragranular pH rapidly modulates exocytosis in adrenal chromaffin cells*. Journal of neurochemistry, 2006. **96**(2): p. 324-334.
95. K. Pihel, E. R. Travis, R. Borges, R. M. Wightman, *Exocytotic release from individual granules exhibits similar properties at mast and chromaffin cells*. Biophysical journal, 1996. **71**(3): p. 1633.
96. A. Gil, S. Viniegra, L. M. Gutiérrez, *Temperature and PMA affect different phases of exocytosis in bovine chromaffin cells*. European Journal of Neuroscience, 2001. **13**(7): p. 1380-1386.
97. L. A. Sombers, N. J. Wittenberg, M. M. Maxson, K. L. Adams, A. G. Ewing, *High Osmolarity and L-DOPA Augment Release via the Fusion Pore in PC12 Cells*. ChemPhysChem, 2007. **8**(17): p. 2471-2477.
98. C. Amatore, S. Arbault, I. Bonifas, Y. Bouret, M. Erard, M. Guille, *Dynamics of full fusion during vesicular exocytotic events: release of adrenaline by chromaffin cells*. ChemPhysChem, 2003. **4**(2): p. 147-154.
99. A. Yildiz, R. D. Vale, *Total internal reflection fluorescence microscopy*. Cold Spring Harbor protocols, 2015. **2015**(9): p. pdb. top086348.
100. A. L. Mattheyses, S. M. Simon, J. Z. Rappoport, *Imaging with total internal reflection fluorescence microscopy for the cell biologist*. J Cell Sci, 2010. **123**(21): p. 3621-3628.
101. J. G. Burchfield, J. A. Lopez, K. Mele, P. Vallotton, W. E. Hughes, *Exocytotic vesicle behaviour assessed by total internal reflection fluorescence microscopy*. Traffic, 2010. **11**(4): p. 429-439.
102. T. Lang, I. Wacker, J. Steyer, C. Kaether, I. Wunderlich, T. Soldati, H. Gerdes, W. Almers, *Ca²⁺-triggered peptide secretion in single cells imaged with green fluorescent protein and evanescent-wave microscopy*. Neuron, 1997. **18**(6): p. 857-863.
103. M. W. Allersma, M. A. Bittner, D. Axelrod, R. W. Holz, *Motion matters: secretory granule motion adjacent to the plasma membrane and exocytosis*. Molecular biology of the cell, 2006. **17**(5): p. 2424-2438.
104. L. Jiang, J. Fan, L. Bai, Y. Wang, Y. Chen, L. Yang, L. Chen, T. Xu, *Direct quantification of fusion rate reveals a distal role for AS160 in insulin-stimulated fusion of GLUT4 storage vesicles*. Journal of biological chemistry, 2008. **283**(13): p. 8508-8516.

105. J. K. Jaiswal, V. M. Rivera, S. M. Simon, *Exocytosis of post-Golgi vesicles is regulated by components of the endocytic machinery*. Cell, 2009. **137**(7): p. 1308-1319.
106. J. Schmoranzer, M. Goulian, D. Axelrod, S. M. Simon, *Imaging constitutive exocytosis with total internal reflection fluorescence microscopy*. The Journal of cell biology, 2000. **149**(1): p. 23-32.
107. L. M. Johns, E. S. Levitan, E. A. Shelden, R. W. Holz, D. Axelrod, *Restriction of secretory granule motion near the plasma membrane of chromaffin cells*. The Journal of cell biology, 2001. **153**(1): p. 177-190.
108. M. Ohara-Imaizumi, C. Nishiwaki, T. Kikuta, K. Kumakura, Y. Nakamichi, S. Nagamatsu, *Site of Docking and Fusion of Insulin Secretory Granules in Live MIN6 β Cells Analyzed by TAT-conjugated Anti-syntaxin 1 Antibody and Total*. Journal of Biological Chemistry, 2004. **279**(9): p. 8403-8408.
109. Y. Wu, Y. Gu, M. K. Morphew, J. Yao, F. L. Yeh, M. Dong, E. R. Chapman, *All three components of the neuronal SNARE complex contribute to secretory vesicle docking*. J Cell Biol, 2012. **198**(3): p. 323-330.
110. J. Schmoranzer, S. M. Simon, *Role of microtubules in fusion of post-Golgi vesicles to the plasma membrane*. Molecular biology of the cell, 2003. **14**(4): p. 1558-1569.
111. I. Krylyshkina, K. I. Anderson, I. Kaverina, I. Upmann, D. J. Manstein, J. V. Small, D. K. Toomre, *Nanometer targeting of microtubules to focal adhesions*. The Journal of cell biology, 2003. **161**(5): p. 853-859.
112. M. Kaksonen, C. P. Toret, D. G. Drubin, *A modular design for the clathrin-and actin-mediated endocytosis machinery*. Cell, 2005. **123**(2): p. 305-320.
113. C. J. Merrifield, M. E. Feldman, L. Wan, W. Almers., *Imaging actin and dynamin recruitment during invagination of single clathrin-coated pits*. Nature cell biology, 2002. **4**(9): p. 691.
114. R. H. Chow, L. Rüdén, E. Neher, *Delay in vesicle fusion revealed by electrochemical monitoring of single secretory events in adrenal chromaffin cells*. Nature, 1992. **356**(6364): p. 60.
115. G. A. De Toledo, R. Fernandez-Chacon, J. Fernandez, *Release of secretory products during transient vesicle fusion*. Nature, 1993. **363**(6429): p. 554.
116. Z. Zhou, S. Mislér, R. H. Chow, *Rapid fluctuations in transmitter release from single vesicles in bovine adrenal chromaffin cells*. Biophysical Journal, 1996. **70**(3): p. 1543-1552.
117. K. L. Engisch, N. I. Chernevskaya, M. C. Nowycky, *Short-term changes in the Ca²⁺-exocytosis relationship during repetitive pulse protocols in bovine adrenal chromaffin cells*. Journal of Neuroscience, 1997. **17**(23): p. 9010-9025.
118. A. Albillos, G. Dernick, H. Horstmann, W. Almers, G. Alvarez de Toledo, M. Lindau, *The exocytotic event in chromaffin cells revealed by patch amperometry*. Nature, 1997. **389**(6650): p. 509.
119. G. Dernick, L. Gong, L. Tabares, G. Alvarez de Toledo, M. Lindau, *Patch amperometry: high-resolution measurements of single-vesicle fusion and release*. Nature Methods, 2005. **2**(9): p. 699.
120. E. Alés, L. Tabares, J. M. Poyato, V. Valero, M. Lindau, G. Alvarez de Toledo, *High calcium concentrations shift the mode of exocytosis to the kiss-and-run mechanism*. Nature Cell Biology, 1999. **1**(1): p. 40.
121. L. Tabares, M. Lindau, G. A. De Toledo, *Relationship between fusion pore opening and release during mast cell exocytosis studied with patch amperometry*. 2003, Portland Press Limited.

122. L. Gong, I. Hafez, G. Alvarez de Toledo, M. Lindau, *Secretory vesicles membrane area is regulated in tandem with quantal size in chromaffin cells*. Journal of Neuroscience, 2003. **23**(21): p. 7917-7921.
123. A. Oberhauser, I. Robinson, J. Fernandez, *Do caged-Ca²⁺ compounds mimic the physiological stimulus for secretion?* Journal of Physiology-Paris, 1995. **89**(2): p. 71-75.
124. A. F. Oberhauser, I. M. Robinson, J. M. Fernandez, *Simultaneous capacitance and amperometric measurements of exocytosis: a comparison*. Biophysical journal, 1996. **71**(2): p. 1131-1139.
125. G. Dernick, G. A. de Toledo, M. Lindau, *Exocytosis of single chromaffin granules in cell-free inside-out membrane patches*. Nature Cell Biology, 2003. **5**(4): p. 358.
126. U. Becherer, M. Pasche, S. Nofal, D. Hof, U. Matti, J. Rettig, *Quantifying exocytosis by combination of membrane capacitance measurements and total internal reflection fluorescence microscopy in chromaffin cells*. PLoS one, 2007. **2**(6): p. e505.
127. M. Okamoto, M. Ohara-Imaizumi, N. Kubota, S. Hashimoto, K. Eto, T. Kanno, T. Kubota, M. Wakui, R. Nagai, M. Noda, S. Nagamatsu, T. Kadowaki., *Adiponectin induces insulin secretion in vitro and in vivo at a low glucose concentration*. Diabetologia, 2008. **51**(5): p. 827-835.
128. M. Pasche, U. Matti, D. Hof, J. Rettig, U. Becherer, *Docking of LDCVs is modulated by lower intracellular [Ca²⁺] than priming*. PLoS One, 2012. **7**(5): p. e36416.
129. A. Meunier, O. Jouannot, R. Fulcrand, I. Fanget, M. Bretou, E. Karatekin, S. Arbault, M. Guille, F. Darchen, F. Lemaître, C. Amatore, *Coupling amperometry and total internal reflection fluorescence microscopy at ITO surfaces for monitoring exocytosis of single vesicles*. Angewandte Chemie International Edition, 2011. **50**(22): p. 5081-5084.
130. X. Liu, A. Savy, S. Maurin, L. Grimaud, F. Darchen, D. Quinton, E. Labbé, O. Buriez, J. Delacotte, F. Lemaître, M. Guille-Collignon, *A dual functional electroactive and fluorescent probe for coupled measurements of vesicular exocytosis with high spatial and temporal resolution*. Angewandte Chemie, 2017. **129**(9): p. 2406-2410.
131. K. Kisler, B. N. Kim, X. Liu, K. Berberian, Q. Fang, C. J. Mathai, S. Gangopadhyay, K. D. Gillis, M. Lindau, *Transparent electrode materials for simultaneous amperometric detection of exocytosis and fluorescence microscopy*. Journal of biomaterials and nanobiotechnology, 2012. **3**(2A): p. 243.
132. D. M. Omiatek, A. Cans, M. L. Heien, A. G. Ewing, *Analytical approaches to investigate transmitter content and release from single secretory vesicles*. Analytical and bioanalytical chemistry, 2010. **397**(8): p. 3269-3279.
133. W. J. Betz, F. Mao, G. S. Bewick, *Activity-dependent fluorescent staining and destaining of living vertebrate motor nerve terminals*. Journal of Neuroscience, 1992. **12**(2): p. 363-375.
134. W. J. Betz, G. S. Bewick, *Optical analysis of synaptic vesicle recycling at the frog neuromuscular junction*. Science, 1992. **255**(5041): p. 200-203.
135. G. Miesenböck, D. A. De Angelis, J. E. Rothman, *Visualizing secretion and synaptic transmission with pH-sensitive green fluorescent proteins*. Nature, 1998. **394**(6689): p. 192.
136. J. A. Steyer, H. Horstmann, W. Almers, *Transport, docking and exocytosis of single secretory granules in live chromaffin cells*. Nature, 1997. **388**(6641): p. 474.
137. G. Hu, A. Henke, R. J. Karpowicz Jr, M. S. Sonders, F. Farrimond, R. Edwards, D. Sulzer, D. Sames, *New fluorescent substrate enables quantitative and high-throughput examination of vesicular monoamine transporter 2 (VMAT2)*. ACS chemical biology, 2013. **8**(9): p. 1947-1954.

138. M. Lee, N. G. Gubernator, D. Sulzer, D. Sames, *Development of pH-responsive fluorescent false neurotransmitters*. Journal of the American Chemical Society, 2010. **132**(26): p. 8828-8830.
139. N. G. Gubernator, H. Zhang, R. G. W. Staal, E. V. Mosharov, D. B. Pereira, M. Yue, V. Balsanek, P. A. Vadola, B. Mukherjee, R. H. Edwards, D. Sulzer, D. Sames, *Fluorescent false neurotransmitters visualize dopamine release from individual presynaptic terminals*. science, 2009. **324**(5933): p. 1441-1444.

Chapter 2: Fluorescent and electroactive false neurotransmitter partially replaces dopamine in PC12 cell vesicles

2.1 Introduction

Vesicular exocytosis, an intracellular membrane trafficking pathway, is an ubiquitous mechanism of intercellular communication. Membrane docking vesicles fuses with cellular membrane allowing subsequently release of biochemical messengers to the extracellular environment [1]. This vesicle based scheme of release can account for quantal hypothesis [2] and was experimentally suggested by electron microscopy [3]. Even though electron microscopy is able to track vesicle exocytosis, observation of the dynamics of exocytosis with infinitely small quantities of release as well as short time require higher time and spacial resolution. Besides, random occurrence of exocytosis, either in terms of location or moment, obviously increase the difficulties of detection. In order to investigate exocytotic process, our group has established a novel method combining TIRFM with amperometry for imploding advantages from each sole technique [4]. pH-sensitive FFN102 (fluorescent false neurotransmitters), a synthetic analogue of endogeneous neurotransmitter, was employed as dual signal probe and used in coupled monitoring of the secretion from BON N13 cells [5]. Contrary to those traditional pH-sensitive fluorescent probes linked with vesicular luminal proteins or peptide, FFN102 exhibits low steric hindrance and high specificity in proactive staining vesicles by recognition with VMAT (vesicular monoamine transporter) [6, 7]. In the meanwhile, Its phenolic hydroxyl structure endows the active electrochemical property, thus offering the opportunity for analyzing single release kinetics and amount though amperometry.

We report here the loading of FFN102 in PC12 cells, a widely used model in fundamental investigation of exocytosis as well as pharmacological and neurotoxic applications [8]. Indeed, PC12 cells are easy-proliferated cells that can be used straight forward as a secretory cell model with homogeneous physiological characteristics, compared to the chromaffin cells obtained from animal. Dopamine initially stored in the secretory vesicles of PC12 cells ascribed to the vesicle monoamine transporter (VMAT) [9] was used as the electrochemical signal standard. Taking advantage of attractive time resolution of amperometry [10, 11], the impact of FFN102 loading on the kinetics as well as amount of secretory release was fully examined. We show that the internalization of FFN102 in PC12 secretory vesicles leads to the replacement of a fraction of dopamine in secretory vesicles without any other modification of the secretion process.

2.2 Materials and methods

2.2.1 Reagents and solutions

FFN102 was synthesized in the lab according to the procedure reported by Lee et al. [6]. All aqueous solutions were prepared using 18.2 MΩ ultra-pure water (Milli-Q, Millipore). Unless stated, all chemicals were obtained from Sigma-Aldrich and used without further purification.

2.2.2 Cell culture and sample preparation

PC12 cells were purchased from the American Type Culture Collection (Manassas, VA). The cells were maintained in RPMI-1640 media, supplemented with 10% heated inactivated horse serum (Life technologies), 5% heated inactivated fetal bovine serum (Life technologies) and 1% penicillin streptomycin solution (Life technologies) in a 5% CO₂, 100% humidity atmosphere at 37 °C . Cells were grown on cell culture flask with filter cap and were sub-cultured approximately every 4-5 days or when coverage in the flask reached 100%. Throughout the cell culture's lifetime, the medium was refreshed every 2 days.

PC12 cells were migrated to human placenta collagen (Bornstein and Traub type IV, Sigma-Aldrich Co.) coated 50 mm glass bottom dish (MatTek Corporation, Ashland, MA) 48 h before the electrochemical experiment (3×10^5 cells/dish) and incubated within complete growth medium. Cells were fed with 20 μM FFN102 supplemented medium for 1 h before the experiment in order to implement the efficient loading of secretory vesicles.

2.2.3 Fabrication of carbon fiber microelectrode

The carbon fiber working electrodes were fabricated by aspirating 10 μm diameter carbon fibers (Thornel P-55S, Cytec Engineered Materials, Greenville, SC, USA) into glass capillaries (GC120F-10, Clark Electromedical Instruments). Then the capillary was subsequently pulled by a vertical micropipette puller (PB-7, Narishige) into two identical part with short protruding carbon fiber at the tapered end. To limit the working area on the tip, poly-oxyphenylene was electropolymerized onto the surface of protruding carbon fiber as an insulating layer. After that, a drop of mercury was back-filled into the capillary as an electrical contact. The CFE was cut into appropriate length and beveled at an angle of 45° for 5 min on a diamond particle whetstone microgrinder (EG-4, Narishige Co., London, UK). Only the electrodes showing very stable baseline in amperogram were used for single cell detection.

2.2.4 Epi-fluorescence observation

Cell samples were inspected with Invert fluorescent microscope (Observer D1, Carl Zeiss AG).

For tracing the vesicles inside PC12 cell with FFN102 as fluorescent reporter, mercury lamp (LEIS TUNGSELEK TRONIK, Type: LQ-HXP 102-z/100.26B) was employed as light source for excitation and the emission light was filtered by an optical filter (band-pass: D460/40) before recording by EM-CCD.

2.2.5 Single cell experiment

Electrochemical recording of exocytosis from single PC12 cells were performed inside Faraday cage. Before the experiment, the cells were rinsed three times with PBS and were maintained in HEPES physiological saline adjusted to pH 7.4 (150 mM NaCl, 5mM KCl, 1.2 mM MgCl₂, 5 mM Glucose, 10 mM HEPES and 2 mM CaCl₂) throughout the experiment at room temperature. The working electrode was positioned by a micromanipulator (Model MHW-103, Narishige Co., London, UK) in contact with the membrane of independent PC12 cell. A glass microcapillary containing K⁺ stimulant (100 mM KCl, 55mM NaCl, 1.2 mM MgCl₂, 5 mM Glucose, 10 mM HEPES and 2 mM CaCl₂) was positioned by another micromanipulator at about 20 μm away from the cell. All the amperograms were collected from individual cell stimulated by 60s' K⁺ injection. Each cell was detected only once.

During the experiment, the electrode was held at a constant potential vs. a Ag/AgCl reference electrode using a commercially available picopotentiostat (model AMU-110, Radiometer Analytical Instruments, Copenhagen, Denmark). The output was digitized at 40 kHz and the current was recorded as a function of time. In order to avoid surface fouling, the CFE was polished between each successive detection.

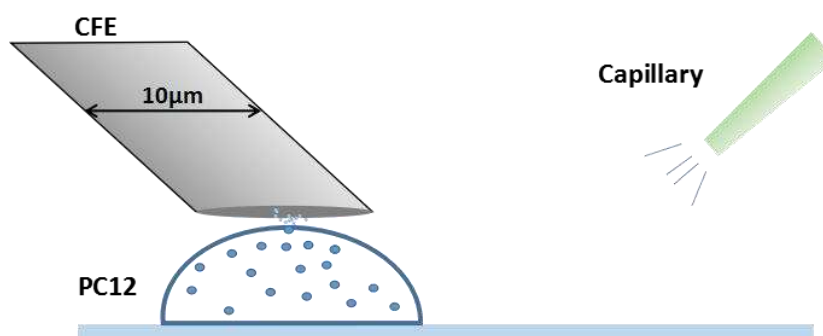


Fig. 2.1 Experiment configuration (“artificial synapse”) in amperometric measurement. Carbon fiber electrode contacting the apical membrane of a single PC12 cell and stimulation capillary injecting KCl solution.

2.2.6 Data analysis

Each amperometric trace recorded during cell secretion was visually inspected and false positive peaks were manually rejected. Double peaks, those with more than one peak (parts overlapping), and those without a smooth decline to the baseline were removed. All the

remained peaks with their maximum current 3 times higher than the fluctuation (0.3 pA) of the baseline current were identified as exocytotic spikes and were collected from amperogram. Feet displaying the typical pre-spike feature with the current higher than 10% and lower than 50% of the maximum peak current were selected for analysis. Each spike characteristics, i.e., the maximum oxidation current I_{\max} (pA), the width at half height t_{FWHM} (ms), the total electrical charge Q (fC) were analyzed by lab-made software. All values were reported as the mean \pm SEM.

2.3 Results and discussion

2.3.1 Cyclic voltammetry of dopamine and FFN102 on CFE

Fig. 2.2 displays cyclic voltammograms of 100 μ M dopamine and 100 μ M FFN102 dissolved in PBS (pH 7.4) recorded by CFE, using Ag/AgCl as a reference electrode. In cyclic voltammetry, 100 mV/s was applied as a scan rate and the scanning potential was ramped between -0.2V and 1.0V. As we can see in the configuration, both dopamine and FFN102 exhibit an irreversible oxidation process, which is presented as the disappearance of centrosymmetric reduction plateau on the reverse cycle. The plateau on the positive scan cycle of dopamine indicates that dopamine's oxidation potential is around 0.6V. While for FFN102, although its complete oxidation showing as plateau is not so obvious, we can still vaguely recognize that the oxidation potential of FFN102 appears around 0.8V. Taking advantage of the oxidation potential distinction between dopamine and FFN102, we designed the next experiment to explore the impact of FFN102 loading on secretory release via selectively detecting dopamine or dopamine in addition with FFN102 through amperometry.

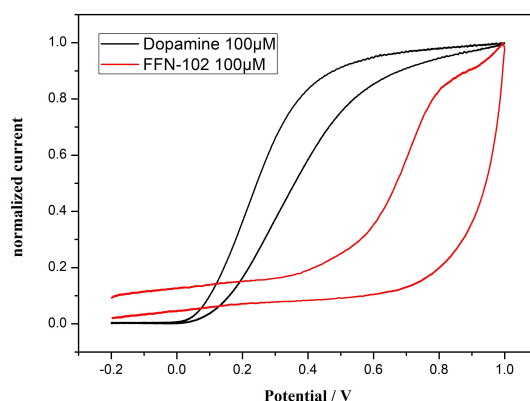


Fig. 2.2 Normalized CVs (obtained by CFE) of dopamine (black) and FFN102 (red) in PBS solution, pH 7.4. Initial potential -0.2V (vs. Ag/AgCl); scan rate 100mV/s. The CVs were all background (PBS)-subtracted.

2.3.2 Cellular uptake and release of FFN102

As shown Fig. 2.4 (left), the morphology of PC12 cell tends to be 2D-stretched instead of 3D-spherical after the attachment. All the individual PC12 cells well-attached on the coverslip, after visual examination, are chosen as proper candidates for electrochemical detection. Employing fluorescent property of FFN102, its gradual loading into the vesicles of PC12 cells was checked with epi-fluorescence. The time-lapse imaging for the dynamic view of FFN102's penetrating process done by Xiaoqing LIU, a previous PhD student, indicated the complete uptake can be accomplished in 60 min [12], see in Fig. 2.3 . In other words, we only need to confirm the loading outcome with 1h incubation of FFN102 before each amperometry test. Fluorescence imaging of pre-incubated cells revealing FFN102 replenished vesicles are presented in Fig. 2.4 (middle). The small bright spots appeared in the inner side of cell are considered as cellular vesicles stained by FFN102, according to the previous research. And the shaded portion in the center of cell is identified as nucleus. In contrast, when the cultured medium was not supplemented with FFN102, cells exhibited no fluorescence. Hence, cells with clear bright spots indicate efficient internalization of FFN102 and can be picked as target cells of our amperometry test. Moreover, we realized that almost all of PC12 cells (>95%) on the coverslip is able to be visualized after FFN102 feeding when excited with mercury lamp, taking the epi-fluorescent image of a growing cluster of PC12 cells as a representative here (Fig. 2.4 right). It definitely shows that FFN102 can be relatively evenly-accumulated into vesicles in PC12 cells, displaying its good biological affinity to PC12 cells.

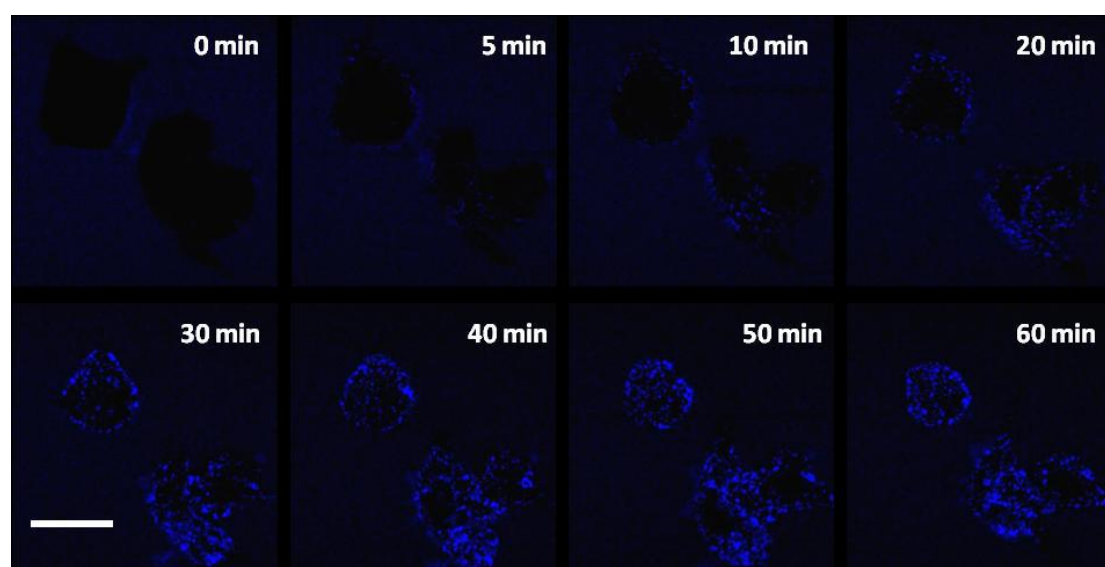


Fig. 2.3 A representative example of the selective uptake of FFN102 by PC12 cells. Sequential images of PC12 cells incubated in 20 μ M 1 from 0 min to 60 min and the small blue spots were their vesicles stained by FFN102; images were acquired by confocal microscope; scale bar: 10 μ m. Figure adapted from reference [12].



Fig. 2.4 One representative group of the uptake of FFN102 by PC12 cells. (Left) PC12 cells observed at bright field; (Middle) epi-fluorescent image of two separated PC12 cells acquired after 1h incubation by 20 μ M FFN102; (Right) the overall uptake consequence.

To ensure the depolarization induced release of FFN102 from PC12 cells during amperometry measurement, the fluorescence from PC12 cells was rechecked after the stimulation with highly concentrated KCl solution. Detected cells exhibited a lower fluorescence level after secretion, consistent with the depletion of FFN102 in vesicle lumen.

2.3.3 Amperometric trace depicting release from single cell

Release of neurotransmitters from PC12 single cells under stimulation was selectively monitored. Amperometric detection of exocytosis was performed with both FFN102 pre-incubated cells and non-incubated cells as control. Typical amperometric trace from stimulated PC12 cell are shown in Fig. 2.5, and the blue arrow in the figure indicates the moment when K⁺ solution was injected by the microinjector. As expected, the spikes started to appear few seconds after the beginning of stimulation. This seconds' delay may due to the diffusion of depolarizer from capillary to target cell. All the secretory release were recorded as a series of amperometric spikes in chronological order of their occurrence. In the trace, each spike was corresponding to an individual exocytotic event from a single secretory vesicle. Attributed to the millisecond time resolution of amperometry, the trace provides kinetic quantitative information about the exocytotic process.

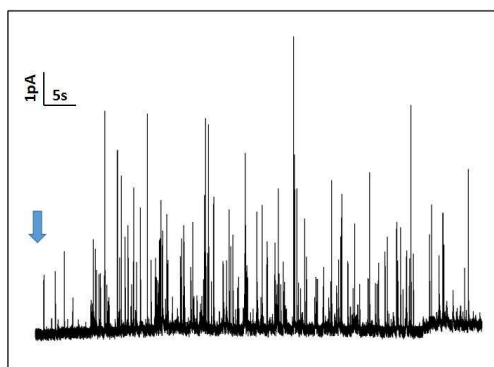


Fig. 2.5 A representative amperometric data from a single PC12 cell. The blue arrow above the trace indicates the application of stimulus(100mM K⁺).

2.3.4 Parameters depicting spike feature

For the analysis of individual amperometric events, the determination of each spike parameters must pursue for accuracy since each spike characteristic contributes to the final statistic result. Rather than relying on some algorithms to designate the beginning and the end of spikes automatically, in our case we applied visual trace examination to precisely extract each single amperometric spike. In the mean time, all the possible spike overlaps, false signals were manually removed. Among spike features discovery, the establishment of spike baseline is one of the most critical step. Baselines were defined by strictly implementing the criterion for each spike: baseline current kept constant for at least 10ms before the raise section of spike and maintained for another 10ms after complete signal decay. All the spikes larger than 1.5 pA (about 3 times the noise of signal, about 0.3 to 0.4 pA in our experiments, extracted from baseline acquisitions at the beginning of the trace) were collected. In a fraction of exocytosis recorded with amperometry, a small increase in current is observed preceding the main current peak (Fig. 2.6). This feature has been termed as foot portion of the spike and related to the release of transmitters through the initial fusion pore. Two categories of this pre-spike feature have been previously described. The first category displays a much gentle and slow current elevating prior to the rapid rising of the spike. The second category constitutes a slight increase of current followed by a stable current showing as a plateau before leading up to the spike. In this work, we took both pre-spike features into consideration for statistic analysis.

The spike parameters for the follow-up analysis were obtained as shown in Fig. 2.6. For the depicting main body of the spike, parameters include the maximal current of the spike i_{max} ,

the rise time t_{rise} , defined as the time counted from 25% current of the maximum to 75% current of the maximum on the ascending part of the spike, the half spike width $t_{1/2}$ defined as the time interval of exocytosis at half of its magnitude, the fall time t_{fall} , defined as the time separating 75% of the maximum from 25% of the maximum on the descending part, and the charge Q calculated as current integrated with time under the spike which intuitively demonstrates the quantity of molecules released according to Faraday's law. For the feet, the parameters are the foot current i_{foot} defined as the final current measured at the terminal of the foot portion, the foot duration t_{foot} , and the foot charge Q_{foot} representing as the area under the curve of foot portion. All the foot portion were identified under visual examination.

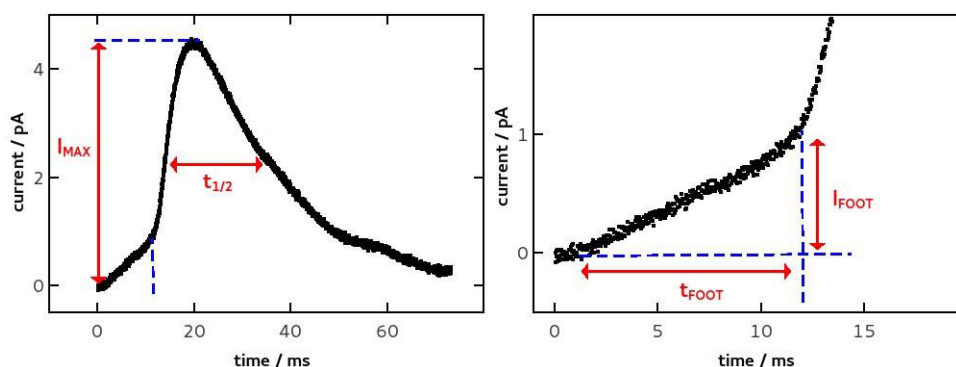


Fig. 2.6 Left: typical recorded spike displaying a prespike foot with the representation of maximum oxidation current I_{max} , duration at half peak height $t_{1/2}$; the released charge Q being the area under the curve. Right: enlarged view of the prespike foot with the representation of the foot current I_{foot} manually determined through time t_{foot} .

2.3.5 Amperometric data analysis

According to the result obtained by cyclic voltammetry, the oxidation potential of dopamine and FFN102 are 0.6 V and 0.8 V. To ensure that all the detected molecules released from cell could be oxidized transiently, amperometric traces were recorded maintaining the CFE potential at 650 mV or 900 mV. Indeed, these potential values were also reported to allow fast oxidation of dopamine and FFN102 at CFE [13]. Amperometric detection of exocytosis was performed with both FFN102 pre-incubated cells and control cells. Additionally, exocytosis from PC12 cells without FFN102 treatment were also monitored at both 0.65 V and 0.9 V, respectively, as a control to eliminate the interfere induced by detection potential.

2.3.5.1 Exocytotic frequency during secretion

Firstly, we inspected the variation of cell state especially their exocytosis occurrence caused

by FFN102 loading. For counting the number of exocytotic events from each cell, either single amperometric spikes or optically distinguished overlapping spikes were included to reflect the entire process of secretion during stimulation. Time computing was starting off from the appearance of first spike as effective response to external stimulant on amperometric trace.

Fig. 2.7(top) represented the average number of exocytotic events accumulated with time during stimulation under 650 mV before and after loading of FFN102. The error bar displayed the standard error of the mean of the collected data. As we all know that under 650mV, merely dopamine discharged from secretory vesicles is selectively oxidized. In other words, the accumulated frequency shown in this configuration only related to exocytosis from dopamine-contained vesicles. Therefore, comparing the two curves, we easily realize that manipulation of loading FFN102 slightly enhance the occurrence of exocytosis concerned with dopamine but the rate was still comparable to those unloaded PC12 cells. Then the exocytotic behavior was detected with higher potential - 900mV, which can record the oxidation of both dopamine and FFN102. For cells with no internalization of FFN102, the secretory events we observed was only related to dopamine release. While for FFN102 treated cells, higher monitoring potential revealed the exocytotic activity of both dopamine-included and FFN102-included vesicles. The comparison between the two curves in the Fig. 2.7(bottom) reminded us that the occurrence rate of exocytosis related to both dopamine and FFN102 was a bit higher than that of merely dopamine-related exocytosis. Comparison of this two configurations, the similar growth magnitude of exocytosis frequency concerned about dopamine, dopamine and FFN102, respectively, provided us powerful evidence that FFN102 entered dopamine-stored secretory vesicles. The non-exaggerated enhancement of exocytotic occurrence after FFN102 incubation can be rationally ascribed to the refreshment of growth medium for FFN102 feeding.

To further verify that the exerted detection potential has no influence on exocytosis properties, we investigated the frequency of exocytosis from unloaded PC12 cells. As we see in Fig. 2.8, the trend of number of events accumulated as a function of time is more or less the same when detected under different potential, suggesting the irrelevance between detected potential and the occurrence of exocytosis. Moreover, this result illustrates that the divergence of exocytosis frequency concerned dopamine release appeared in the top and bottom configuration of Fig. 2.7 may simply lead by distinct cell generations.

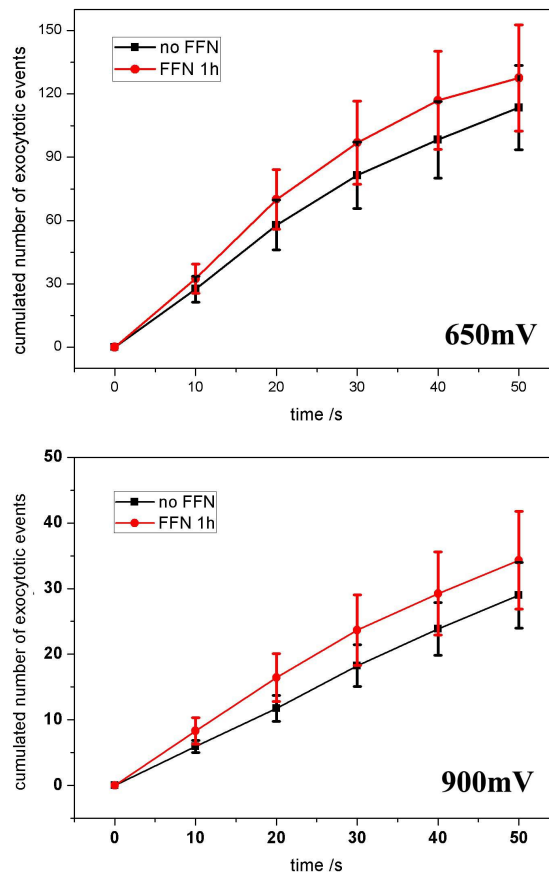


Fig. 2.7 Cumulated exocytotic occurrence from PC12 cell lines with and without FFN102 incubation under different potential (650mV (top); 900mV (bottom)). The accumulated number of events is revealed as the time-course of the experiments and the error bar represents the standard error of the mean. The spikes were counted from the amperograms from 16 individual cells in each experiment condition.

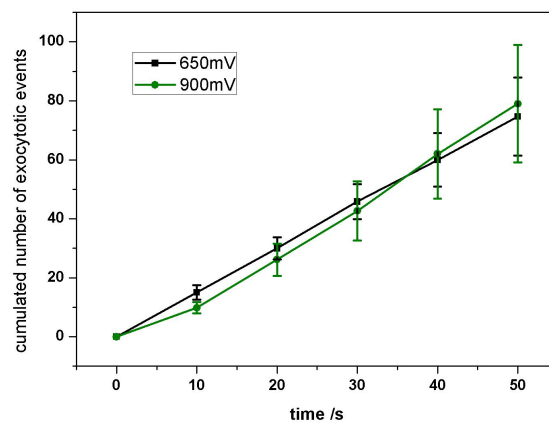


Fig. 2.8 Exocytotic occurrence measured by amperometry from the same generation of PC12 cell lines under different potential (650mV , 900mV) as a control. The spikes were counted from the amperograms from 6 individual cells in each experiment condition.

2.3.5.2 Exploration of kinetics of exocytotic release

Albeit we have already figured out that the applied potential does not vary the occurrence of exocytosis, there is still another query waiting for answer, that is, whether the high applied potential can influence the process of secretory release in terms of single exocytotic event. To unveil the doubt, we inspected the mean value of each spike parameters obtained from PC12 cells in the control group (non-FFN102 supplement) within the same generation under different potential. The spikes was analyzed as described above, and the corresponding exocytotic parameters are summarized in Table 2.1. The five key parameters: t_{rise} , t_{fall} , $t_{1/2}$, Q , and I_{max} represent the general morphology of the spike, thus briefly displaying the kinetics of exocytosis. Comparing the two groups of parameters, all the features of spike nearly kept consistent when a higher potential applied shift from 650mV to 900mV. Hence, it is easily summarized that the detection potential has approximately no impact on the process of secretory release.

Table. 2.1 Spike parameters obtained from K^+ stimulated PC12 cells under different potentials as a control. Reported values are mean \pm s.e.m

	t_{rise} / ms	t_{fall} / ms	$t_{1/2}$ / ms	Q / fC	I_{max} / pA
650mV (6cells, 346spikes)	6.12 ± 0.15	15.12 ± 0.25	21.25 ± 0.36	75.69 ± 2.79	2.75 ± 0.09
900mV (6cells, 384spikes)	6.19 ± 0.14	14.93 ± 0.25	21.21 ± 0.34	75.40 ± 2.42	2.85 ± 0.08

Next, we examined the main experimental groups. The mean value of each spike parameters from these group is shown in Table 2.2 . As it's confirmed that the applied potential itself has no impact on kinetics of secretory release, the discrepancy of parameter value reflected on the two groups without FFN102 incubation can only be caused by the varied generation of cells. In order to get rid of this discrepancy, normalization was applied to the value of each parameter recorded from the non FFN102-incubated cells in the two groups. And the values of parameter collected from FFN102 exposed samples were displayed as a ratio using corresponding control as reference (Fig. 2.9 and Fig. 2.10). Judging on the frequency of exocytosis, we have verified that FFN102 is internalized into dopamine-contained vesicles. Therefore, the obvious charge diminish from the selective oxidation of dopamine compared with black and red columns must be owing to the partial substitution of dopamine with FFN102. Interestingly, the oxidation of both dopamine and FFN102 after FFN102 feeding shows a broader and flatter spike in comparison with that recorded from the non FFN102-incubated cells, specific performing as larger value of t_{rise} , t_{fall} , and $t_{1/2}$, but lower I_{max} (orange column vs. Black column). The probable explanation for the morphology change is that the diffusion rate of FFN102 from vesicle lumen to the extracellular solution is smaller

than that of dopamine. Furthermore, it's worth noting that the charge Q integrated with time under the spike preserved its value after FFN102's loading. It indicates that the average amount of molecules released from vesicles is not altered by FFN102 and directly proves that the mechanism of FFN102's uptake is to partially replace endogeneous dopamine instead of expanding the vesicle capacity. The shortened time-course of current rising as well as falling with respect to dopamine oxidation after FFN102 incubation may possible due to the replacement of dopamine by newly-came FFN102 in the fast-release domain.

Table. 2.2 Spike parameters obtained from K⁺ stimulated PC12 cells: pre-incubation conditions "FFN102", CFE potential E_{CFE}, number of analyzed spikes N, rising time of spike t_{rise}, falling time of spike t_{fall}, duration at half peak heigth t_{1/2}, detected charge Q, and peak current I_{max}. Secretion was monitored at 16 single cells in each experimental condition. Reported values are mean ±s.e.m

FFN102	E _{CFE} / mV	N	t _{rise} / ms	t _{fall} / ms	t _{1/2} / ms	Q / fC	I _{max} / pA
-	650	393	6.46 ± 0.10	14.76 ± 0.17	21.21 ± 0.21	63.58 ± 1.80	2.45 ± 0.06
20 μM 1h	650	434	5.62 ± 0.08	13.29 ± 0.15	18.91 ± 0.18	55.86 ± 1.66	2.33 ± 0.06
-	900	315	4.70 ± 0.20	13.98 ± 0.28	18.68 ± 0.44	66.98 ± 2.11	2.82 ± 0.08
20 μM 1h	900	379	5.22 ± 0.16	14.56 ± 0.24	19.78 ± 0.36	67.08 ± 2.23	2.75 ± 0.10

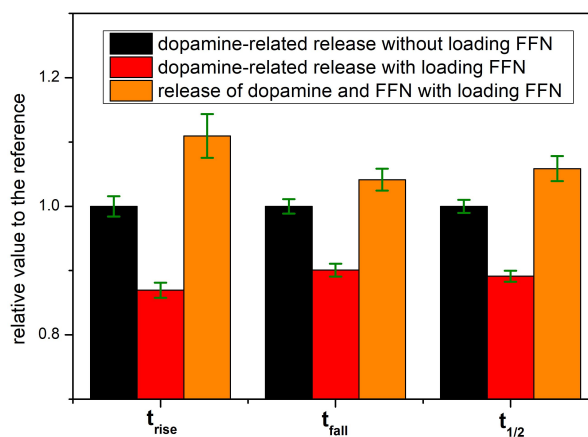


Fig. 2.9 Ratio value of t_{rise}, t_{fall} and t_{1/2} with control cells as reference. Bars represent the relative mean ±SEM for the different experimental condition.

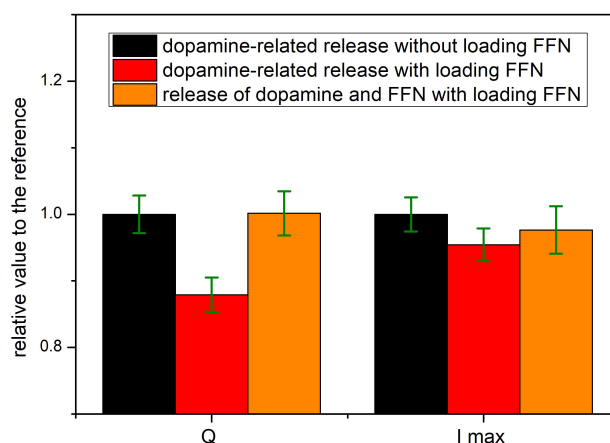


Fig. 2.10 Ratio value of Q and I_{max} with control cells as reference. Bars represent the relative mean \pm SEM for the different experimental condition.

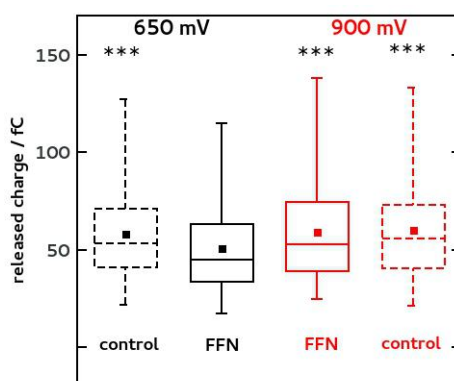


Fig. 2.11 Distribution of detected charge during secretion. In black: selective detection of dopamine (650mV vs Ag/AgCl). In red: detection of dopamine and FFN102 (900mV vs Ag/AgCl). solid lines: pre-incubation with FFN102. Dashed line : controls. *** $p < 10^{-5}$; p -values obtained from Mann-Whitney-Wilcoxon test (R software).

Fig. 2.11 specially shows the features of the detected charge distributions. The median of the detected charges from control cells (CFE potential held at 650 mV or 900 mV) and from treated cells with CFE held at 900mV were not significantly different between each other (p -values > 0.3 , Mann-Whitney-Wilcoxon test). The replacement ratio of dopamine by FFN102 can be estimated as ca. 12% mol. This value is determined assuming that oxidation process involves two electrons for the FFN102 molecule same as for dopamine and that diffusion coefficients are comparable. These assumptions seem reasonable owing to the close structure of the two molecules: size and nature of the oxidized group. The concentration of the internalized FFN102 can be estimated considering a vesicle diameter of

ca. 160-200 nm [14, 15] and a released fraction 40%-60% of transmitters content [16]. The uptake of FFN102 leads to the internalization of ca. 60×10^3 molecules per vesicles with the corresponding concentration, 15-45 μM , higher than the incubation concentration.

2.3.5.3 Preliminary glimpse on vesicular capacity

To further study the impact on secretory vesicles initiated by FFN102's loading, we analyzed the statistical logarithmic distribution of the charge. Fig. 2.12 shows the histogram of the charge per exocytotic event. And the green curves display the Gauss Fit results. Since the charge is relative to the amount of detected molecules released from the vesicle according to Faraday's law, legitimately assuming that released molecules occupy the constant part of total number of molecules stored in the vesicle lumen, we can hope to glimpse primarily the variation of vesicular capacity caused by the passive loading. The similar peak position of Gauss Fit Curves from Fig. 2.12E and Fig. 2.12F in the control group evidences that PC12 cells maintain their vesicular volume when different potentials were applied. Taking this conclusion as a prerequisite, we inspected the logarithmic distribution of the charge from the other two experimental groups. Fig. 2.12A and Fig. 2.12B indicate no drastic difference on the shape of the curve which represents the trend of distribution of dopamine in all the detected vesicles from FFN102 loaded PC12 cells is comparable to that from PC12 cells without loading. When taking the signal of FFN102 into consideration, as shown in Fig. 2.12D, the analogous curve (vs. Fig. 2.12C) points out a rather similar distribution of charge, both the morphology and the position, compared to those non-loaded PC12 cells. It implies almost the same vesicular volume distribution were owned in between non-loaded PC12 cells and FFN102 loaded PC12 cells. The deviation of peak position in Fig. 2.12B compared to that in Fig. 2.12A and the similar of the charge at the zenith of the peak in Fig. 2.12A, C and D reflect again that portion of endogeneous dopamine was replaced by FFN102.

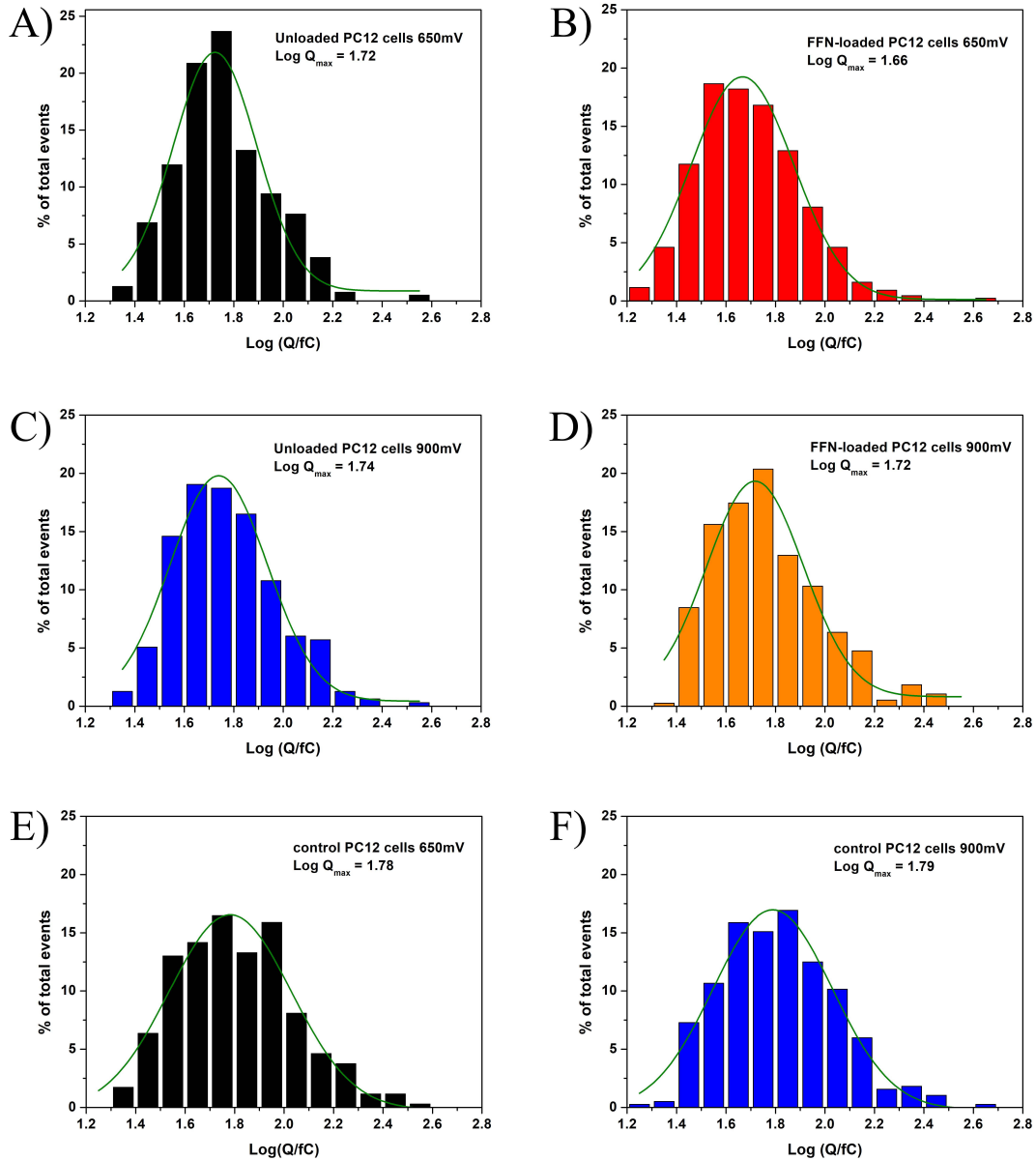


Fig. 2.12 Statistical logarithmic distributions of the charge Q (fC) obtained from each exocytotic spike under condition described in the scheme: Group1: secretory release from A) unloaded PC12 and B) FFN102-loaded PC12 detected with 650mV; Group2: secretory release from C) unloaded PC12 and D) FFN-loaded PC12 recorded with 900mV; Group3 as a control: secretory release from non-loading PC12 detected under E) 650 mV and F) 900 mV.

2.3.5.4 Early stage of fusion pore opening

Among all the exocytotic events recorded via amperometric detection, slow increase of current followed by a quick enhancement to the maximum was monitored within a small fraction. This slow increase of current appeared close to the main spike is called the foot portion and has been reported as a representation of neurotransmitters leaked through the fusion pore formed at its early stage [17]. Thus the PSF can directly reflect the formation of fusion pore. Three features of the foot portion are traditionally considered: the lifetime of

the foot (t_{foot}) is a stability indicator of the first stage of fusion pore opening; the current of the foot (I_{foot}) shows the transient flux of molecules through the pore; while the charge of the foot (Q_{foot}) is dependent on the accumulated amount of molecules released via the pore during its lifetime.

Table. 2.3 Parameters of PSF obtained from three groups of amperometry detection in parallel. Group1: PSF from unloaded PC12 and FFN102-loaded PC12 under 650 mV (selectively dopamine detected); Group2: PSF from unloaded PC12 and FFN102-loaded PC12 under 900 mV (dopamine and FFN102 detected); Group3 as a control: PSF from non-loading PC12 detected under 650 mV and 900 mV. Foot incidences were calculated as ratio values of the number of events exhibiting a well defined foot divided by the total number of clean, non-overlapping amperometric events. The data was presented as mean with standard error of the mean as error bar.

	Detect Condition	$t_{\text{foot}}/\text{ms}$	$I_{\text{foot}}/\text{pA}$	$Q_{\text{foot}}/\text{fC}$	PSF%
Group1	“null” 650mV	7.09 ± 0.38	0.63 ± 0.04	1.98 ± 0.31	19.43 ± 2.64
	FFN102 650mV	6.37 ± 0.32	0.48 ± 0.02	1.28 ± 0.11	19.20 ± 1.78
Group2	“null” 900mV	7.37 ± 0.59	0.67 ± 0.05	3.17 ± 0.65	20.14 ± 3.15
	FFN102 900mV	7.80 ± 0.48	0.70 ± 0.05	2.80 ± 0.41	20.73 ± 2.44
Control	“null” 650mV	9.05 ± 0.59	0.66 ± 0.04	2.65 ± 0.32	20.31 ± 5.03
	“null” 900mV	8.73 ± 0.72	0.66 ± 0.03	2.74 ± 0.45	24.84 ± 4.34

The prespike feet with current foot values I_{foot} from 10% up to 50% of the maximum peak current were selected for analysis as depicted. The observed frequency ratio of 20% of spikes exhibiting a foot is lower than the 30% value reported by Sombers et al. [18] and similar to the one reported at chromaffin cells [19]. It is presumably related to the shape of the typical spikes recorded at our PC12 cells varied from the shape reported for some other PC12 cell line [20, 21]. The parameters of pre-spike feature (PSF) were showed as mean value with S.E.M as error bar in Table 2.3. Two sets of typical parameters from the control group are quite similar, indicating an equivalent formation of fusion pore under different potential. Besides, the incidence of PSF are also comparable. Therefore, we can deduce that applied potential does not affect the fusion pore opening at the very beginning period. Staring back to the data of experimental group, in agreement with the phenomenon we observed during whole release process, the representative parameters of PSF are found to slightly decrease when detected dopamine after FFN102 incubation, shown in Table. 2.3 Group 1. While paying attention to the Group 2 detecting both dopamine and FFN102, the value of each parameter is almost restored to the level of unloaded PC12. The decrease of signal from dopamine and the recovery of signal from both molecules recertificate the replacement mechanism of FFN102’s loading. Moreover, the remaining shape of pre-spike portion after

the loading of FFN102 suggests the consistent process of secretory release through initial fusion pore compared to unloaded PC12. Plus with the maintenance of pre-spike occurrence rate of the two sets in each group, we believe that loading of FFN102 causes no divergence on the nature process of fusion pore opening.

Table. 2.4 Pre-incubation conditions "FFN102", detected released charge Q, detected foot charge Q_{foot}. CFE potential was held at 650 mV. Secretion was monitored at 16 single cells in each experimental condition. Reported values are mean \pm s.e.m

FFN102	Q/ fC	Q _{foot} / fC
-	78.1 \pm 3.8	1.97 \pm 0.31
20 μ M 1h	70.9 \pm 2.9	1.28 \pm 0.11

Interestingly, when cells were pre-incubated with FFN102, FFN102 has an enhanced contribution to the released charge through the initial fusion pore. Indeed, FFN102 replaces ca. 35% of the dopamine during foot duration whereas this ratio falls to 12% during the whole spike duration. The table presents the values of the charges related to spikes exhibiting foot portion. The averaged released charge is significantly higher for spikes featuring a foot (78.1 \pm 3.8 fC) than for spikes without foot (63.6 \pm 1.8 fC). This trend has already been reported for L-DOPA treated chromaffin cells [22] and PC12 cells [18]. The loading of FFN102 in secretory vesicles of PC12 cells is thus analog to the L-DOPA one. This uptake is consistent with the enrichment of a fast diffusion compartment in the vesicle (so called "halo") [19, 23] and supports a recently introduced model relying on highly compacted chromogranin nanodomains floated within a much loose bulk [24]. This conclusion also echoes with our previous speculation that short lifetime of dopamine release after FFN102 supplement is ascribed to the highly occurrence of dopamine replacement in fast-release domain.

2.4 Conclusion and perspective

In this chapter, we mainly discuss about the biological effect on exocytotic process induced by loading of FFN102 using PC12 cell line as our cell model. Through the current trace obtained by amperometry, we concluded that the uptake of FFN102 leads to the partial replacement of dopamine in secretory vesicles. Besides, the incidence and the kinetics for exocytotic vesicular release also maintain after the incubation of this signal probe. The non-intrusive mode of loading for cell activity promotes FFN102 as a rather precious probe in biological investigation. The partial replacement of dopamine could allow to monitor exocytotic events through electrochemical detection of dopamine and this approach could

be of interest to overcome the possible shortcoming of the high oxidation potential of FFN. In the meanwhile, the location of exocytosis as well as the secretory release process of monoamines can all be visualized with FFN102 enrichment inside vesicles as a fluorescent probe. Furthermore, it's also worth noting that FFN102 represented an overrelease pattern at the beginning of fusion pore opening, indicating the storage in fast diffusion compartment of the vesicles.

Notes: Based on this chapter, we have published a relative article entitled: Electroactive fluorescent false neurotransmitter FFN102 partially replaces dopamine in PC12 cell vesicles [25].

2.5 Reference

1. Z. P. Pang, T. C. Südhof, *Cell biology of Ca²⁺-triggered exocytosis*. Current opinion in cell biology, 2010. **22**(4): p. 496-505.
2. J. Del Castillo, B. Katz, *Local activity at a depolarized nerve-muscle junction*. The Journal of physiology, 1955. **128**(2): p. 396-411.
3. J. D. Robertson, *The ultrastructure of a reptilian myoneural junction*. The Journal of Cell Biology, 1956. **2**(4): p. 381-394.
4. A. Meunier, O. Jouannot, R. Fulcrand, I. Fanget, M. Bretou, E. Karatekin, S. Arbault, M. Guille, F. Darchen, F. Lemaître, C. Amatore, *Coupling amperometry and total internal reflection fluorescence microscopy at ITO surfaces for monitoring exocytosis of single vesicles*. Angewandte Chemie International Edition, 2011. **50**(22): p. 5081-5084.
5. X. Liu, A. Savy, S. Maurin, L. Grimaud, F. Darchen, D. Quinton, E. Labbé, O. Buriez, J. Delacotte, F. Lemaître, M. Guille-Collignon, *A dual functional electroactive and fluorescent probe for coupled measurements of vesicular exocytosis with high spatial and temporal resolution*. Angewandte Chemie, 2017. **129**(9): p. 2406-2410.
6. M. Lee, N. G. Gubernator, D. Sulzer, D. Sames, *Development of pH-responsive fluorescent false neurotransmitters*. Journal of the American Chemical Society, 2010. **132**(26): p. 8828-8830.
7. N. G. Gubernator, H. Zhang, R. G. W. Staal, E. V. Mosharov, D. B. Pereira, M. Yue, V. Balsanek, P. A. Vadola, B. Mukherjee, R. H. Edwards, D. Sulzer, D. Sames, *Fluorescent false neurotransmitters visualize dopamine release from individual presynaptic terminals*. science, 2009. **324**(5933): p. 1441-1444.
8. R. Westerink, A. Ewing, *The PC12 cell as model for neurosecretion*. Acta Physiologica, 2008. **192**(2): p. 273-285.
9. J. P. Henry, C. Sagné, C. Bedet, B. Gasnier, *The vesicular monoamine transporter: from chromaffin granule to brain*. Neurochemistry international, 1998. **32**(3): p. 227-246.
10. R. M. Wightman, J. A. Jankowski, R. T. Kennedy, K. T. Kawagoe, T. J. Schroeder, D. J. Leszczyszyn, J. A. Near, E. J. Diliberto Jr, O. H. Viveros., *Temporally resolved catecholamine spikes correspond to single vesicle release from individual chromaffin cells*. Proceedings of the National Academy of Sciences, 1991. **88**(23): p. 10754-10758.
11. T. J. Schroeder, J. A. Jankowski, K. T. Kawagoe, R. M. Wightman, C. Lefrou, C. Amatore, *Analysis of diffusional broadening of vesicular packets of catecholamines released from biological cells during exocytosis*. Analytical chemistry, 1992. **64**(24): p. 3077-3083.

12. X. Liu, *More transparency in bioanalysis of exocytosis: application of fluorescent false neurotransmitters in coupling methodology of electrochemistry with fluorescence microscopy at ITO microelectrodes*. 2016, Paris 6.
13. C. Amatore, S. Arbault, M. Guille, F. Lemaître, *Electrochemical monitoring of single cell secretion: vesicular exocytosis and oxidative stress*. Chemical reviews, 2008. **108**(7): p. 2585-2621.
14. D. Schubert, M. LaCorbiere, F. G. Klier, J. H. Steinbach, *The modulation of neurotransmitter synthesis by steroid hormones and insulin*. Brain research, 1980. **190**(1): p. 67-79.
15. T. Kishimoto, T. Liu, H. Hatakeyama, T. Nemoto, N. Takahashi, H. Kasai, *Sequential compound exocytosis of large dense-core vesicles in PC12 cells studied with TEPIQ (two-photon extracellular polar-tracer imaging-based quantification) analysis*. The Journal of physiology, 2005. **568**(3): p. 905-915.
16. D. M. Omiatek, Y. Dong, M. L. Heien, A. G. Ewing, *Only a fraction of quantal content is released during exocytosis as revealed by electrochemical cytometry of secretory vesicles*. ACS chemical neuroscience, 2010. **1**(3): p. 234-245.
17. R. H. Chow, L. Rüdén, E. Neher, *Delay in vesicle fusion revealed by electrochemical monitoring of single secretory events in adrenal chromaffin cells*. Nature, 1992. **356**(6364): p. 60.
18. L. A. Sombers, H. J. Hanchar, T. L. Colliver, N. Wittenberg, A. Cans, S. Arbault, C. Amatore and A. G. Ewing, *The effects of vesicular volume on secretion through the fusion pore in exocytotic release from PC12 cells*. Journal of Neuroscience, 2004. **24**(2): p. 303-309.
19. C. Amatore, S. Arbault, I. Bonifas, M. Guille, F. Lemaître, Y. Verchier, *Relationship between amperometric pre-spike feet and secretion granule composition in chromaffin cells: an overview*. Biophysical chemistry, 2007. **129**(2-3): p. 181-189.
20. R. I. Trouillon, A. G. Ewing, *Single cell amperometry reveals glycocalyx hinders the release of neurotransmitters during exocytosis*. Analytical chemistry, 2013. **85**(9): p. 4822-4828.
21. R. I. Trouillon, A. G. Ewing, *Actin controls the vesicular fraction of dopamine released during extended kiss and run exocytosis*. ACS chemical biology, 2014. **9**(3): p. 812-820.
22. C. Amatore, S. Arbault, I. Bonifas, Y. Bouret, M. Erard, A. G. Ewing, L. A. Sombers, *Correlation between vesicle quantal size and fusion pore release in chromaffin cell exocytosis*. Biophysical journal, 2005. **88**(6): p. 4411-4420.
23. L. Sombers, M. Maxson, A. Ewing, *Loaded dopamine is preferentially stored in the halo portion of PC12 cell dense core vesicles*. Journal of neurochemistry, 2005. **93**(5): p. 1122-1131.
24. A. Oleinick, I. Svir, and C. Amatore, *'Full fusion' is not ineluctable during vesicular exocytosis of neurotransmitters by endocrine cells*. Proc. R. Soc. A, 2017. **473**(2197): p. 20160684.
25. L. Hu, A. Savy, L. Grimaud, M. Guille-Collignon, F. Lemaître, C. Amatore, J. Delacotte, *Electroactive fluorescent false neurotransmitter FFN102 partially replaces dopamine in PC12 cell vesicles*. Biophysical Chemistry, 2018.

Chapter 3: Exploration of myosin II 's role in regulation of fusion pore opening

3.1 Introduction

Study of vesicular exocytosis has attracted more and more attention over the past 25 years because of its great significance in cell interactions. During exocytosis, the expansion of fusion pore opens the channel for biochemical molecules escaping to the extracellular space [1, 2]. It's the highly regulated secretion of messengers that modulates various activities in multi-cellular organisms. Studies suggested that the release of hormones with large molecular weight was usually observed with complete insertion of vesicle construction in the cellular membrane via spacious "omega" figure [3, 4]. Other studies showed that the initially formed tiny fusion pore allowed the secretory release of some small neurotransmitters such as dopamine [5, 6]. It is obvious that fusion pore is crucial in regulating secretory release, either in terms of its content or its temporal and releasing behaviour. Hence, exploring the dimension of fusion pore and figuring out mechanisms of fusion pore evolution are of outstanding importance.

Myosin II is a well known molecular motor associated with actin filaments. Recent studies have unveiled that myosin II is responsible for fusion pore dynamics via regulating relative motion of cortical actin filaments [7]. For example, Ryo et al. clarified that myosin II prolonged luminal proteins' release in PC12 cells by slowing down fusion pore closure [8]. This work first related the dynamics of fusion pore to the activity of myosin II using PC12 cell as investigated cell model. However, due to the intrinsic limitation of acquisition rate from camera, the temporal resolution of sequential image is not sufficient to monitor the transformation of fusion pore. In addition, on account of the imaging principle of TIRF as well as light scattering, quantitative tracking of fusion pore dimension cannot be fulfilled with fluorescence recording. Indeed, fusion pore evolution has been more widely investigated by electrochemical techniques including patch clamp and amperometry at single cell level. Patch clamp measurement records the growth of cellular membrane area caused by fusion pore variation via monitoring membrane electrical capacitance. With respect to the fast response of patch clamp, the occurrence time of fusion pore formation as well as the relative membrane surface supplement caused by integration of vesicular membrane and cellular membrane are easily obtained. Whereas amperometry implies the general fusion pore development process via monitoring flux of catecholamine release. Experimental evidence from patch clamp has been accumulated suggesting a role of myosin II in promoting the

dilation of fusion pore from chromaffin cells [9, 10]. Amperometric data adds to a growing body of evidence showing that myosin II contributes to facilitate the fusion pore opening in chromaffin cells with fast vesicle cargo discharge. However, so far capturing the actual dimension of fusion pore still encountered some challenge. Extracting the fusion pore development kinetics motivated by myosin II can only rely on simulations.

Recently, a theoretical model has been proposed and successfully applied to translate the kinetics of release to the dynamics of fusion pore at single vesicle level in chromaffin cells [11]. To comprehend the role of myosin II in regulation of fusion pore dilation during exocytosis in PC12 cells, we recorded the release of dopamine from each exocytotic events via amperometry with pharmacological perturbation of myosin II. Y27632 as a ROCK inhibitor was used to restrain the signaling cascade that drives phosphorylation and activation of myosin II [12]. Considering the analogous structure as well as the exocytotic behaviour of dense core vesicles in chromaffin cells and PC12 cells, the fusion pore radius was reconstructed by mechanically applying the same simulation. We show that myosin II extends the duration of dopamine release by slowing down the expansion of fusion pore.

3.2 Materials and methods

3.2.1 Cell culture and sample preparation

PC-12 cells were purchased from the American Type Culture Collection (Manassas, VA). Cells were maintained in RPMI-1640 complete growth media with 10% heated inactivated horse serum (Life technologies), 5% heated inactivated fetal bovine serum (Life technologies) and 1% penicillin streptomycin solution (Life technologies) in a 5% CO₂, 100% humidity atmosphere at 37 °C . Cells were grown in cell culture flask and were sub-cultured approximately every 4-5 days. Throughout the cell culture's lifetime, the medium was refreshed every 2 days. 48h before the electrochemical experiment, PC-12 cells were sub-cultured on human placenta collagen (Bornstein and Traub type IV, Sigma-Aldrich Co.) coated 50 mm glass bottom dish (MatTek Corporation, Ashland, MA). All the complete growth medium was filtered by 0.22 µm filtration membrane before use.

3.2.2 Single cell experiment

Y27632 dihydrochloride purchased from Sigma Aldrich was diluted to 2 mM with distilled water and stored in 4 °C . Cell sample was rinsed three times with PBS and maintained in HEPES physiological saline (150 mM NaCl, 5 mM KCl, 1.2 mM MgCl₂, 5 mM Glucose, 10 mM HEPES and 2 mM CaCl₂) during experiment at room temperature. The solution was prepared with distilled water and adjusted to pH 7.4. For the pharmacological inhibition of myosin II,

Y27632 was further diluted to 10 μM with corresponding buffer solution and preincubated with cells 10 min before amperometry test.

Micro-CFE was fabricated and polished in the same way as mentioned in Chapter 2. It was positioned by a micromanipulator (Model MHW-103, Narishige Co., London, UK) with 45° to gently touch the membrane of an independent cell to mimic as an artificial synapse. During the experiment, a constant potential 650 mV was applied on CFE vs. Ag/AgCl reference electrode using a commercially available picopotentiostat (model AMU-110, Radiometer Analytical Instruments, Copenhagen, Denmark). The output was digitized at 40 kHz and the current was recorded as time-course. Electrochemical recording was performed on an inverted microscope (Observer D1, Carl Zeiss AG) inside Faraday cage. For triggering exocytosis from PC-12 cells, a glass microcapillary containing KCl stimulant(100 mM KCl, 55 mM NaCl, 1.2 mM MgCl_2 , 5 mM Glucose, 10 mM HEPES and 2 mM CaCl_2) was positioned by another micromanipulator at about 20 μm away from the cell. All the amperograms were collected from individual cell stimulated within 60s. Each cell was detected only one time.

3.2.3 Cell viability test

The LIVE/DEAD® Viability/Cytotoxicity Kit purchased from ThermoFisher was applied for discriminating live cells against dead ones. Cell sample was rinsed three times with PBS and incubated in HEPES physiological saline. Cells were preincubated with Y27632 10 μM 30 min before membrane staining while in the control group cells were maintained in pure HEPES buffer in the same period of time. After that, calcein-AM and ethidium homodimer-1 were added into samples to obtain the final concentration 2 μM and 4 μM , respectively. Samples were incubated in a 5% CO_2 , 100% humidity atmosphere at 37 °C for another 1h and then examined with inverted fluorescent microscope.

3.2.4 Electrochemical signal filter

Fig. 3.1C represents part of initial amperogram obtained by potentiostat AMU-110 and e-corder 401 system associated with eDAQ_Chart software. Even with the Faraday cage, periodic fluctuations still appeared on the current baseline. To figure out the origin of noise, Fourier transform was applied to decompose original signal as a function of time into the frequencies. As we can see from Fig. 3.1A, an obvious peak emerges at 50 Hz (partial enlargement in Fig. 3.1B) accompanying with several small peaks with frequency higher than 250 Hz. 50 Hz is exactly the frequency of AC, thus it is identified as the main source of the background noise. In addition, according to the physiological characteristics of our cells, exocytosis is not able to be occurred with frequency higher than 250Hz under stimulation.

Therefore, we consider those high frequency oscillation as uncertain interference signal. To purify the current recorded, we artificially removed the sharp peak at 50Hz as well as frequency signal higher than 250Hz on the Fourier frequency domain representation and mathematically re-operate the treated FFT spectrum to the function of time. Fig. 3.1D shows the amperogram from Fig. 3.1C filtered by Fourier transform. Compared with original spectrum, the undulations on baseline in the filtered trace are significantly eliminated and the details in both pre-spike and post-spike features are hence highlighted.

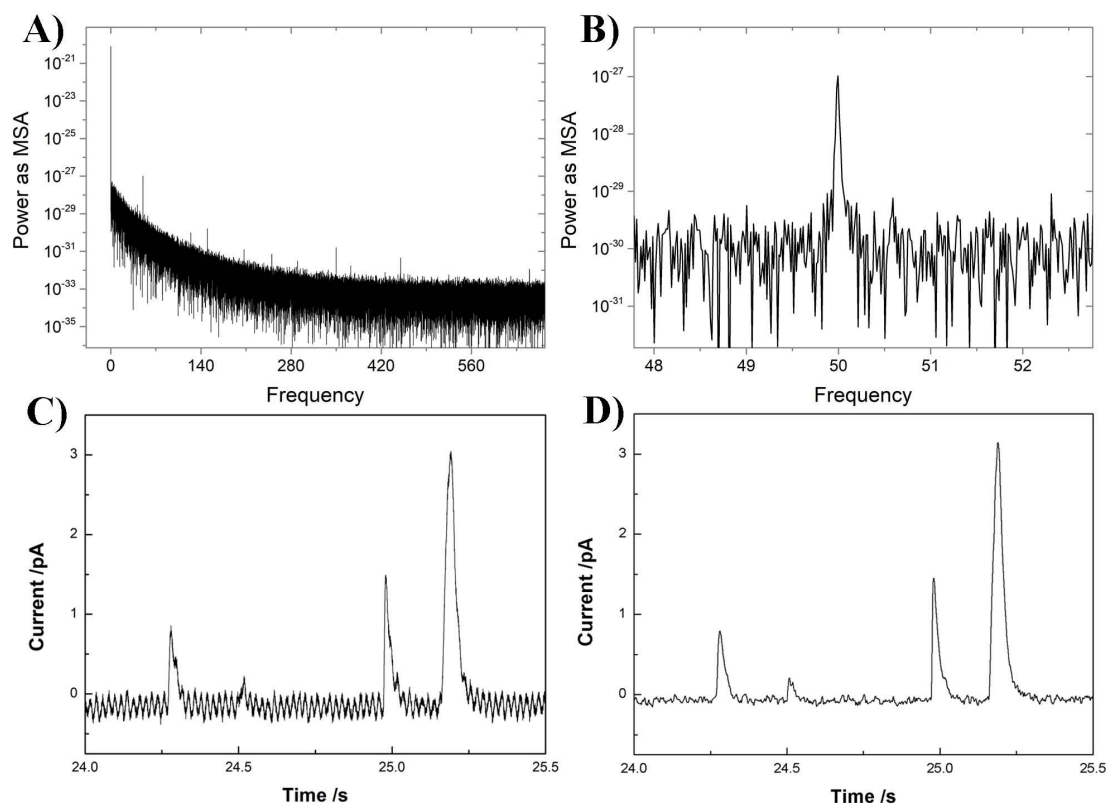


Fig. 3.1 Illustration of Fourier transform treatment. A) overall FFT spectrum powered as mean squared amplitude of frequency obtained from the original amperometric sequence. B) Zoom-in FFT spectrum around 50Hz. C) fragment of initial recorded amperogram. D) amperogram of Fig.C after application of filtering procedure described in the text.

3.2.5 Data analysis

Filtered amperometric traces were visually inspected. All the complete orphan peaks with their maximum current higher than 0.3 pA were identified as exocytotic spikes and collected separately with our lab-made programme. The 0.3 pA threshold was high enough for amperometric signals to be discerned from noise and sufficient for the majority of spikes in all treatment groups to be included in the data analysis. Spike characteristics including but not limited to the maximum oxidation current I_{\max} (pA), the width at half height I_{FWHM} (pA), the total electrical charge Q (fC) were analyzed by lab-made software. All values were

reported as the mean \pm SEM of the data. Pre-spike feature with the foot current between 10% and 50% of the maximum peak current were collected for κ determination. The dynamics of fusion pore expansion were reconstructed from amperometric spikes via simulation. The simulation was set up as interpreted in the first section of supporting information, and the reconstruction of fusion pore radius was performed by Alexander Oleinick.

3.3 Results and discussion

3.3.1 Experimental condition determination

The dose of Y27632 for inhibiting the activity of myosin II in commonly cultured PC-12 cells has not been clearly mentioned in previous publications. As myosin II has been proposed to facilitate vesicular movement along the cytoskeleton, then the alteration on the frequency of exocytotic events must be the most intuitive embodiment of myosin II inhibition. In addition, consulting the reduced number of exocytotic events caused by ML-7 treatment [10], another myosin II associated kinase inhibitor with analogous interference mechanism as Y27632, we probed the proper amount of Y27632 via comparing the frequency of secretory release pre- and post- supplement. 10 min's preincubation with 10 μ M Y27632 has been established for efficient blocking the phosphorylation and activation of myosin II in HL-60 cells previously [12], hence, we followed their protocol.

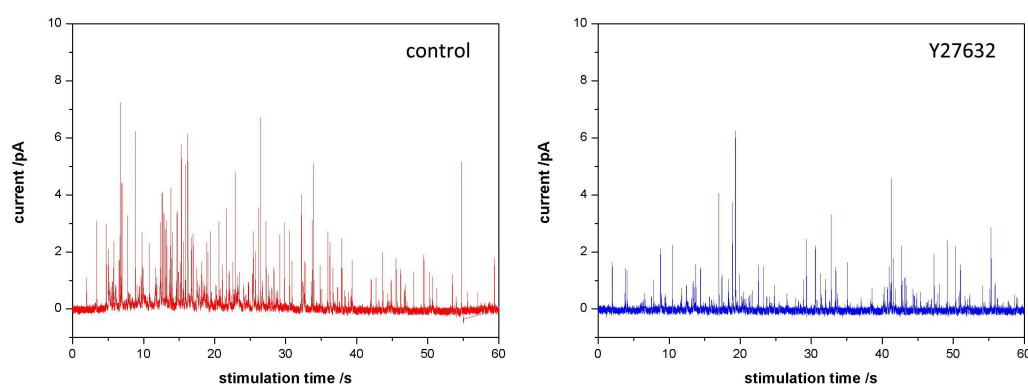


Fig. 3.2 Representative real-time recorded amperograms from PC12 cells with (right) and without (left) Y27632 treatment.

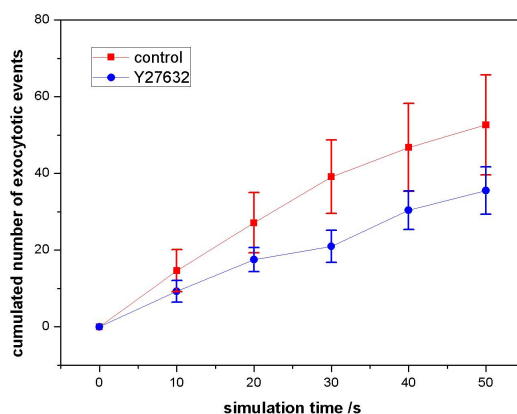


Fig. 3.3 Comparison of cumulated number of exocytotic events during stimulation within and without Y27632 incubation. For equality, timing starts from the point when the first secretory release occurred as a response of stimulation. Amperograms from 8 cells were examined in each condition.

Within our experimental condition, we realized that 10 min incubation with 10 μ M Y27632 did not lead to the deformation of our adherent cells, representing the maintenance of cell status. During the stimulation, cells treated with Y27632 performed relative weak responding behaviour to the K^+ , showing distinct low frequency of exocytosis in the whole process compared to that without any treatment (see in Fig. 3.3). To further ensure that the attenuated response to stimulation is not the representative of cells in low viability due to drug cytotoxicity, we carried on the cell viability test. The LIVE/DEAD[®] Viability/Cytotoxicity Kit was applied as a quick and easy two-color assay to determine viability of cells. In a population of cells, live cells are selectively stained with green-fluorescent calcein-AM to indicate intracellular esterase activity and dead cells are labeled by red-fluorescent ethidium homodimer-1 to indicate loss of plasma membrane integrity. As shown in Fig. 3.4, even though cells were submerged in Y27632 contained buffer for 1h30min, over 99.9% of cells displayed extremely high activity, comparable to the viability in control group. It sufficiently demonstrates that during our exocytosis detection, which last around 1h for one sample, cells have their normal state maintained either being treated with Y27632 or not. The decline on occurrence of exocytosis is clarified to be related to the mute of myosin II. Hence, we reasonably considered that both the incubation time and the dose of Y27632 are proper for myosin II activity inhibition. This condition have thus be applied for the bulk electrochemical data collection.

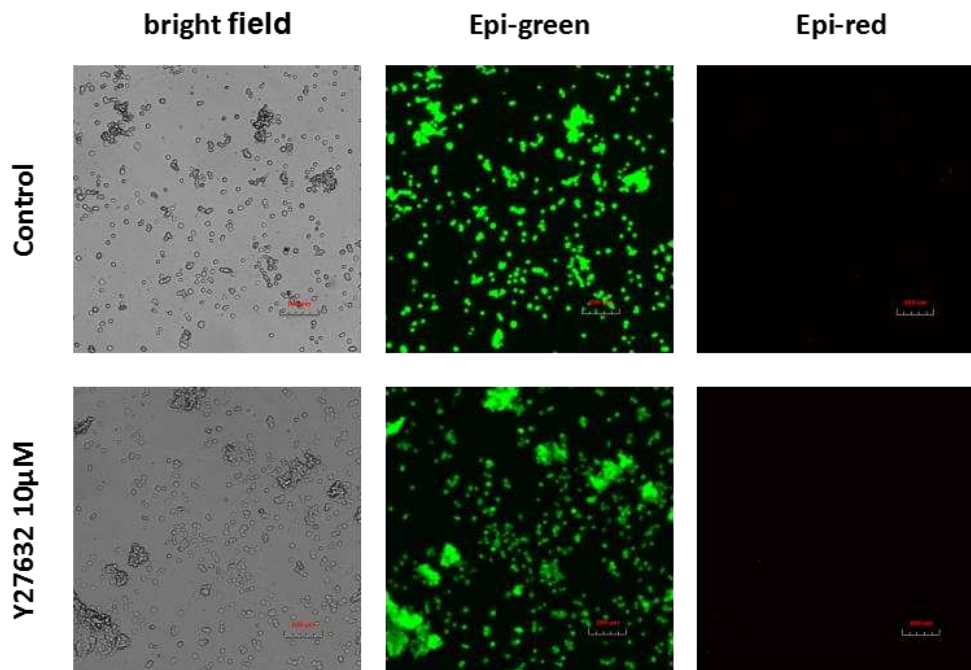


Fig. 3.4 Cell viability test: An example group of epi-fluorescent images from PC12 cells sample co-stained by green-fluorescent calcein-AM as live cell marker and red-fluorescent ethidium homodimer-1 as dead cell marker without (control) and with drug incubation (Y27632 10 μ M 1h30min).

3.3.2 General variation on kinetics of exocytotic release

To explore the alternation of exocytotic kinetics, the morphology of amperometric spike is always the first consideration to appear in mind. Five parameters are considered as the characterizations of spike: the rise time of half peak width $t_{1/2\text{rise}}$ (the time separating 50% of the maximum from 100% of the maximum on the ascending part of the spike), the fall time of half peak width $t_{1/2\text{drop}}$ (the time separating 100% of the maximum from 50% of the maximum on the descending part of the spike), the half peak width $t_{1/2}$ (the sum of $t_{1/2\text{rise}}$ and $t_{1/2\text{drop}}$), the released charge Q , and the current amplitude I_{max} . The mean values of each parameter obtained from cells with and without Y27632 treatment are listed in Table 3.1.

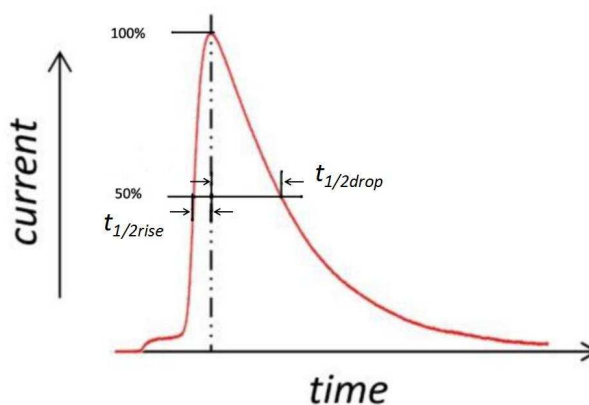


Fig. 3.5 Schematic diagram of $t_{1/2\text{rise}}$ and $t_{1/2\text{drop}}$.

The average amount of molecules released from secretory vesicles seems not be influenced by myosin II freezing when compared the mean charge of spikes. Generally, it suggests that the inhibition of myosin II does not alter the amount of dopamine release from PC12 cell vesicles in stimulated exocytotic condition. It is in accordance with the maintenance of catecholamine content released from chromaffin cells after myosin II inactivation[9, 13]. Moreover, Fig. 3.6 displays the distribution of charges under each amperometric spikes. Compared by the Mann-Whitney test, the charge distributed according to the same probability distribution as featured by a large value of $p = 0.64$ (i.e. there is no statistical difference between the two distributions). It can be illustrated as that dopamine released from secretory vesicles follow its instincts after the muted activity of myosin II. In addition to the conclusion obtained from average value of charge, it further convinces that unphosphorylated myosin II does not contribute to the manipulation of amount of cargo secreted through fusion pore.

Table. 3.1 Spike parameters obtained from K^+ stimulated PC-12 cells. Cells without any treatment were shown as control group. The data was presented as average value with standard error of the mean as error bar.

	$t_{1/2}/ms$	$t_{1/2rise}/ms$	$t_{1/2drop}/ms$	Q/fC	I_{max}/pA
Control (12cells, 246spikes)	27.66 ± 0.65	8.45 ± 0.31	19.12 ± 0.41	53.57 ± 2.45	1.61 ± 0.09
Y27632 10 μ M 10min (12cells, 194spikes)	24.47 ± 0.54	7.28 ± 0.26	17.19 ± 0.33	55.44 ± 3.13	1.76 ± 0.10

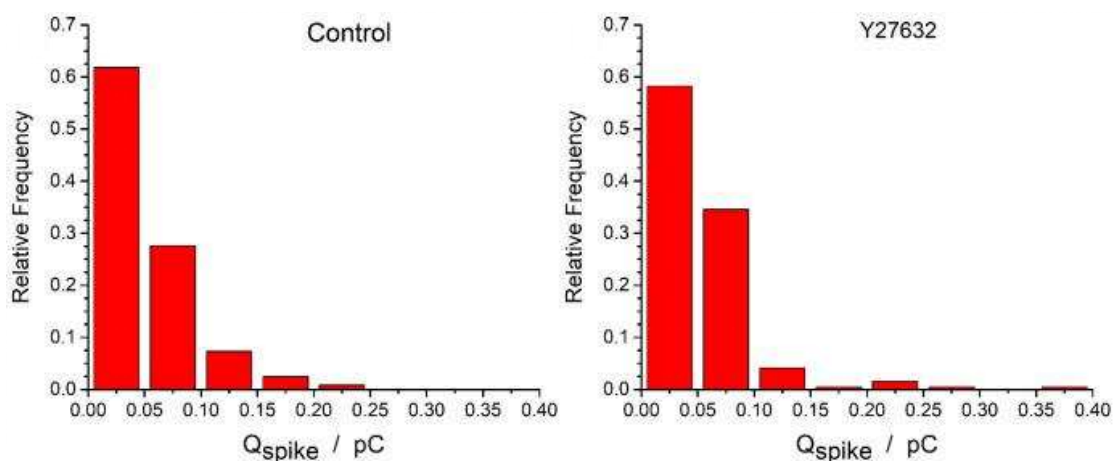


Fig. 3.6 Distribution of quantal size under each amperometric spike with (right) and without (left) Y27632 treatment. Mann-Whitney test: $p = 0.64$

The half peak width and the maximum current represent the breadth and the amplitude of the spike, respectively, while the rise time and fall time from the half peak width display the

steepness. All these four parameters generally describe the average morphology of the spike. The data from the Table 3.1. demonstrates that the inhibition of myosin II activity causes relative rapid release with high flux since the average values of four parameters depicting the narrower but taller spike after the treatment. It may be further deduced to the overall consequence that the inhibition of myosin II plays a positive role on secretory release. To verify this point, we continue inspecting the distribution of parameters to figure out the arresting of myosin II activity results in which extent of release variation at the single vesicle level.

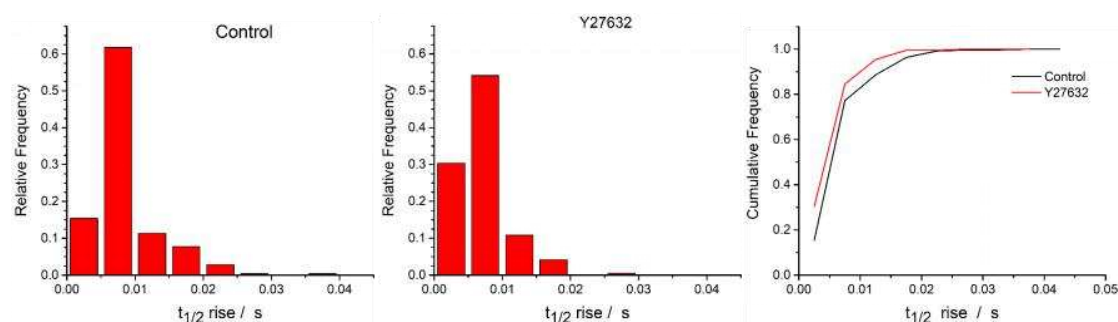


Fig. 3.7 Statistic distribution of time of the rising section at half peak width. Mann-Whitney test: $p = 0.001$

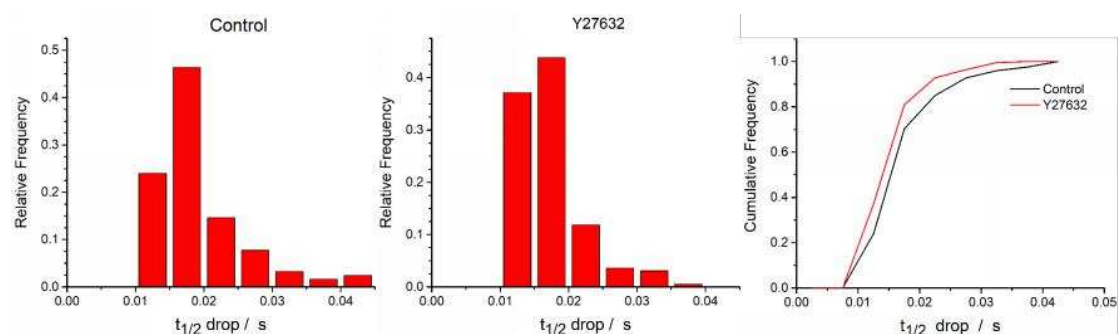


Fig. 3.8 Statistic distribution of time of the falling section at half peak width. Mann-Whitney test: $p = 0.0002$

The current at rise section of half peak width is mainly driven by the real-time fusion pore size, hence the corresponding time could reflect the expansion rate of fusion pore. For the drop section, it depicts a complex process regulated by both fusion pore size and diffusion, however, the diffusion control occupies most of the time, thus its time roughly reflects the duration of the diffusion regulated step depends on the maximum pore size. Looking forward to dig out the relation between myosin II and fusion pore opening, we analyze the duration of ascending branch and descending branch at half peak width.

It can be seen in Fig. 3.7, the rise time at half peak width mostly concentrates in between 5

to 10 ms, regardless of implementation of Y27632 incubation. The p value from Mann-Whitney test indicates statistical difference in these two groups of data. When focusing on this high incidence region, it is not hard to realize that the duration of ascending part overall shifts to the short range. Considering the rising time locally reflects the rate of fusion pore opening, the shift observed on the distribution of rise time is evaluated to be related to the inhibition of myosin II activity that acts on the modification of release kinetics through regulating fusion pore expansion. Furthermore, comparison of the time of descending part also shows an overall prominent shift to short range with p value far less than 0.1 (Fig. 3.8). It approximately reflects a relative fast release through size-fixed fusion pore after the inhibition of actin filaments movement. Hence, we realize that myosin II acts on not only the expansion rate but also the terminal size of fusion pore.

So far, we have seek out that myosin II certainly makes an impact on fusion pore expansion during exocytosis. In order to further decipher the variations on fusion pore evolution caused by myosin II, fusion pore dynamics were reconstructed by means of simulations from amperometric spikes recorded at single vesicle level.

3.3.3 Effect of myosin II inhibition on fusion pore radius

Single exocytotic event monitored by amperometry using an “artificial synapse” configuration can be simply explicated as follows: The opening of fusion pore at the beginning of exocytosis leads to a rapid significant increase of the surface area of the matrix exposed to the solution. It gives rise to a sharp increase of the released flux of neurotransmitter that can be recorded as current with rapid growth. When this expansion terminates and the fusion pore maintains at its maximum radius R_{pore} , this flux, or current as its representative, decreases following an exponential decay to clear up the vesicle initial dopamine content. Details about fusion pore expansion process reconstruction based on spike pattern are elaborated in the supporting information of this thesis. Here, we omit the theoretical calculation and display the simulation data obtained by the reconstruction procedure.

Table. 3.2 Number of single spikes and pre-spike features considered in fusion pore expansion process.

	Number of detected cells	Amount of single spikes	Number of PSF
Control	12	246	42
Y27632 10 μ M 10min	12	194	29

The transport rate of catecholamines within matrix K was determined as described

previously through the calibration of current during PSF [11, 14]. In each experimental condition exocytosis from 12 individual cells were monitored, gaining 246 and 194 single spikes, respectively, from normal grown samples and Y27632 treated samples. Among them, 42 PSF from control group and 29 PSF from drug interference group were used in the K value acquisition. In our case, the appearance of PSF is a bit low, ca. 16% of the events, compared to ca. 30% reported in the literature [14]. It is possibly due to the relative low amplitude of spike observed from our PC12 cells that submerges weak PSF current into background noise. The mean K value obtained from control group and Y27632 treated group were extremely close, hence we select the overall average value 122.57 s^{-1} as the transport rate for the simulation of fusion pore opening dynamics for both control and Y27632 treated spikes. As mentioned in the introduction, 80nm was applied as the general vesicle radius of our PC12 cells. Knowing κ value and vesicle size, each amperometric spike with single exponential decay is converted to time-course of fusion pore expansion following

$$R_{pore}(t) = [i(t) \times R_{ves} / \kappa] / \left[q_{ves}^{tot} - \int_0^t i(u) du \right],$$

as illustrated in Fig. 3.9 [11]. To determine the statistical significance of the changes in fusion pore expansion process, two quantitative features were generally considered. The first one is its maximal size, R_{pore}^{max} , the terminal value of fusion pore radius during release, which is represented as Y-ordinate of the plateau on radius curve. The other one is the expansion rate in its radial direction, that is the slope of pore expansion as a function of time $v_{open} = dR_{pore}(t) / dt$, typically presented in its maximum value, v_{open}^{max} .

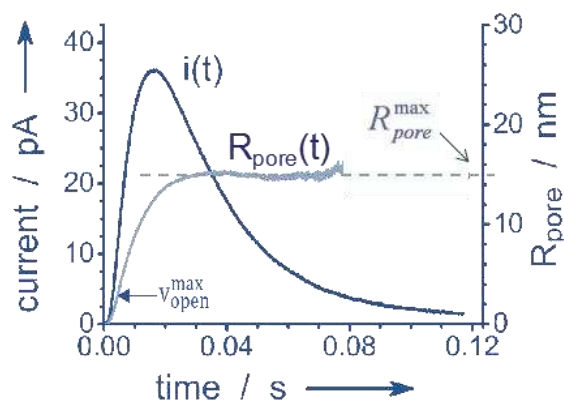


Fig. 3.9 Graphic illustration of key characteristics of fusion pore expansion

Table. 3.3 Number of single spikes representing single and double exponential tail investigated in our survey.

	Number of detected cells	Amount of single spikes	Spikes with single exponential tail	Spikes with double exponential tail
Control	12	246	147	99
Y27632 10 μ M 10min	12	194	105	89

The number of classic single exponential tail and double exponential tail extracted from amperograms in each experimental condition are listed in Table 3.3. Since our theoretical model is based on the release displaying single exponential decay, the reconstruction of fusion pore expansion presented here only considers 147 spikes and 105 spikes with single exponential tail, respectively, from control group and drug treatment group. Those spikes with double exponential tail are discussed later.

3.3.3.1 Effects on maximal fusion pore radius

As we illustrate in the simulation part, the single exponential decay of current corresponds to a fixed vesicle opening angle α with known diffusion rate K within the matrix following the equation[15].

$$i \sim \exp[-k_{\rho}^{diff} t] = \exp[-\alpha \kappa t]$$

Therefore, the absolute value of the slope of current decay which become linear in log scale is directly proportional to the terminal opening of fusion pore during release. In other words, the distribution of the slope from logarithmic analysis will clear reflect the distribution of ultimate size of fusion pore. By comparing the overall arrangement of the slope, the variation trend of fusion pore in its maximum size due to the interference myosin II activity can be deduced.

Fig. 3.10 demonstrates the comparison of the slope distributions from the linear descending part of logarithmic plots of current between control group and Y27632 treated group. The p value calculated from the two groups of data via Mann-Whitney test indicates significant statistic difference of distribution. See from the histogram, it is obvious that the slope emerges in a much higher frequency between -60 s^{-1} and -70 s^{-1} after myosin II inhibition, at the same time the slope with absolute value smaller than 50 shows corresponding reduction of the occurrence. High degree of inclination demonstrates fusion pore with larger opening angle during the diffusion control process. Thereafter, it indicates an overall enlargement of terminal fusion pore radius resulted from the restriction of myosin II activity.

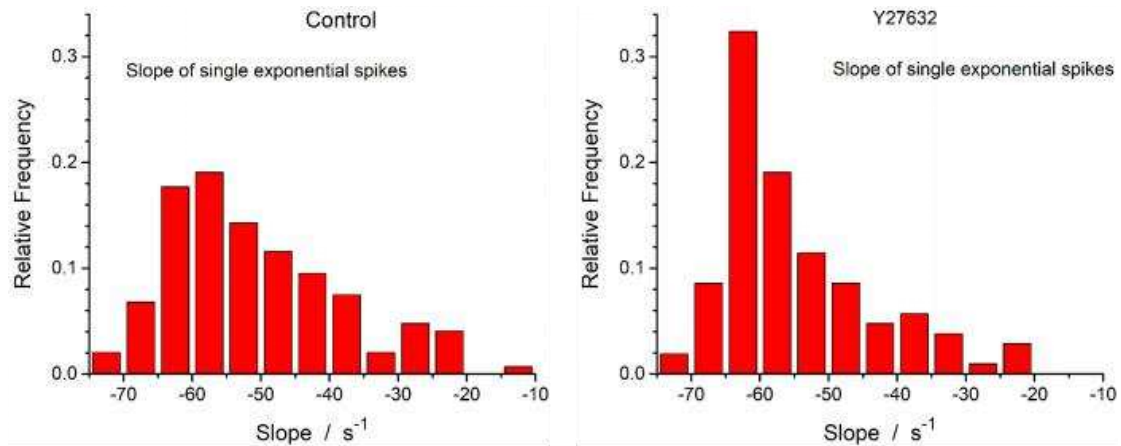


Fig. 3.10 Distribution histogram of the slopes of single exponential spike in log plots without (left) and with (right) Y27632 incubation. Mann-Whitney test: $p = 0.007$

Hereafter, 147 spikes and 105 spikes with single exponential tail in control group and Y27632 treated group are translated to the time-course of fusion pore expansion. For each single exponential spike, the final size of fusion pore can be easily read out from the plateau on each reconstruction curve (as shown in Fig.3.9). Hundreds of ultimate fusion pore radius from two experimental condition are presented as distribution histogram in Fig. 3.11. It should be noted that the average value of K calibrated from PSF and the average value of vesicle radius were applied for fusion pore opening reconstruction, hence dimensions of pore radius obtained from the simulation should be considered in the sense of average pore radius. However, the normalized time dependent dynamics (i.e. $R_{\text{pore}}(t)/R_{\text{pore_max}}$) of the fusion pore is extracted precisely. As shown in Fig. 3.11, the maximal radius of fusion pore is always smaller than ca. 40nm. It is a large size but still smaller than one half of mean vesicle radius (80nm), satisfying the restrained condition for the simplified reconstruction procedure that $R_{\text{pore}}(t)/R_{\text{ves}}$ should be less than 0.7.

By inspecting the variation on the distribution, direct evidence of myosin II's role in regulating fusion pore emerges. Judging by the p value of Mann-Whitney test, the two groups of radius displays obvious distinction in their distribution mode. Although the upper limit for the maximum pore radius in both case are the same (40-45 nm), the overall arrangement of radius shifts to larger size. The prominent high appearance of fusion pore with 35-40 nm as their terminal size is observed after the inhibition of myosin II activity. In the meanwhile, release behaving exponential decay via fixed fusion pore with radius in between 25-35 nm occurs in a relative low frequency. In other words, the introduction of Y27632 caused the enlargement of the terminal fusion pore size while still maintained the upper limit of its distribution. Thus the influence initiated by Y27632 can be interpreted as

modestly unraveling of the constraint for fusion pore to swell to its maximal dimension.

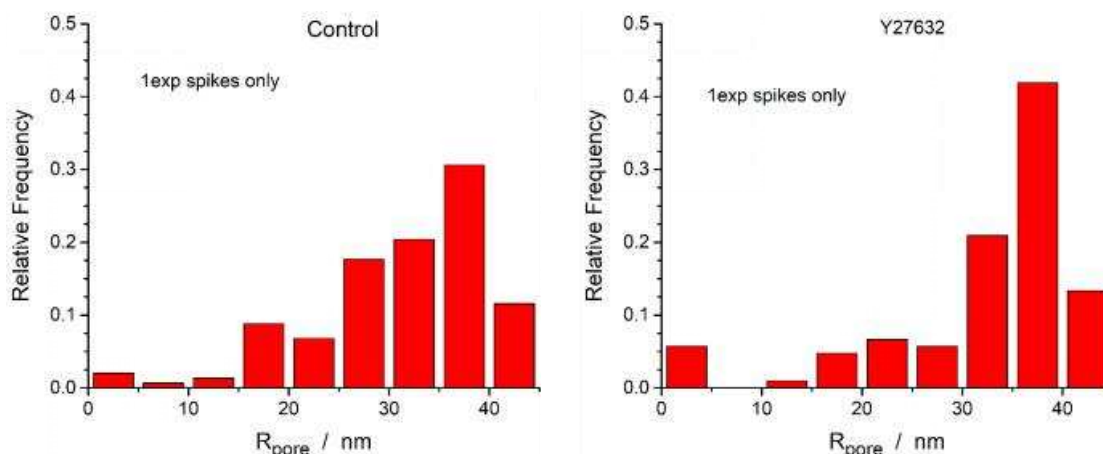


Fig. 3.11 Distribution of calculated maximum fusion pore radius with (right) and without (left) Y27632 incubation. K is defined as 122.57 s^{-1} and 80 nm is applied as the average value of vesicle radius for fusion pore opening reconstruction. Mann-Whitney test: $p = 0.068$

3.3.3.2 Effects on maximal expansion rate

Before the fusion pore enlarges to its maximum, its radial expansion rate is determined by the balance between the driving force exerting on the pore edge and the demand of system to relax the inner energy via viscous dissipation. Accordingly, $R_{\text{pore}}(t)$ enlarges exponentially at the beginning of its expansion. After this stage, the rate of expansion gradually tends to 0 while the fusion pore reaches its maximum size. $v_{\text{open}}^{\text{max}}$ hence indicates the expansion velocity before the pore edge may interact with some non-lipid biological structures that ultimately slow down its dilation. A distinct mode of distribution of $v_{\text{open}}^{\text{max}}$ is displayed after Y27632 treatment (Fig. 3.12), although the upper limit of distribution maintains. The lower occurrence of events with maximal expansion rate of fusion pore less than $3 \mu\text{m/s}$ is observed after Y27632 treatment, while the population with maximal opening rate higher than $6 \mu\text{m/s}$ displays significant growth in the meanwhile. It demonstrates an overall shift of maximal expansion rate of fusion pore to larger value. Indeed, the cumulative distribution depicts the same trend (Fig. 3.13). Moreover, the mean value of maximal expansion rate ensures the acceleration of maximal expansion rate with Y27632 application. As we elucidate above, higher velocity of expansion indicates less obstacles encountered before reaching some non-lipid rigid structures. Hence, it is reasonable to suppose that the action of Y27632 assist to eliminate the hindrance on the way for fusion pore expansion, which is not surprising and consistent with the conclusion we obtained from the distribution of maximal fusion pore radius.

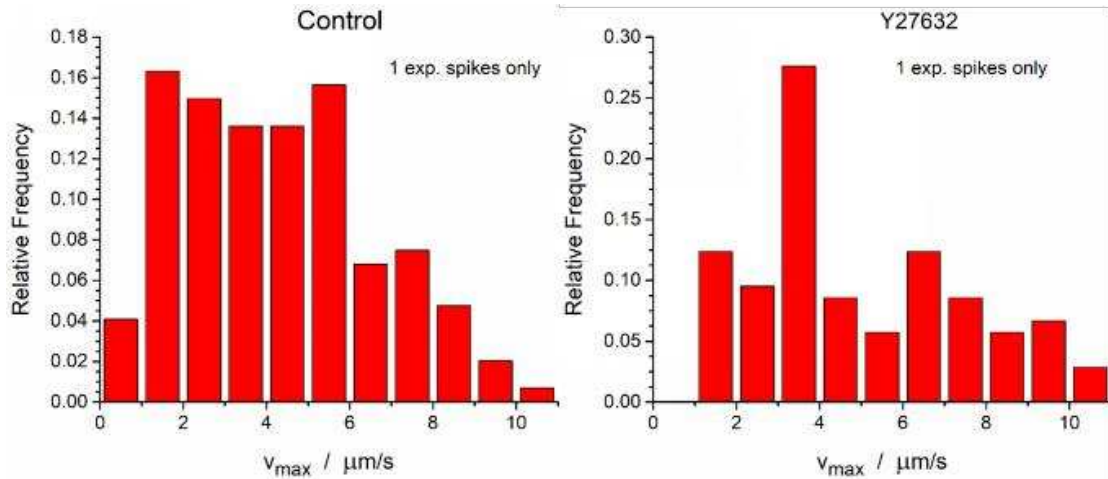


Fig. 3.12 Relative occurrence of exocytosis depends on the distribution of maximal fusion pore expansion rate distribution without (left) and with (right) Y27632 incubation. Mann-Whitney test: $p = 0.028$.

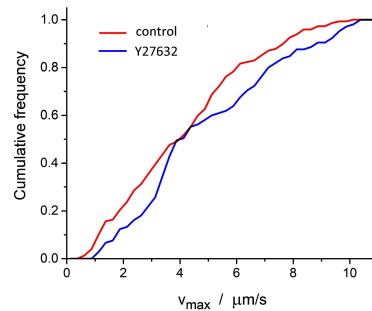


Fig. 3.13 Cumulative distribution of fusion pore maximal expansion rate shown in Fig.3.12 without (red) and with (blue) Y27632 incubation. The mean value of v_{max} in control group is $4.23\mu\text{m/s}$, and in Y27632 treated group is $4.97\mu\text{m/s}$.

It is surprised that in control group, v_{open}^{max} distributes in an uniform pattern with relative high occurrence in between 1 to 6 $\mu\text{m/s}$, while for Y27632-modified condition, v_{open}^{max} presents a smooth appearance in a wide range excluding a sharp rise at 3 to 4 $\mu\text{m/s}$. We have no clear explanation for the irregular pattern of distribution, but one possible view to consider is that it may be due to the small amount of samples containing foot portion. Since v_{open}^{max} is the maximal expansion rate from individual events controlled by single elementary process, the difference from independent exocytosis would cause outstanding manifestation without enormous sampling. Despite this, their distributions still can generally reflect the variation on the initial fusion pore expansion resulting from the incubation of Y27632.

Considering that actin filaments have been reported to assemble as a coat or ring structure

around the fused vesicle during release [16, 17], the inert relative movement of actin filaments prevailed by inhibition of myosin II may weaken its contractile force on the edge of fusion pore to liberate its opening. Besides, deregulated actin depolymerization induced by mute of ROCK with Y27632 also slightly impairs the bounding structure of actin surrounding the fusion pore, reducing the resistance of pore expansion.

3.3.4 Second exponential behaviour on the decay branch of spikes

Interestingly, in our case we observed some of the events display decay branches involving double exponential tail (see from Table. 3.3), similar as reported by Ewing and his colleagues [18]. It can be rationalized by the two-pool model established recently [19]. Within this model, the matrix adopt a composite grainy structure in which highly compacted chromogranins nanodomains are floated in a much loose bulk. The special structure allows the catecholamine cations stored in less condensed areas to diffuse at significant rates to sustain the fast-releasing mode current, that is the first exponential decay. When the vesicles have unloaded their free-releasing content, those catecholamines stored in tightly compacted domains may migrate into fast-releasing pool. This slow kinetic exchanges display the second exponential behaviour with gentle decline of current. It has been shown that if the fusion pore is not able to reach its sufficient size, then the fast domain cannot be discharged rapidly for the slow-releasing pool contribution to be observable. At this condition, only the fast pool release is recorded by amperometry, giving rise to spikes displaying single exponential tail and corresponding to the partial release of content in the vesicle.

The over representation of two exponential tail of release recorded when myosin II is inhibited is consistent with model of fast and slow compartment in vesicles (Fig. 3.14). As described above, inhibition of myosin II activity leads to faster expansion of the fusion pore without changing the maximum pore size. Consequently the cargo stored in "fast compartment" is exhausted in a faster way and subsequently, the release from the slow compartment can be detected with higher efficiency. In addition, the inhibition of myosin II caused the second exponential decay with larger slope, as apparent from the distribution in Fig. 3.15. It represents prominent slow-releasing mode. Simulations show that the slope of second exponential tail is associated with several factors such as diffusion rate from fast release pool to external space, the bilateral exchange rate between slow and fast release pool. Since a complete model for elaborating the kinetics on the second exponential decay has not been established yet, the specific analysis of the difference observed from second

exponential tail will be left for resolving in the near future.

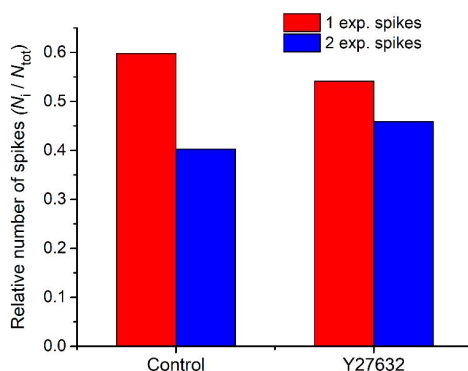


Fig. 3.14 Relative number of spikes present single exponential decay and double exponential decay in two experimental conditions.

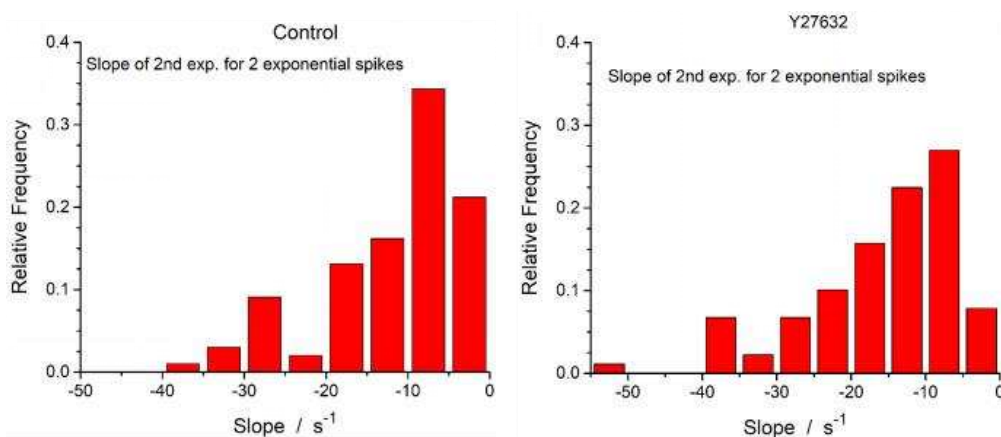


Fig. 3.15 Distribution of the slopes of second exponential tail in log plot from double exponential spikes with (right) and without (left) Y27632 incubation. Mann-Whitney test: $p = 0.005$

3.4 Conclusion and perspective

In this chapter, we investigate the role of myosin II in the regulation of fusion pore opening via amperometry using an “artificial synapse” configuration. The fast semi-analytical simulation established in previous work acts as a useful tool for interpreting the real time enlargement of fusion pore radius from recorded current amperometric spikes. Y27632 was applied as a non-toxic retard for inhibition of myosin II activity. The combination of molecular motor inhibitor and sensitive detection technique as well as theoretical simulation has allowed us to present direct evidence about how myosin II influence the fusion pore expansion. It is realized that the temporary myosin II inhibition maintained the amount of cargo released through fusion pore while speeding up the releasing process. The simulation of fusion pore expansion indicates that suppression of myosin II activity induced larger fixed

fusion pore in general without crossing the upper range. Moreover, the maximal expansion velocity of fusion pore was also raised by temporary myosin II silence. In addition, the double exponential spike tails occasionally observed in current spike was briefly illustrated by purposed two-pool releasing model. The higher occurrence of double exponential tail after interference of myosin II further convince the relative unrestrained opening of fusion pore. In light of the observations presented here, it is reasonable to conclude that myosin II have an overall inhibition effect on the fusion pore development without disturbing the inherent release amount.

The reconstruction of fusion pore radius based on real-time recorded current is capable to present kinetics of pore expansion in details, providing unprecedented evidence with high time resolution. Hence, it presents a wide application prospects in exocytosis research field. In this work, we revealed the modulation of fusion pore expansion influenced by the myosin II, one of important proteins participating in the complex physiological processes. However, our strategy is not limited to this research. It opens the possibility to study the function of other actin filaments' activity such as the polymerization, depolymerization and can be even extended to unveil the mystery of other proteins identified as key players in regulating release step.

3.5 References

1. C. Amatore, S. Arbault, M. Guille, F. Lemaître, *Electrochemical monitoring of single cell secretion: vesicular exocytosis and oxidative stress*. Chemical reviews, 2008. **108**(7): p. 2585-2621.
2. D. M. Omiatek, A. Cans, M. L. Heien, A. G. Ewing, *Analytical approaches to investigate transmitter content and release from single secretory vesicles*. Analytical and bioanalytical chemistry, 2010. **397**(8): p. 3269-3279.
3. D. Zenisek, J. A. Steyer, M. E. Feldman, W. Almers, *A membrane marker leaves synaptic vesicles in milliseconds after exocytosis in retinal bipolar cells*. Neuron, 2002. **35**(6): p. 1085-1097.
4. M. Lindau, W. Almers, *Structure and function of fusion pores in exocytosis and ectoplasmic membrane fusion*. Current opinion in cell biology, 1995. **7**(4): p. 509-517.
5. J. W. Taraska, D. Perrais, M. Ohara-Imaizumi, S. Nagamatsu, W. Almers, *Secretory granules are recaptured largely intact after stimulated exocytosis in cultured endocrine cells*. Proceedings of the National Academy of Sciences, 2003. **100**(4): p. 2070-2075.
6. T. Tsuboi, G. A. Rutter, *Multiple forms of "kiss-and-run" exocytosis revealed by evanescent wave microscopy*. Current Biology, 2003. **13**(7): p. 563-567.
7. J. Villanueva, V. Torres, C. J. Torregrosa-Hetland, V. Garcia-Martinez, I. López-Font, S. Viniegra, L. M. Gutiérrez, *F-actin–myosin II inhibitors affect chromaffin granule plasma membrane distance and fusion kinetics by retraction of the cytoskeletal cortex*. Journal of Molecular Neuroscience, 2012. **48**(2): p. 328-338.

8. R. Aoki, T. Kitaguchi, M. Oya, Y. Yanagihara, M. Sato, A. Miyawaki, T. Tsuboi, *Duration of fusion pore opening and the amount of hormone released are regulated by myosin II during kiss-and-run exocytosis*. *Biochemical Journal*, 2010. **429**(3): p. 497-504.
9. P. Ñeco, C. Fernández-Peruchena, S. Navas, M. Lindau, L. M. Gutiérrez, G. Álvarez de Toledo, E. Alés, *Myosin II contributes to fusion pore expansion during exocytosis*. *Journal of Biological Chemistry*, 2008. **283**(16): p. 10949-10957.
10. K. Berberian, A. J. Torres, Q. Fang, K. Kisler, M. Lindau, *F-actin and myosin II accelerate catecholamine release from chromaffin granules*. *Journal of Neuroscience*, 2009. **29**(3): p. 863-870.
11. A. Oleinick, I. Svir, C. Amatore, *'Full fusion' is not ineluctable during vesicular exocytosis of neurotransmitters by endocrine cells*. *Proc. R. Soc. A*, 2017. **473**(2197): p. 20160684.
12. G. E. Peng, S. R. Wilson, O. D. Weiner, *A pharmacological cocktail for arresting actin dynamics in living cells*. *Molecular biology of the cell*, 2011. **22**(21): p. 3986-3994.
13. P. Ñeco, D. Giner, S. Viniestra, R. Borges, A. Villarroel, L. M. Gutiérrez, *New roles of myosin II during vesicle transport and fusion in chromaffin cells*. *Journal of Biological Chemistry*, 2004. **279**(26): p. 27450-27457.
14. A. Oleinick, F. Lemaître, M. Guille-Collignon, I. Svir, Christian Amatore, *Vesicular release of neurotransmitters: converting amperometric measurements into size, dynamics and energetics of initial fusion pores*. *Faraday discussions*, 2013. **164**: p. 33-55.
15. C. Amatore, A. I. Oleinick, I. Svir, *Reconstruction of aperture functions during full fusion in vesicular exocytosis of neurotransmitters*. *ChemPhysChem*, 2010. **11**(1): p. 159-174.
16. T. D. Nightingale, D. F. Cutler, L. P. Cramer, *Actin coats and rings promote regulated exocytosis*. *Trends in cell biology*, 2012. **22**(6): p. 329-337.
17. J. Wang, D. A. Richards, *Spatial regulation of exocytic site and vesicle mobilization by the actin cytoskeleton*. *PloS one*, 2011. **6**(12): p. e29162.
18. R. Trouillon, A. G. Ewing, *Amperometric measurements at cells support a role for dynamin in the dilation of the fusion pore during exocytosis*. *ChemPhysChem*, 2013. **14**(10): p. 2295-2301.
19. R. Hu, B. Ren, C. Lin, A. Oleinick, I. Svir, Z. Tian, C. Amatore, *How "Full" is "Full Fusion" during Exocytosis from Dense Core Vesicles? Effect of SDS on "Quantal" Release and Final Fusion Pore Size*. *Journal of The Electrochemical Society*, 2016. **163**(9): p. H853-H865.

Chapter 4: Simultaneous monitoring of both neurotransmitter release and fusion pore development

4.1 Introduction

Vesicular exocytosis is an ubiquitous process for intercellular communication in neurons and endocrine cells achieved via intracellular membrane trafficking pathway. It involves the fusion of chemical messengers full-loaded secretory vesicle with the cellular membrane for the formation of the nanometric fusion pore and the subsequent release of messengers through the minute pore to synaptic or extracellular fluids. As the most direct and crucial step for signal exchange domination, fusion pore opening with its corresponding secretory release sustains a popular research area within exocytosis investigation. In the early stage of exocytosis study, it was generally considered that the expansion of fusion pore ended in a complete integration into the cellular membrane that resulted in a full vesicle content release [1, 2]. However, the inevitable view of “full fusion” tendency has recently aroused controversy with the appearance of evidence about fusion pore closure or flicker (“kiss and run” mode) [3, 4], among which fluorescent microscopy provided the strongest support for multiple exocytosis mode [5, 6]. The visualization of fusion pore evolution was mainly accomplished via tracking fluorescence distribution from single secretory vesicle by tagging vesicle membrane-resident protein with fluorescent protein (e.g. VAcHT-GFP) or introducing a fluorescent styryl dye as membrane optical probe [7]. Although the background fluorescence can be technically excluded by employing thin-layer illumination methodology such as TIRFM [8], the temporal resolution (e.g. ~tens to hundreds of milliseconds/frame) limited by camera still hinders fluorescent microscopy’s application in instant and detailed exocytotic description. This intrinsic drawback is embodied more evidently when optically recording the transient neurotransmitter release (e.g. ~few to tens of milliseconds within whole process, PC12 cells) by loading fluorescent chemicals into vesicular lumen. Conversely, as the most widely used electrochemical technique for exocytosis investigation, amperometry performs remarkable advantages such as sufficient temporal resolution and sensitivity in small messengers’ release monitoring. The massive flux of neurotransmitter is precisely quantifiable based on amperometric spike. With reasonable analytical simulation, extraction of the dynamics of fusion pore expansion including both extent and rate during secretory release is further implemented [9]. For example, most releasing events from endocrine cells have been verified to be entirely proceeded through a tiny fusion pores whose dimension are much smaller than those of vesicles [10, 11]. Even though the

detection principle of amperometry brings superior time resolution, it also limits amperometry's application in recording small molecule discharge process during exocytosis. In other words, amperometry becomes completely "blind" to the experience of fusion pore along with termination of neurotransmitters release.

Inspired by the complementary features of these two technologies, a combined TIRFM and amperometry detection method was previously implemented and successfully applied in the investigation of secretory release at single vesicle level [12]. Taking advantage of the high spatio-temporal resolution of coupling detection, with the assistance of electroactive probe inside vesicular lumen and fluorescent probe labeled on vesicular membrane we achieved recording both neurotransmitter release and the whole evolution process of fusion pore simultaneously during single exocytotic events. Two commonly reported fates of fusion pore can be identified: "open and close" and "full opening".

4.2 Materials and methods

4.2.1 Fabrication of transparent ITO microelectrode device

The ITO device was fabricated following the protocol designed previously in the lab [13]. A thin film of ITO (90%In₂O₃, 10%SnO₂; 150 ± 10 nm thickness; ACM, Villiers Saint Frédéric, France) was beforehand sputtered onto optical glass slides (22 mm × 22 mm × 0.13 mm) to form a thin layer with low electrical resistance (≤20 ohms per square) and transparency. ITO surface was successively rinsed with distilled water, ethanol, isopropanol, and subsequently treated with oxygen plasma for 2 min at 400 mTorr. Then a positive photoresist, AZ9260 (Clariant GmbH, Germany), was deposited onto ITO substrate to cover the entire surface without any bubble. The AZ9260-covered ITO substrate was then spun at 2000 rpm for 60 s with acceleration of 300 rpm to produce a homogeneous thin layer (10 μm thickness) of photoresist. Hereafter, ITO substrate was pre-baked on a hotplate at 110 °C for 160 s to get rid of volatile solvents and exposed to UV light (20mW/cm²) for 70 s through a specific mask design for ITO microelectrode molding. The substrate was then immersed in 1:4 (v/v) AZ400K-H₂O mixture to remove exposed AZ9260. After surface cleaning with distilled water, the substrate was gently agitated in highly concentrated HCl solution till the disappearance of unprotected ITO region and rinsed with water. At the end of wet etching step, photoresist covering multiple ITO microelectrodes was removed by acetone to unveil multiple microelectrodes on the glass surface. For further limiting a specific working region, a negative photoresist SU-8 3010 was dispensed to cover the entire surface of etched ITO substrate. Then it was spin-coated at 500 rpm for 10s with acceleration of 100 rpm, followed

by a faster spin-coating at 3000 rpm for 30 s with acceleration of 500 rpm to gain a thin SU-8 3010 film of 10 μm thickness. After soft pre-baking on the hotplate at 110 $^{\circ}\text{C}$ for 4 min, SU-8 3010 covered ITO substrate was then exposed to UV light (20mW/cm²) for 17 s through a specific mask design, followed by post-baking at 65 $^{\circ}\text{C}$ for 1 min and 95 $^{\circ}\text{C}$ for 2 min. Unexposed SU-8 3010 region was developed within SU-8 developer to merge the specific working region on ITO substrate. Finally, the thoroughly cleaned ITO microelectrodes chip was fixed on the Petri dish with 1.5 cm diameter hole in the center (P50G-1.5-14-F, MatTek Cultureware, Ashland, MA) by polydimethylsiloxane (PDMS).

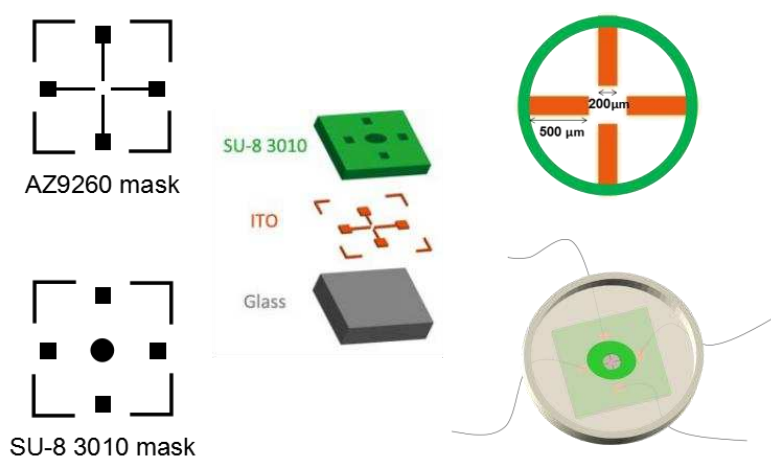


Fig.4.1 Illustration of ITO microelectrode device fabrication. Left: patterns of mask for AZ9260 layer and SU-8 3010 layer; Middle: composition of ITO microelectrode chip with different layers obtained by using the photoresists AZ9260 and SU8-3010, respectively; Right: assembled ITO device with enlarged view of defined working areas of ITO microelectrodes. ITO microelectrode bands are shown in orange and defined to 200 μm width/500 μm length by the isolation layers of SU-8 3010 displayed in green.

4.2.2 Cell culture and sample preparation

PC12 cells (CRL-1721.1) were purchased from the American Type Culture Collection (Manassas, VA) and incubated in RPMI-1640 complete growth media with 10% heated inactivated horse serum (Life technologies), 5% heated inactivated fetal bovine serum (Life technologies) and 1% penicillin streptomycin solution (Life technologies) in a 5% CO₂, 100% humidity atmosphere at 37 $^{\circ}\text{C}$ following official protocol. Throughout the cell culture, cells were grown in cell culture flask with medium refreshed every 2 days and were sub-cultured approximately every 4-5 days. PC12 cells were sub-cultured on human placenta collagen (Bornstein and Traub type IV, Sigma-Aldrich Co.) coated lab-made ITO microelectrode device 2 days before electrochemical test. After 1 day's growth, cells were transfected with VMAT2-pHluorin (designed and provided by Robert Edwards Lab) using Lipofectamine 3000 as transfection reagent in optimal condition. The transfection procedure is described in

supporting information. For L-DOPA enrichment test, PC12 cells were sub-cultured on human placenta collagen (Bornstein and Traub type IV, Sigma-Aldrich Co.) coated 50 mm glass bottom dish (MatTek Corporation, Ashland, MA) 2 days in advance. The complete growth medium used was filtered by 0.22 μm filtration membrane before use.

4.2.3 L-DOPA enrichment amperometric test with CFE

Cell sample in glass bottom dish was rinsed with PBS and incubated in a 100 μM L-3,4-dihydroxyphenylalanine (abbreviated as L-DOPA) supplemented HEPES containing 150 mM NaCl, 5mM KCl, 1.2 mM MgCl_2 , 5 mM Glucose, 10 mM HEPES and 2 mM CaCl_2 at 37 $^\circ\text{C}$ for 1 h before the experiment in order to achieve the enrichment of dopamine into secretory vesicles. The solution was prepared with distilled water and adjusted to pH 7.4. Micro-CFE was fabricated and used in the same way as mentioned in Chapter 2. A constant potential 650 mV was applied at CFE vs. a Ag/AgCl reference electrode using a commercially available picopotentiostat (model AMU-110, Radiometer Analytical Instruments, Copenhagen, Denmark). The output was digitized at 40 kHz to record current as time-course. Electrochemical recording was performed on an inverted microscope (Observer D1, Carl Zeiss AG) inside Faraday cage. A glass microcapillary containing isotonic KCl stimulant (100 mM KCl, 55 mM NaCl, 1.2 mM MgCl_2 , 5 mM Glucose, 10 mM HEPES and 2 mM CaCl_2) was positioned at about 20 μm away from the cell to trigger exocytosis. All the amperograms were collected from individual cell stimulated within 60s. Each cell was detected only once.

4.2.4 Coupling detection on living cells

Recording of exocytosis with amperometry combined with TIRFM were performed on an inverted microscope (Observer D1, Carl Zeiss AG) inside Faraday cage. Cells grown on ITO device were rinsed three times with PBS and incubated in a 100 μM L-DOPA contained HEPES at 37 $^\circ\text{C}$ for 1 h before the experiment. During coupling detection, cells were maintained in HEPES physiological saline adjusted to pH 7.4 at room temperature. Specified potential 650mV was applied between ITO band and Ag/AgCl reference electrode by a commercially available picopotentiostat (model AMU-110, Radiometer Analytical Instruments, Copenhagen, Denmark). The output was digitized at 40 kHz and the current was recorded as a function of time. A glass microcapillary containing K^+ stimulant was positioned at about 20 μm away from the inspected cell regulated by micromanipulator as shown in Fig. 4.2. All the amperograms were collected from individual cell polarized by 60s' K^+ injection with the same component as used in CFE detection .

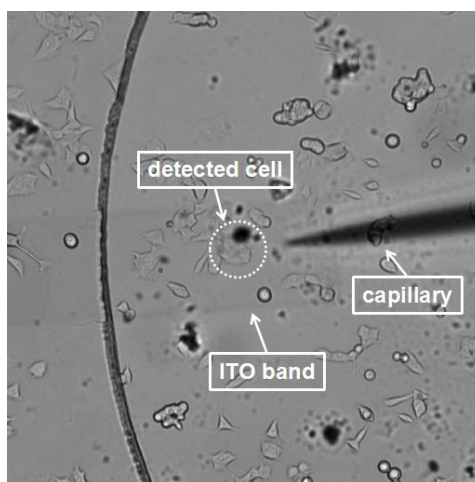


Fig. 4.2 Inverted microscopy image of experimental configuration. ITO microelectrode was displayed as a narrow and transparent band under bright field. Cells were randomly attached on the surface of device including the ITO microelectrodes. A glass microcapillary with sharp tip was positioned close to the target cell for K^+ injection.

Optical tracing of status of vesicular membrane during exocytosis was implemented by evanescent field illumination. Laser beam with wavelength 488 nm was focused at the back focal plan of a high numerical aperture objective lens (1.45NA, PlanApo, Zeiss). The ITO device was placed above the 100 \times TIRFM objective with immersion oil (sulphur in diiodomethane refractive index $n=1.52$, Nonfluorescence, Olympus) as optical contact assistant during test. Interference reflection microscopy technique was applied to help focusing on ITO electrodes-cell interface. Laser was guided into the objective at an angle beyond the critical angle θ_c and underwent total internal reflection at the glass-cell surface. Scattered and back-reflected excitation light was blocked at the emission path by a dichroic mirror (FT 495 nm) and a band-pass filter (BP 525/50 nm, Chroma Technology). Images were recorded at 30 ms/frame by digital camera system (EM-CCD, C9100-13, Hamamatsu).

The fluorescent/electrochemical signals were displayed and recorded with eDAQ Chart software (AD Instruments) and HClmage software (Hamamatsu), respectively. Each image captured by EM-CCD could also produce a pulse signal monitored by e-corder (eDAQ) data recorder using eDAQ Chart software (Fig. 4.4). The first recorded voltage pulse indicated the start time of movie. Manual offline time correction then allowed us to synchronize the movie and the amperometric signals. Each cell was detected only once. Unless stated, all chemicals were obtained from Sigma-Aldrich and used without further purification.

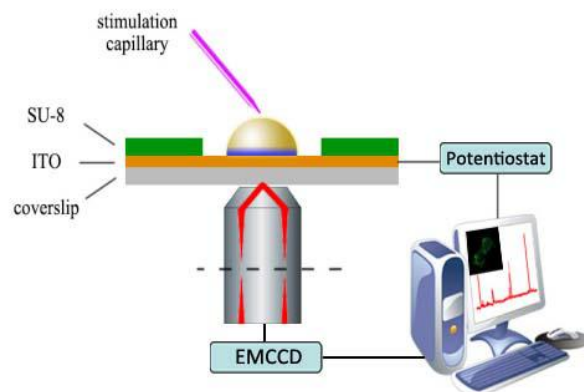


Fig. 4.3 Setup for TIRFM/ampereometry coupling detection; the fluorescent/electrochemical signals were concurrently collected through transparent ITO band and displayed on computer screen.

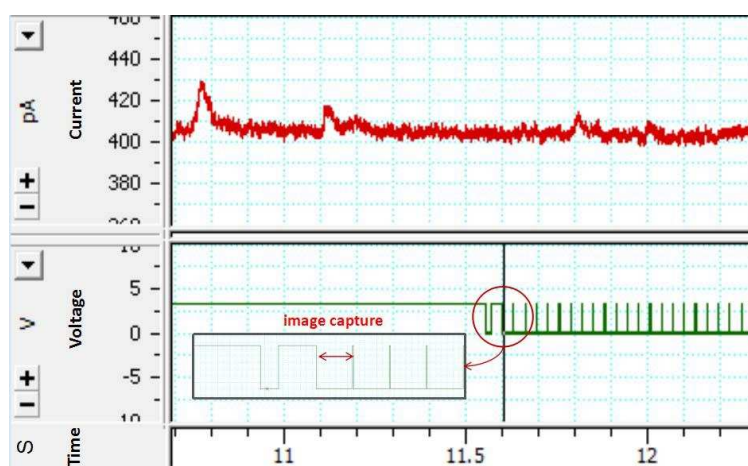


Fig. 4.4 The synchronization of amperometric and fluorescent signals. Zoom in: voltage pulse caused by frame capture.

4.2.5 Data analysis

Amperometric trace recorded was visually inspected. Signals were designated as exocytotic spikes if their maximum current values were 3 times higher than the noise of the baseline current recorded prior to each signal. Spike characteristics, e.g. the maximum oxidation current I_{\max} (pA), the width at half height t_{FWHM} (ms), and the total electrical charge Q (fC) were analyzed by lab-made software.

Using TIRFM, exocytotic event is visually identified as a sudden appearance of small bright dot followed with gradual variation of fluorescent intensity in a successive frames (“flash”). One pixel represents approximate 160 nm at the cell surface in this case. Fig. 4.5 shows a typical example of vesicle image at the beginning of exocytosis and the end of full collapse. Fluorescent probes stained on the vesicular membrane were transferring to the cellular

membrane along with the fusion progressively. This spreading led to the dim of signals in the center while at the same time lighted up the surrounding region. Minimized pixel regions describing individual vesicle was defined relying on the distribution of fluorescence recorded (Fig. 4.5). The dimension of region of interest (ROI) obtained from experiment was also matched with theoretical derivation taking point spread function of image capture system into consideration. The Gaussian root mean square (RMS) width of the airy pattern in one dimension was used to estimate the size of the vesicles captured as fluorescent dots. Equating the peak amplitude of the airy pattern and Gaussian profile RMS width σ yields in our set-up :

$$\sigma \approx 0.21\lambda / NA \approx 0.21 \times 515nm / 1.45 \approx 75nm$$

Noting that NA is the objective numerical aperture and λ is the wavelength of emission light. On account of the approximate value of vesicle radius in PC12 cells, which is in the range 80 nm, then the diameter of pre-fused vesicle displayed should be $2R_{vesicle} + 2\sigma$, around 2pixel. Rationally considering that vesicle may not appear precisely at the center of pixel, the region representing pre-fused vesicle should be boarder than calculated value. To achieve semi-quantification of the fusion between vesicular membrane and cellular membrane, the first ROI we selected including center area with 2 pixels in radius for depicting fluorescence in the centre of events (Fig. 4.6). While annular ring with 4 pixels in radius surrounding the center was defined as second ROI and acted as the indicator for characterizing the lateral fluorescence spreading away from the site of exocytosis. Via tracing the entire footprint of the average fluorescence intensity variation in ROIs, distribution of optical probes on both membranes were able to be informed. In addition with the dynamics of secretion monitored by amperometry, fusion pore evolution could be tightly linked to the corresponding release, thus providing a comprehensive understanding of the last stage of exocytosis.

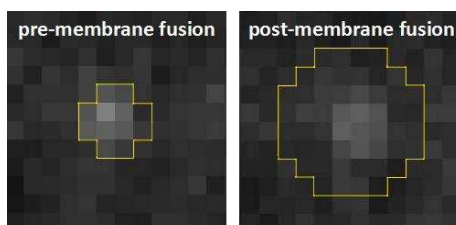


Fig. 4.5 Representative example of single vesicle observed using TIRFM pre- and post-complete fused with cellular membrane. Each square reveals one pixel.

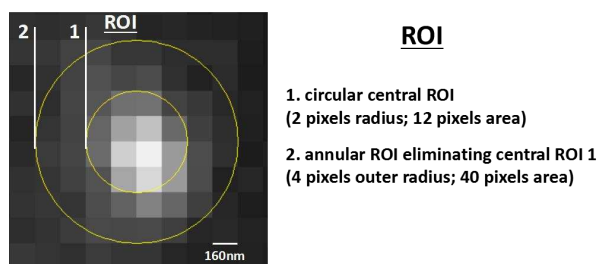


Fig. 4.6 The schematic illustration of the region of interest (ROI) selected for subsequent image analysis. ROIs were centered on fusion site. Noting that the actual pixels participated in average fluorescence calculation were those with their majority of area included in the circle.

Image analysis was executed with ImageJ software. Successive frames (30 frames before “flash” and 500 frames after “flash”) were substacked and average fluorescence in each ROI was (2px, 4px radius) measured from each frame. Average fluorescence in ROIs preceding increase (10 frames) F_0 was subtracted from the fluorescence value to quantify excess fluorescence $F-F_0$. Normalization was operated by dividing this corrected fluorescence intensity ($F-F_0$) with the average fluorescence before increase F_0 (10 frames in the ROI).

4.3 Results and discussion

4.3.1 Vesicle content enrichment with L-DOPA

According to the previous work in our lab, compared to CFE, current noise from ITO electrode was a non-evasive limitation when applied to constant-potential amperometry for detection of neurotransmitter release from single cell during exocytosis. Fig. 4.7 demonstrated the current noise of ITO electrode measured with various surface dimensions at 900 mV vs. silver/silver chloride. On the basis of the linear relationship between noise and working area, we can estimate that with our ITO band ($500 \mu\text{m} \times 200 \mu\text{m}$), baseline fluctuation should be approximately 10 pA at high potential. Noting that the average maximum current of dopamine release from individual exocytotic events recorded with CFE is in between 2 to 3 pA, although the working potential in this project was lower, 650 mV, which may help weaken the background, the noise was still a foreseeable serious obstruction for exocytosis recording. Considering relative high noise as the intrinsic drawback, for sake of improving the S/N ratio of exocytotic release monitoring with amperometry using ITO, signal enhancement is desperately needed.

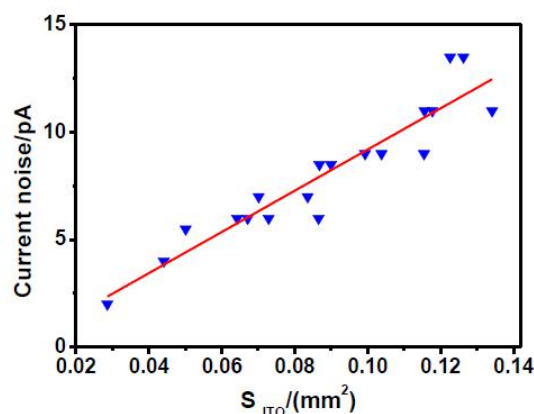


Fig. 4.7 The electrical noise of ITO microelectrodes in PBS (pH=7.4) measured at the potential 900 mV vs. Ag/AgCl as a function of surface dimensions ($y=95.9x-0.4$, $R^2=0.875$). Figure adapted from reference [13].

Inspired by the adequate enrichment of dopamine into vesicle lumen reported by Sombers et.al., we referred their loading procedure to carry out vesicular content filling in our PC12 cell line [14, 15]. L-DOPA can active permeate through the cellular membrane. As a substrate of decarboxylase, L-DOPA was converted into dopamine and addressed to vesicles through monoamine transporter. Here, we examined the amperometric signal enhancement owing to dopamine supplement. As shown in table 4.1, the average detected charge from exocytotic events experienced an evident increase from 85.6 ± 10.8 fC to 203.3 ± 14.7 fC within a 60 min incubation of 100 μ M L-DOPA. Peak current (peak height) also displayed an obvious enhancement after L-DOPA incubation. The augmentation of I_{max} and Q were in the same ratio ca. 2.5. Accordingly, average value of t_{FWHM} related to the width of the peak were practically maintained. The distributions of t_{FWHM} from control cells and L-DOPA loaded cells with p value $\gg 0.01$ presented in Fig. 4.8 further indicates similarity of t_{FWHM} in these two groups (p=0.65, WMW test). All the variation on features of detected spikes depict the secretory release with higher amount and flux but same duration resulting from the incubation of L-DOPA. It confirms the successful vesicle content enrichment of dopamine without disturbing the dynamics of fusion pore development. The significant elevation of the amount of dopamine stored inside vesicles should enhance the electrochemical signal recorded by ITO during coupling detection.

Table. 4.1 Main features of the detected spikes at control cells “none” and pre-incubated cells “100 μ M 1h”; detected charge Q , peak current I_{max} , and duration at half peak height t_{FWHM} . Secretion was monitored at 12 single cells in each experimental condition. Reported values are mean \pm SEM

L-DOPA	Q /fC	I_{max} /pA	t_{FWHM} /ms
none	85.6 ± 10.8	2.3 ± 0.2	28.4 ± 1.8
100 μ M 1h	203.3 ± 14.7	6.3 ± 0.5	27.1 ± 1.0

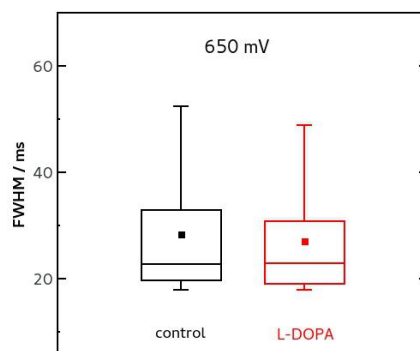


Fig. 4.8 Feature of the duration at half peak height distributions in detection of dopamine (650mV) at control cells and L-DOPA loaded cells. Horizontal lines correspond to the three first quartiles, whiskers span the 5%-95% range and plain dot indicates the mean value. p value=0.65 obtained from Mann-Whitney-Wilcoxon test (R software).

4.3.2 Discrepancy of current spike recorded from ITO microelectrode and CFE

Sole amperometry measurement of exocytotic release from single living cell is routinely to be achieved by positioning CFE on the cell apex forming an “artificial synapse”. For ensuring optical signal penetration in our coupling detection system, transparent ITO is applied as conductive substrate on the bottom of cell for electrochemical signal collection. In both case, as soon as the electroactive molecules are released through fusion pore to external space, they are immediately (ca. μ s) oxidized at the electrode surface, detected as a sharp current spike lasting tens of milliseconds. However, distinct quantitative and temporal parameters for characterization of exocytosis of PC12 cells from the apex measurement with CFE and the basal measurement with ITO were observed as reported for other cell types [16, 17]. Fig. 4.9 shows the typical example of current spikes intercepted from amperogram recorded with our ITO device and 10 μ m CFE, respectively. The characteristics of secretions recorded at the apex with CFE differed from those at the bottom with ITO. Although duration of secretory release are systematically analogue recorded from the apex and the base of the cell, the maximum oxidation current I_{max} was approximate 4 times lower at the apical pole. In other words, the flux of dopamine discharged from apical located vesicle was in a much slower kinetics compared to that from basal vesicle. In addition, the mean amount of dopamine released

from each exocytotic event is also larger from the basal located vesicle than from the apical one.

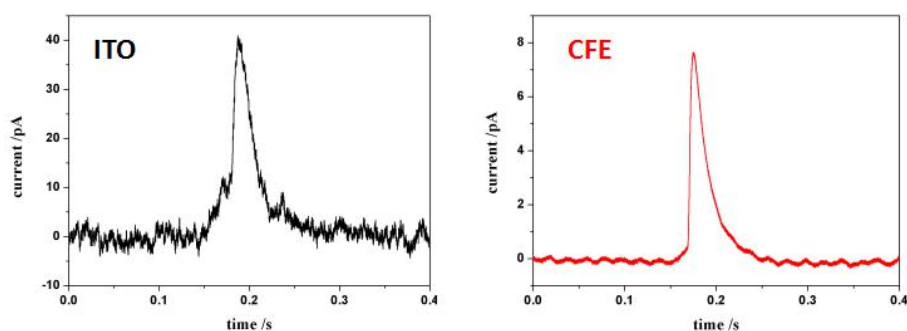


Fig. 4.9 Typical example of amperometric spikes representing exocytosis from L-DOPA loaded vesicles in PC12 cells recorded by ITO and CFE.

The suspicion of electrode materials as the source of the discrepancy on electrochemical behaviour was surmised once. However, it was challenged by the discovery that electrochemical behavior of adrenaline (catecholamine released during exocytosis from some cells) was consistent in vitro either detected at ITO or carbon electrodes[18]. In addition, this discrepancy can neither be ascribed to the slight difference of the gap between cell and detection electrode. The working area of either CFE or ITO is thousand times larger than the fusion pore formed during release, ensuring the collection of all released dopamine. Hence, the larger amount of release from basal pole can only be explained by the intrinsic distinct property from the events. To illustrate the distinct characteristic of cellular exocytosis obtained, we propose here two possible explanations/hypothesis as following:

(1) Discrimination on natures of release pools at different location

Our observed results show that exocytotic behaviour are radically different occurred at the basal or apical pole of the cell. In our point of view, the major distinction of amount of dopamine expelled to extracellular space with consistent release duration is either related to the dissimilar luminal storage of dopamine or corresponding to the discriminated fusion pore size developed at the two poles of the cell. Hence, it is rational to doubt that the discrepancy of release is assigned to the inherent heterogeneity on species of secretory pools.

(2) Difference of membrane tension at the top and bottom of cell

Membrane surface tension has been demonstrated to drastically modulate the dynamics of secretion when affected by external factors such as high osmolarity [19]. Membrane at the base pole adheres to the ITO substrate during stimulation and this contact is further

strengthened by Collagen IV. In contrast, membrane at the zenith of cell is directly exposed to the saline. The two distinct physical states of membrane may also contribute to the variation of fusion pore expansion, thus further altering the kinetics of release.

4.3.3 Influence of laser exposure on baseline of amperogram recorded with ITO

Feature of ITO microelectrode has been reported to be seriously affected by the irradiation of 405 nm laser [13]. The current baseline underwent a sudden increase when light with wavelength of 405 nm was exposed to the ITO surface. In addition, the electrical noise showed irregular fluctuation compared to that detected without laser exposure. Therefore, we checked the electrochemical behaviour of ITO band under 488 nm irradiation before coupling measurement. We explored the amperogram recorded by our ITO microelectrode under the potentials in close to 650 mV (potential applied in coupling measurement). The ITO surface was exposed to the laser illumination with critical angle imitating the total internal reflection condition achieved during coupling measurement. As shown in Fig. 4.10, the current baseline demonstrated a tiny raise with several pA under 800 mV. When applied potential was decreased to 600 mV, this baseline increase attenuates to inconspicuous value. It highlights that the influence from laser exposure of 488 nm on current baseline diminishes corresponding to the shrink of potential. In addition, this general slight elevation of baseline is not able to hinder or conceal the recording of current spikes. Moreover, the background noise maintained stable under laser irradiation compared with that recorded in normal condition regardless of potential. It shows that the influence of laser exposure during coupling measurement is sufficiently negligible, confirming the reliability of amperometric spike recorded from ITO.

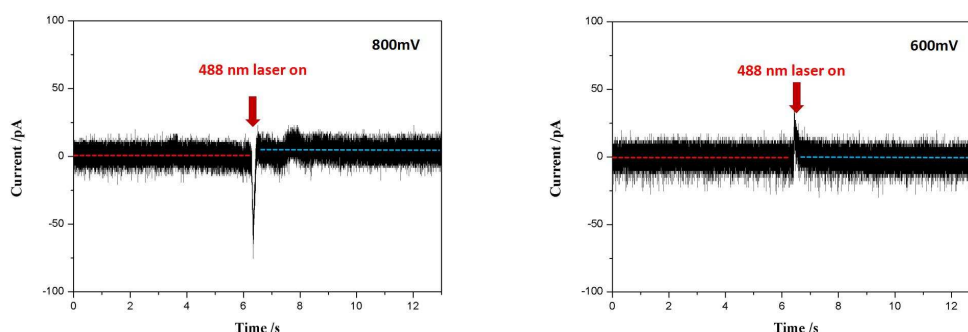


Fig. 4.10 Influence of 488 nm laser irradiation on the current noise with ITO device; Left: amperogram recorded under 800 mV, Right: amperogram recorded under 600mV. The arrow indicates the starting point of laser illumination. Red dash line and Blue dash line represent the current baseline without and with laser exposure, respectively.

4.3.4 Suppression effect of fusion pore on membrane protein diffusion

In terms of single exocytotic event, the initial opening of fusion pore formed through the fusion between vesicle membrane and cellular membrane leads to the vesicle cavity exposing to the external environment with higher pH. pHluorin towards the inner side of vesicle cavity modified on the vesicular membrane hence becomes immediately illuminated through the neutralization process. Hereafter, with various fusion pore evolution mode, pHluorin exhibits different behaviours. For example, it may either be transferred to the cellular membrane and diffused to the surrounding region along with the membrane fusion or maintained on vesicular membrane after the “flicker release” and the closure of fusion pore. Distinct behaviour of pHluorin expressed on vesicular membrane provides insight into the fusion pore evolution process. To use the fluorescence of pHluorin as an optical probe for membrane fusion extent analysis, its spontaneous spreading in the cellular membrane was first considered.

We estimated the ordinary diffusional dispersion pattern of VMAT2-pHluorin on cellular membrane. The value of VMAT2-pHluorin diffusion coefficient in PC12 cells ($0.1 \mu\text{m}^2/\text{s}$) reported by Rao et al. [20] was used and Gaussian function was applied for diffusion profile. Fig. 4.11 displays the variation of full width at 10% maximal intensity and the normalized central intensity of fluorescence plotted against time. It's obvious that in 300ms (~ 10 frames) pHluorin is able to diffuse to an extensive region ($\sim 1 \mu\text{m}$ in radius) with 10% of original fluorescent intensity in the center. However, exocytotic events observed under TIRFM indicate a slow elevation of fluorescence from the surrounding ROI ($\sim 1 \mu\text{m}$ in radius) in a longer period (~ 1 s). Moreover, the enhancement on the peripheral region compassing the exocytotic center can merely be ascribed to the migration of pHluorin from membrane fusion site. The contradiction encountered in between theoretical calculation and experimental observation about pHluorin expansion fully demonstrates that fusion pore junction plays a role in confining the diffusion of VMAT2-pHluorin from vesicular membrane to the cellular membrane. The difference between theoretical estimation and experimental observation about pHluorin expansion is consistent with the confinement of VMAT2-pHluorin by the small fusion pore [21].

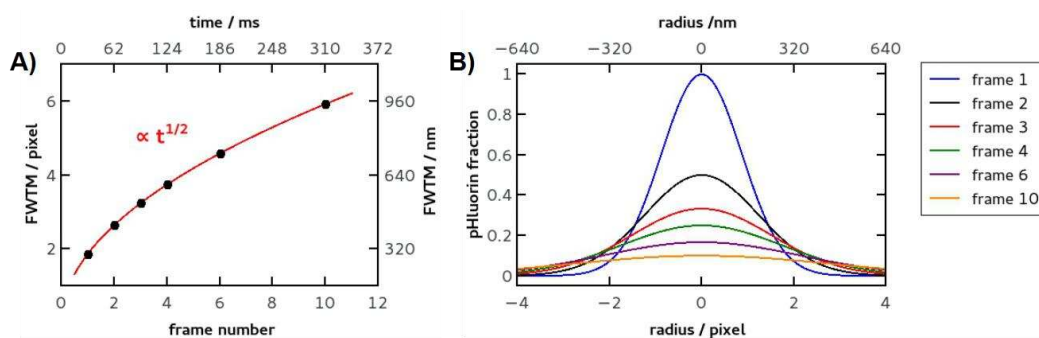


Fig. 4.11 2D-diffusion pattern simulation relying on Gaussian function. A) Full width at 10% of maximum fluorescence intensity changing as a function of time; B) Simulated Gaussian distribution of pHluorin on cellular membrane varying along with the diffusion time centered on zero.

4.3.5 Distinct exocytotic behaviours of vesicles assessed by coupling measurement

Exocytosis can be generally delineated into 4 steps: the loading of vesicle cargo, transportation of mature vesicle to ready-release region, docking to cellular membrane with subsequent fusion pore formation, and the secretory release accompanied with fusion pore expansion. The generation of cargo-enriched vesicle is occurred in the bulk of cell which is the blind zone under TIRFM observation. As soon as vesicle arrives within the TIRF zone close to cellular membrane, the trace of fluorescent labeled vesicle is able to be visually identified. Therefore, transport becomes the first exocytotic behaviour that may be captured by TIRFM. Vesicle membrane labeled by pH-dependent fluorescent protein is dimmed due to the tonical acidic environment inside vesicle lumen. Hence, vesicle's rush into the TIRF zone is monitored as the appearance of weak bright spot in the field of vision. Since the thin evanescent field excited by TIRF is merely hundreds of nanometers originated from membrane, the motion track of vesicle entered in this region is able to be clearly monitored. Vesicle may either retract back to the internal cell with fluorescence vanish, move parallel to the cellular membrane revealed as movement of bright spot in X-Y trajectories, or attach to cellular membrane preparing for release. The first two possibilities are not so related to our research motif, thus they are not fully described here. Attachment arouses the restriction in vesicle motion, visually corresponding to halt of spot movement. Owing to attachment of vesicle on cellular membrane, the biochemical condition of membrane docking is provided for preparation of final cargo delivery in fusion. All these described above is the pre-release process during single exocytotic event, which cannot be monitored with chronoamperometry. Here we pay more attention on exploring the exocytotic behaviour starting from the membrane fusion along with secretory release valuable monitored by simultaneous TIRFM and amperometric measurements.

Fusion of pHluorin labeled vesicular membrane with plasma membrane observed by TIRFM has been reported to induce brightening of pHluorin. This sudden enhancement is triggered by the higher pH of extracellular medium and has been used as a fusion pore opening reporter [22, 23]. Hence, we visually identified the sudden brightening spot as an indicator of single exocytotic event. The significant enhancement of fluorescence centered on the fusion site was considered as the onset of fusion pore development. It was manually aligned with the current spike recorded by amperometry following the time consistency principle (Fig. 4.12). 30 frames prior to fusion and a sequence of frames after release with fluorescence distribution variation were substacked from the movie. The normalized average intensity of fluorescence in ROIs from each frame $(F-F_0)/F_0$ were extracted to assemble the fluorescence trace. Thanks to the track of fluorescence in the annuli, lateral diffusion effect was taken into consideration. Although heterogeneity always exists in among independent exocytotic events, it's undeniable that exocytosis regulated by molecule machine follows specific rules to some extent. Here, relying on information collected from fluorescence trace and amperometric spikes, we generally classify observed exocytosis into two types: "open and close" and "full opening" in terms of fusion pore evolution. The two types of exocytotic behaviour from PC12 cells we observed are coincidence with key exocytotic modes from secretory cells reported in decades of studies [3, 24].

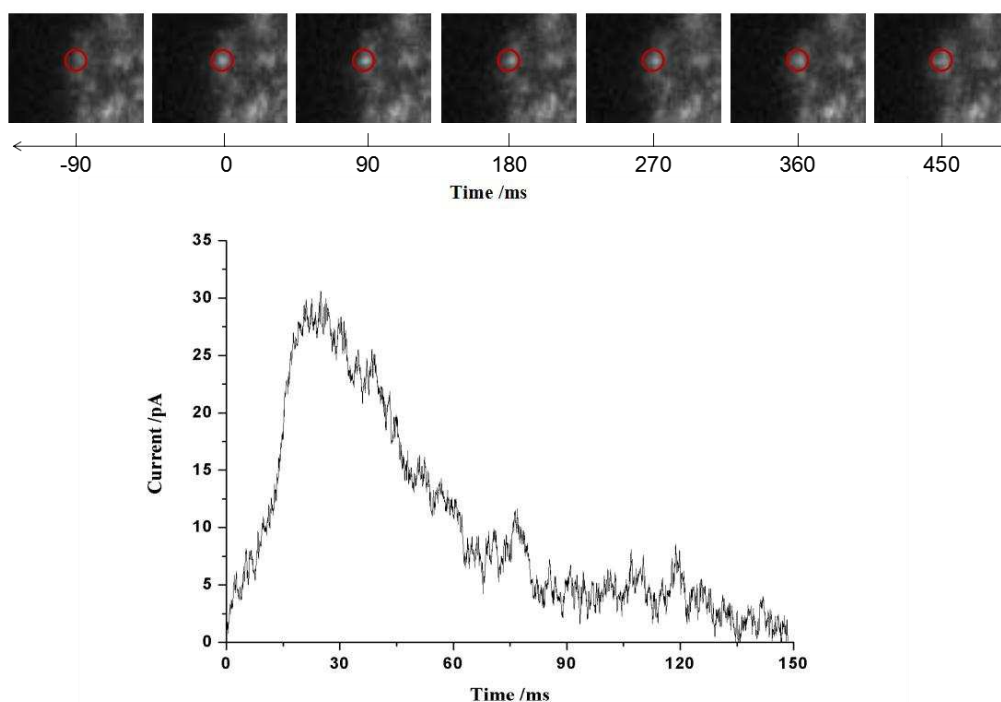


Fig. 4.12 A typical example of temporal correlated amperometric/fluorescent signal from single exocytotic event.

Type I : “open and close”

With respect to the assembly fluorescence trace extracted from TIRFM sequence imaging, exocytosis in this type can be visually divided into four stages (Fig. 4.13) according to fluorescence variation described as follows:

Stage 1: augmentation of central ROI fluorescence accompanied with annular ROI fluorescence increase

Stage 2: central ROI fluorescence decrease whereas annular ROI fluorescence increase (fed by central one)

Stage 3: central ROI fluorescence decrease and annular ROI fluorescence decrease with different rate, consistent with the interdiction of supplement to annulus from central part

Stage 4: central ROI fluorescence synchronous decline with annular ROI fluorescence

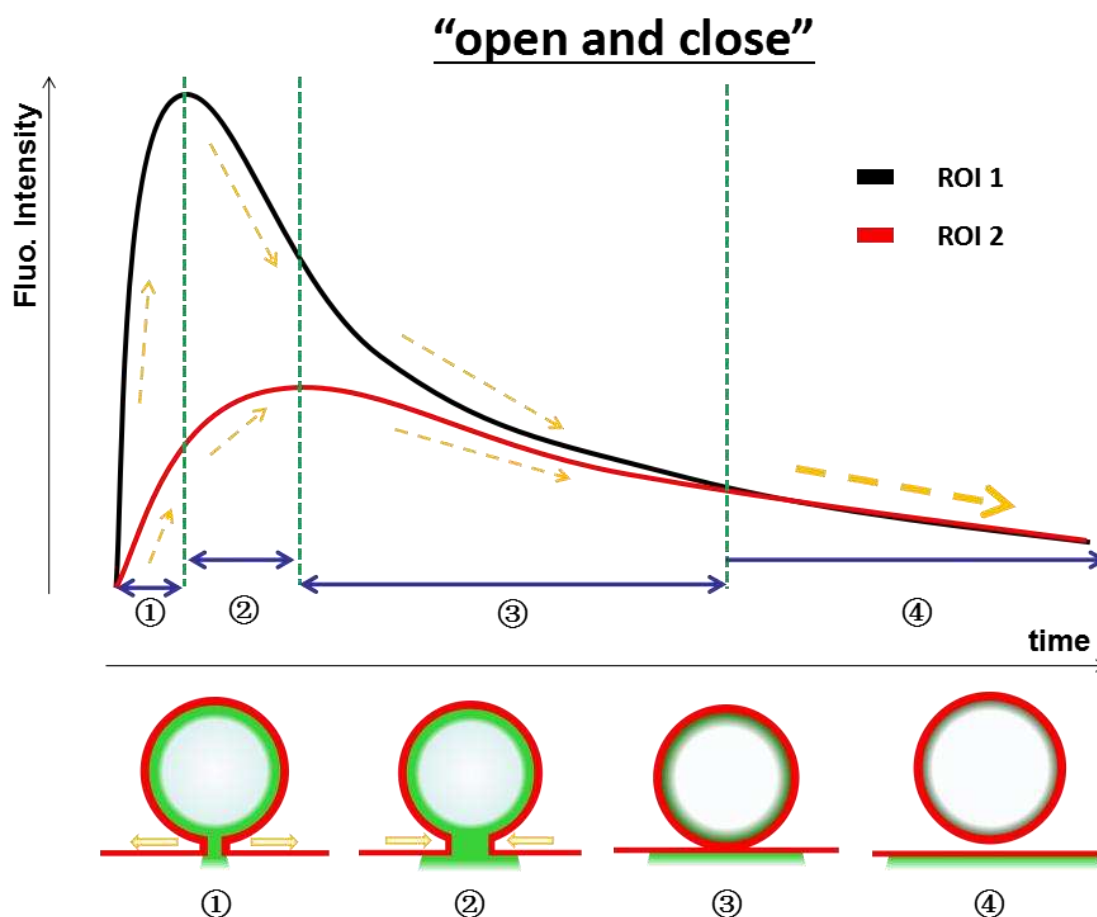


Fig. 4.13 A brief illustration of exocytotic behaviour in “open and close” mode from VMAT2-pHluorin stained PC12 cell. Fluorescence variation in stages were displayed and identified to distinct fusion pore status.

Hereafter, we discourse the attribution of fusion pore status to the fluorescence variation in each stage as well as secretory release taking a typical exocytotic event classified in Type I as

an example (Fig. 4.14). In stage 1, sudden brightening in the center is indisputably identified as the initial membrane fusion. This swift illumination period is well-known attributed to the efflux of proton to extracellular medium via fusion pore that caused the dequenching of pHluorin labeled on the inner membrane of vesicle. Secretory release of small neurotransmitters (mainly dopamine) recorded as a current spike in amperogram was occurred at the very beginning of fluorescence elevation. It demonstrates the initial opening of fusion pore has reached nanometric scale that allows the discharge of small molecules. The half width of secretory release recorded by ITO in this event is in the range of 30 ms, which is comparable to that measured with CFE, indicating a similar neurotransmitter emission. Even though restrained by the acquisition rate of camera, instant expansion of fusion pore at its early stage is out of observation. Fortunately, the application of synchronous amperometry measurement makes a compensation for this missing information. As soon as fusion pore evolution entered into stage 2, the contrast change of fluorescence in different regions of interest was observed. The obvious raise of integrated fluorescence in surrounding region can be interpreted as pHluorin transmission towards the outer ring area. Hence, it is safely to deduce that at this moment vesicle remained effectively in diffusional contact with cellular membrane with weakly lateral leakage of pHluorin occurred around the fusion pore. The rapid dim in the center of fusion site can be considered as the shrink of fusion pore along with the tendency of endocytosis. The continuous slow decrease of fluorescence in the annuli away from the center in both stage3 and 4 is speculated to represent the slow spreading of pHluorin remained on the cellular membrane. The halt of integrated fluorescence enhancement in the peripheral region in between stage 2 and 3 thus reveals the disconnection of vesicular and cellular membrane. The duration of fast decay in central region appeared in stage3 agrees well with measurements of the reacidification of vesicle cavity[25, 26]. Hence, it is most likely that in this stage, internalized vesicle was reacidified and aroused the proton quench of pHluorin in the lumen. At the terminal stage (stage4), with the departure of vesicle away from TIRF zone, fluorescence in each ROIs is merely corresponding to the concentration of residual pHluorin on the plasma membrane. Therefore, the gradual vanish of fluorescence in the whole region can only be ascribed to pHluorin spreading, as judged by the same decay rate displayed in the center and the surroundings.

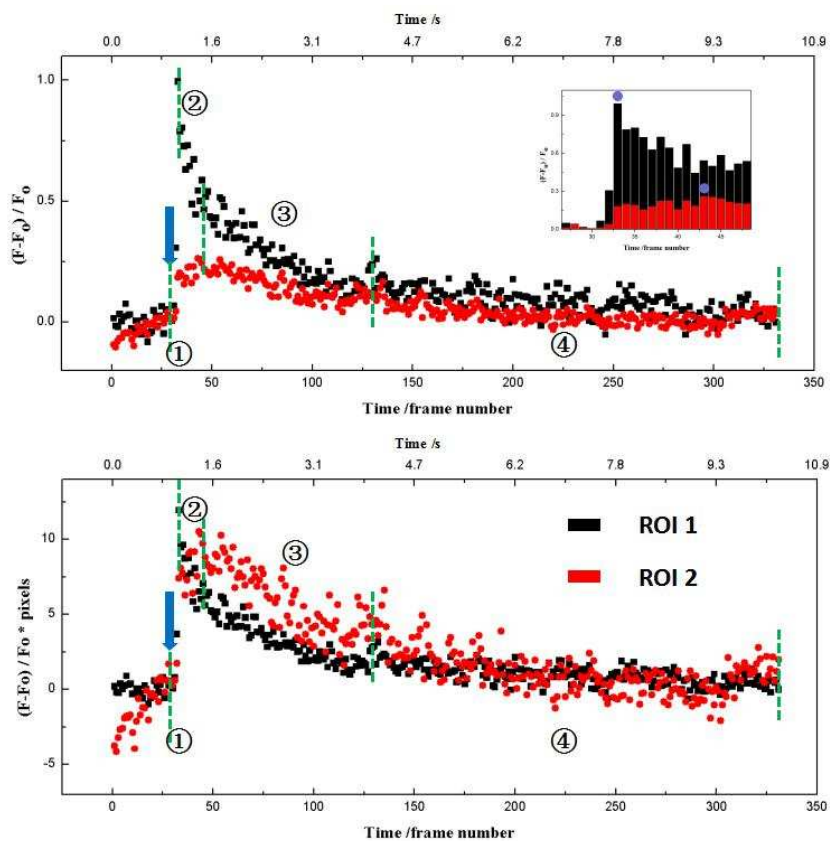


Fig. 4.14 A typical exocytotic event classified in Type I. Top: Average relative fluorescence extracted from each ROIs. Relative fluorescence are plotted as the change of fluorescence ($F-F_0$) divided by the background (F_0) as a function of time. Inset: Zoom in image of average fluorescence variation in stage 1 and 2. Purple dots demonstrate the maximal fluorescence arrival. Bottom: Integrated fluorescence curve in ROIs. Integrated fluorescence was calculated by multiplying relative fluorescence by number of pixel in corresponding ROIs. Blue arrows indicate the appearance of amperometric spike in electrochemical detection. Parameters of the current spike from this event are: $Q=1.57\text{pC}$, $I_{\text{max}}=30.8\text{pA}$, $t_{1/2}=32.4\text{ms}$. Green dash lines separate the vesicle behaviour into 4 stages labeled by serial number.

Type I includes all the events with similar vesicle behaviour of fusion pore expansion followed by closure, or called “extended kiss and run” mode among others [27, 28]. It’s important to note that there is no serious restriction on the degree of pore evolution rhythm or duration of each stage during classification. For example, we also observed some events showing an approximate plateau on the peak of fluorescence in ROI 1 taking fluctuation of fluorescence into account (see in Fig. 4.15). This period with stable fluorescence can be regarded as the elongation of fusion pore opening with its maximal size from transient moment to hundreds of milliseconds in the interval of stage1 and stage2. The maintenance of fluorescence in the center can be explained by the inner supplement of fluorescence loss in the fusion site caused by lateral spreading of pHLuorin to the surrounding region. The

inner supplement of fluorescence may be possibly achieved via dequenching of pHluorin deeply attached inside the vesicle by consequent proton outflow or the migration of pHluorin close to fusion pore with higher chance to be illuminated by neutral medium. In this case, the opening of fusion pore (stage 1) was prolonged compared to that observed from the typical transient extended fusion pore event. Current spike was also recorded at the halfway of central fluorescence enhancement, indicating the tiny size of fusion pore at the very beginning. Additionally, features of the spike showed a release with lower rate compared to the previous example. All the observations reflect a much slow dwell of fusion pore at the beginning of this event.

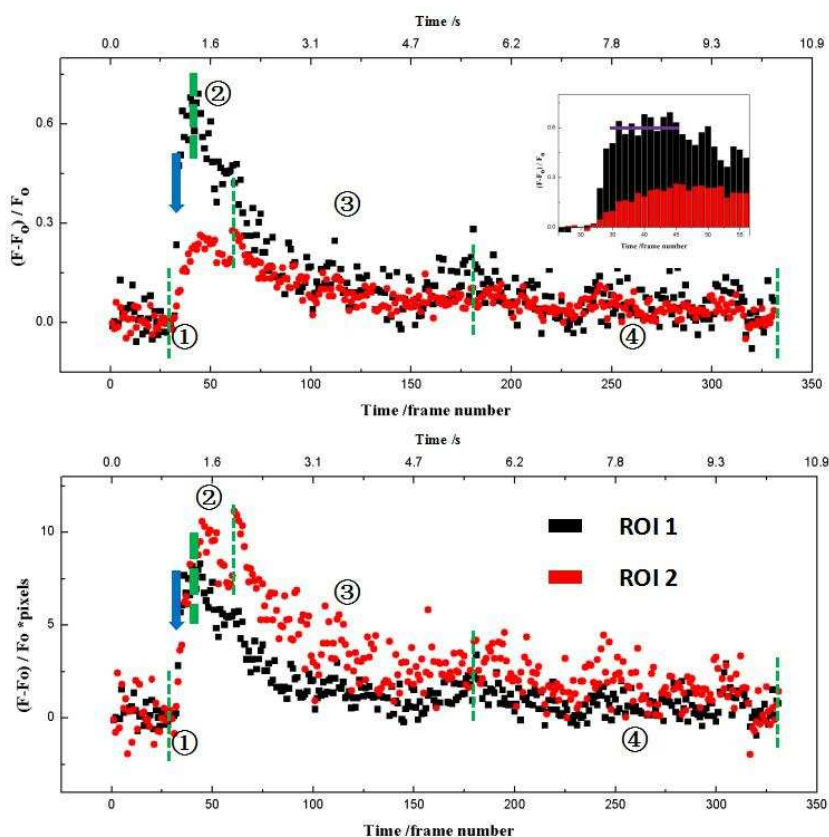


Fig. 4.15 A slightly mutated exocytotic event classified in Type I. Top: Average relative fluorescence in ROIs. Relative fluorescence are plotted as the change of fluorescence ($F-F_0$) divided by the background (F_0) against time. Inset: Amplified average fluorescence variation against time in stage 1 and 2. Purple lines indicate the plateau appeared in between stage 1 and 2. Bottom: Integrated fluorescence curve in ROIs. Integrated fluorescence was calculated by multiplying relative fluorescence by number of pixel in corresponding ROIs. Blue arrows indicate the appearance of amperometric spike in electrochemical detection. Parameters of the current spike from this event are: $Q=0.59\text{pC}$, $I_{\text{max}}=22.9\text{pA}$, $t_{1/2}=23.2\text{ms}$. Vesicle behaviour is separated into 4 stages with green dash line and labeled by serial number. Green dash line for isolating stage 2 was bold for emphasizing the arrival of fluorescence at a plateau.

Type II : “full opening”

Apart from the those events representing typical behaviour that belongs to Type I, in many cases the whole process of exocytosis was observed to advance in another approach. According to the features of fluorescence variation in ROIs, in this type II of exocytosis fusion pore evolution can also be separated into 4 stages (Fig. 4.16).

Stage 1: augmentation of central ROI fluorescence accompanied with annular ROI fluorescence increase with different rate

Stage 2: central ROI fluorescence presenting almost indiscernible decrease with annular ROI fluorescence preservation

Stage 3: central ROI fluorescence decrease whereas annular ROI fluorescence enhance (fed by central one)

Stage 4: central ROI fluorescence synchronous decline with annular ROI fluorescence

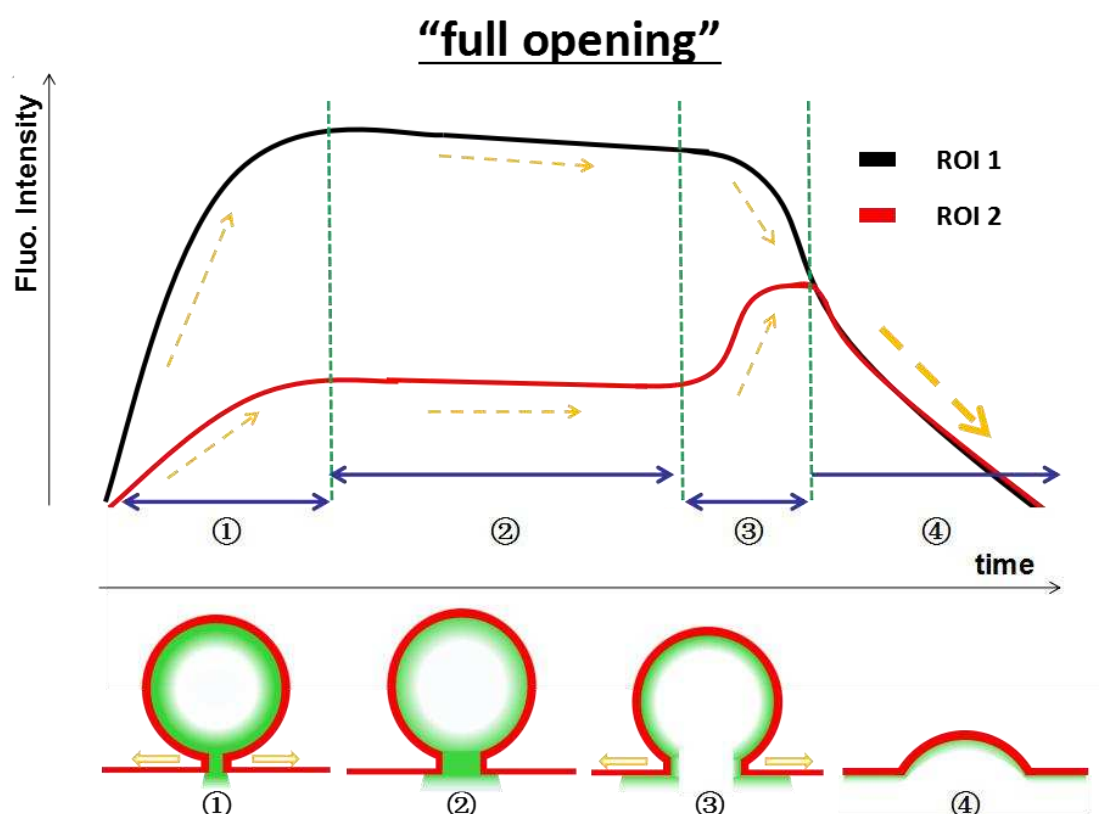


Fig. 4.16 A brief illustration of exocytotic behaviour in “full opening” mode from VMAT2-pHluorin stained PC12 cell. Fluorescence variation in stages were displayed and identified to distinct fusion pore status.

Fluorescence variation rule in Type II exocytosis was also identified to dynamic fusion pore status relying on a representative instance shown in Fig. 4.17. In stage 1, vesicle showed an unanimous behaviour as that recorded in Type I. The sudden enhancement of fluorescence in this stage is undoubtedly ascribed to the fusion pore formation and expansion. However, it

seems that fluorescence in the center experienced a persistent elevation after fusion pore opening. The dim rate of centered fluorescence in stage 2 is almost approaching to zero. At the same time, peripheral fluorescence also arrived at a “steady-state”, representing as a constant intensity within the whole stage. This phenomenon fits well with the status that vesicular membrane maintains connecting to cellular membrane with a stationary fusion pore. Small amount of illuminated pHluorin step over the boundary of ROI 1 and ROI 2 to peripheral region can result in the slightly diminish of centered fluorescence. While this supplement of pHluorin in ROI 2 happens to offset the loss of fluorescence in this region due to the progressive spreading further away into the membrane bulk, thus ensuring the stable fluorescence emission. The evident fade of fluorescence in the centered region accompanied with the elevation of fluorescence in the surrounding region during stage 3 most likely present the collapse of vesicle construction to the cellular membrane. Therefore, the synchronous fluorescence vanish from both ROIs in the last stage is identified as overall pHluorin spreading. In addition, according to Faraday’s law, the amperometric spikes secretory release from this event showed an urgent flux with relative larger amount within a longer time compared to that recorded in Type I. It works in concert with the full release of entire vesicular content allowed by membrane collapse instead of the reasonable partial release due to the final closure of fusion pore.

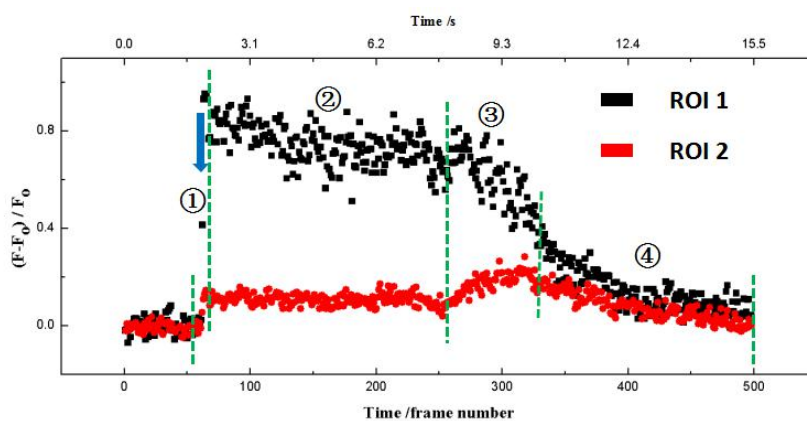


Fig. 4.17 A representative exocytotic event classified in Type II. Average relative fluorescence in ROIs were assembled and displayed in time course. Relative fluorescence are plotted as the change of fluorescence ($F-F_0$) divided by the background (F_0). Blue arrows indicate the appearance of amperometric spike in electrochemical detection. Parameters of the current spike from this event are: $Q=2.47\text{pC}$, $I_{max}=38.8\text{pA}$, $t_{1/2}=44.9\text{ms}$. Green dash lines separate the vesicle behaviour into 4 stages labeled by serial number.

Analogously, exocytotic events sorted into Type II also present consistent behaviour with various duration in each stage. Fig. 4.18 demonstrates an exocytotic event with fast membrane collapse process. Membrane fusion with fixed pore size during stage 2 was reduced to a instant moment, displaying as a transient elevation of centered fluorescence rather than a persistent one. Compared to the representative behaviour of exocytosis in Type II, this vesicle entirely merged into cellular membrane after the formation of fusion pore without any delay.

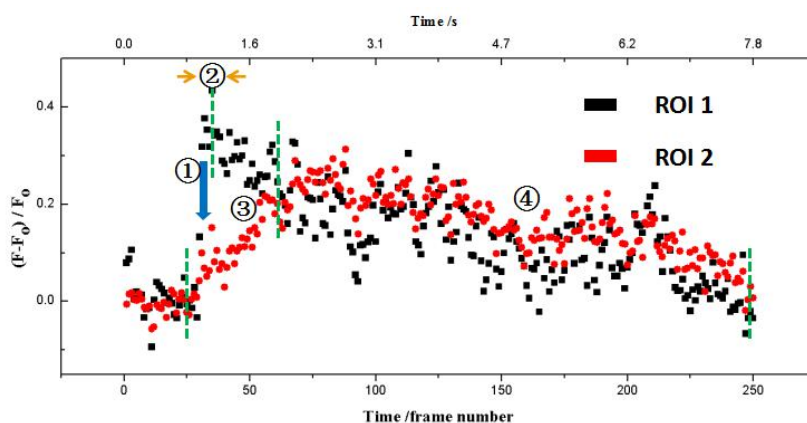


Fig. 4.18 An instance of varied exocytotic event classified in Type II. Changing on vesicle status was recorded as average relative fluorescence in ROIs distinguished along with the time. Relative fluorescence are plotted as the change of fluorescence ($F-F_0$) divided by the background (F_0). Blue arrows indicate the appearance of amperometric spike in electrochemical detection. Green dash lines indicates the boundary in between different stages of vesicle status. Noting that current spike in this event was concealed in a group of two tightly overlapping spikes, the parameters for single spike feature is not presented here.

Rare behaviour of vesicle during exocytosis

Interestingly, except the two main types of exocytosis described above, a bizarre event with two steps of centered fluorescence elevation (indicated with yellow arrows in Fig. 4.19) was observed. This behaviour can be possibly related to an uncommon mode of secretion discovered previously - compound exocytosis [29], during which a second vesicle came from the bulk of cell links to the first vesicle that has already been attached on the cellular membrane with membrane fusion. Then the first plateau arrived during fluorescence enhancement in the fusion site is testified as the fusion pore within a constant diameter after the docking of first vesicle to the cellular membrane. The centered fluorescence kept a specified value following a sudden increase is consistent with behaviour recorded in both Type I and Type II in a part of cases. And the second rapid enhancement with its subsequent maintenance of fluorescence intensity can be simply considered as the appearance of second vesicle adherent on the first vesicle surface in the TIRF zone. The continuous growth

of peripheral fluorescence in ROI 2 during the same period confirms the conjunction of first vesicle with plasma membrane. However, compound exocytosis, which is still controversial to some extent, is not the only possibility to explain this two steps' elevation. Single vesicle with two stages of fusion pore opening offers another feasibility. Miniature fusion pore formed in the first step kept its dimension in seconds and then followed by the second time expansion is also able to cause the fluorescence elevation in the center with two evident plateaus. In addition, It's most likely that the tiny amperometric signal resulted from the small amount of release limited by miniature pore was obscured in background noise due to the technique limitation. Hence, we are not capable of realizing the fusion pore dimension through electrochemical measurement in this event. Although restrained by the measurement, we can only propose possibilities instead of clearly interpreting the vesicle behaviour in this case. It is certain that the behaviour of vesicle hereafter abided by the general mode of Type I indicating vesicle retrieval and its reacidification.

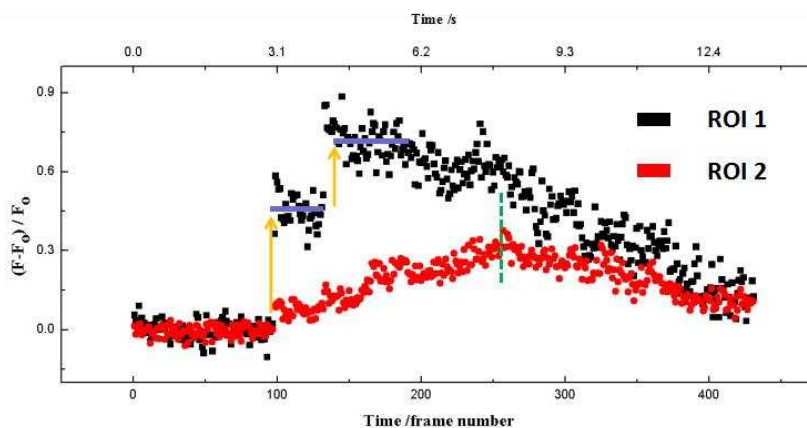


Fig. 4.19 A rare vesicle behaviour observed from VMAT2-pHluorin stained PC12 cell with vesicle content enrichment of L-DOPA. Average relative fluorescence calculated as the change of fluorescence ($F-F_0$) divided by the background (F_0) in ROIs were plotted against time. Yellow arrows prompt the two-step increase of fluorescence in ROI 1 with plateaus marked by purple lines. Green dash lines indicates the zenith of fluorescence in ROI 2 which represents the turning point of vesicle behaviour.

4.3.6 General view of vesicle behaviour in exocytosis

By monitoring fluorescence from region of interests, exocytotic events ($n=21$) from two individual cells were monitored and classified into Type I and Type II excluding those rarely appeared events with complex behaviour. The majority of stimulated events ($n=17$, 81%) were identified as Type I exocytosis while the rest of events ($n=4$, 19%) were sorted into Type II exocytosis. Apparently, stimulated exocytosis in our imaging experiment most likely consist of the transient opening of fusion pore followed by its re-closure rather than full fusion. Therefore, it probably indicates that vesicle exocytosis from PC12 cells triggered by

stimulation prefers the non-full-collapse manner, which is in accordance with the reported conclusion obtained from PC12 cells [28] and other analogous cell model for exocytosis investigation [30, 31]. 8 events were recorded with aligned amperometric/fluorescent signal from “open and close” mode, while 1 event was recorded from “full opening” mode. The failure of fluo-ampero signal alignment is ascribed to the obscure of individual current spike underneath multiple peak stacking, thus inducing the recorded electrochemical signal from these events to be less informative. As shown in table 4.11, the detected charge of release from “open and close” events was in the lower range compared to that from “full opening” event: 0.21-1.6 pC vs. 2.4 pC, respectively. It’s obvious that the charge recorded from “full opening” mode is approximate 1.5 times than the largest charge recorded in “open and close” mode, in accordance with the fact that “full opening” of fusion pore leads to complete release of vesicle cargo whereas “open and close” of fusion pore enables partial release. In additional, from hundreds of secretory events from PC12 cells collected with CFE (data used in Chapter 2), we realized the heterogeneity of catecholamine release as well. Approximately 5% of events displayed outstanding discharge amount out of the others. Although the occupancy of large release looked slightly lower than that observed with ITO during amperometric/fluorescent combined detection, the heterogeneity on release still powerfully proves the existence of two exocytosis mode.

Exocytosis mode	Number of events traced by TIRFM	Number of events with amperometric/fluorescent signal aligned	Detected range of release charge (pC)
“open and close”	17	8	0.21-1.6
“full opening”	4	1	2.4

Table. 4.1 General information derived from “open and close” and “full opening” exocytosis (n=2 cells).

4.4 Conclusion and perspective

In this work, we have identified two typical patterns of vesicle behaviour during exocytosis from PC12 cell line based on observation via electrochemical-optical combined method amperometry with TIRFM. On account of the heterogeneity on local fluorescence variation in fusion site as well as kinetic fluorescence spreading occurring in the surrounding annulus, exocytotic events from PC12 cells were sorted into two types with respect to fusion pore: “open and close” and “full opening”. These two exocytosis modes are consistent with the main forms of exocytosis reported from secretory cells discovered by single detection method. Amperometric spikes synchronously recorded with the sequence imaging

supplemented the amount of released neurotransmitters supporting evidence of heterogeneity in release mode. Moreover, we have observed that in PC12 cells, under regular polarization with K⁺, the "open and close" mode mostly occurs.

This combined observation offers the opportunity to explore the subtle variations not only on vesicular membrane but also on secretory release during the entire exocytotic events. This approach provides electrical and optical measurement for the same event, which is valuable to investigate the discrepancy between interpretation of fusion pore behavior relying only on electrical (amperometry and capacitance measurement) or fluorescence measurements. With the prerequisite of enhancing the signal to noise ratio for both amperometry and fluorescence measurement, this TIRFM and amperometry combined detection affords an attractive potential in quantitative analysis of exocytosis.

4.5 References

1. A. Albillos, G. Dernick, H. Horstmann, W. Almers, G. Alvarez de Toledo, M. Lindau, *The exocytotic event in chromaffin cells revealed by patch amperometry*. *Nature*, 1997. **389**(6650): p. 509.
2. G. Dernick, G. A. de Toledo, M. Lindau, *Exocytosis of single chromaffin granules in cell-free inside-out membrane patches*. *Nature Cell Biology*, 2003. **5**(4): p. 358.
3. L. He, X. Wu, R. Mohan, L. Wu, *Two modes of fusion pore opening revealed by cell-attached recordings at a synapse*. *Nature*, 2006. **444**(7115): p. 102.
4. V. A. Klyachko, M. B. Jackson, *Capacitance steps and fusion pores of small and large-dense-core vesicles in nerve terminals*. *Nature*, 2002. **418**(6893): p. 89.
5. S. O. Rizzoli, R. Jahn, *Kiss-and-run, collapse and 'readily retrievable' vesicles*. *Traffic*, 2007. **8**(9): p. 1137-1144.
6. D. A. Richards, J. Bai, E. R. Chapman, *Two modes of exocytosis at hippocampal synapses revealed by rate of FM1-43 efflux from individual vesicles*. *J Cell Biol*, 2005. **168**(6): p. 929-939.
7. A. A. Alabi, R. W. Tsien, *Perspectives on kiss-and-run: role in exocytosis, endocytosis, and neurotransmission*. *Annual review of physiology*, 2013. **75**: p. 393-422.
8. A. L. Mattheyses, S. M. Simon, J. Z. Rappoport, *Imaging with total internal reflection fluorescence microscopy for the cell biologist*. *J Cell Sci*, 2010. **123**(21): p. 3621-3628.
9. A. Oleinick, I. Svir, C. Amatore, *'Full fusion' is not ineluctable during vesicular exocytosis of neurotransmitters by endocrine cells*. *Proc. R. Soc. A*, 2017. **473**(2197): p. 20160684.
10. L. Ren, L. J. Mellander, J. Keighron, A. Cans, M. E. Kurczyk, I. Svir, A. Oleinick, C. Amatore, A. G. Ewing, *The evidence for open and closed exocytosis as the primary release mechanism*. *Quarterly reviews of biophysics*, 2016. **49**.
11. D. M. Omiattek, Y. Dong, M. L. Heien, A. G. Ewing, *Only a fraction of quantal content is released during exocytosis as revealed by electrochemical cytometry of secretory vesicles*. *ACS chemical neuroscience*, 2010. **1**(3): p. 234-245.

12. A. Meunier, O. Jouannot, R. Fulcrand, I. Fanget, M. Bretou, E. Karatekin, S. Arbault, M. Guille, F. Darchen, F. Lemaître, C. Amatore, *Coupling amperometry and total internal reflection fluorescence microscopy at ITO surfaces for monitoring exocytosis of single vesicles*. *Angewandte Chemie International Edition*, 2011. **50**(22): p. 5081-5084.
13. X. Liu, *More transparency in bioanalysis of exocytosis: application of fluorescent false neurotransmitters in coupling methodology of electrochemistry with fluorescence microscopy at ITO microelectrodes*. 2016, Paris 6.
14. L. A. Sombers, H. J. Hanchar, T. L. Colliver, N. Wittenberg, A. Cans, S. Arbault, C. Amatore, A. G. Ewing, *The effects of vesicular volume on secretion through the fusion pore in exocytotic release from PC12 cells*. *Journal of Neuroscience*, 2004. **24**(2): p. 303-309.
15. L. Sombers, M. Maxson, A. Ewing, *Loaded dopamine is preferentially stored in the halo portion of PC12 cell dense core vesicles*. *Journal of neurochemistry*, 2005. **93**(5): p. 1122-1131.
16. X. Liu, L. Hu, N. Pan, L. Grimaud, E. Labbé, O. Buriez, J. Delacotte, F. Lemaître, M. Guille-Collignon, *Coupling electrochemistry and TIRF-microscopy with the fluorescent false neurotransmitter FFN102 supports the fluorescence signals during single vesicle exocytosis detection*. *Biophysical chemistry*, 2018. **235**: p. 48-55.
17. C. Amatore, S. Arbault, F. Lemaître, Y. Verchier, *Comparison of apex and bottom secretion efficiency at chromaffin cells as measured by amperometry*. *Biophysical chemistry*, 2007. **127**(3): p. 165-171.
18. C. Amatore, S. Arbault, I. Bonifas, M. Guille, F. Lemaître, Y. Verchier, *Relationship between amperometric pre-spike feet and secretion granule composition in chromaffin cells: an overview*. *Biophysical chemistry*, 2007. **129**(2-3): p. 181-189.
19. C. Amatore, S. Arbault, I. Bonifas, F. Lemaître, Y. Verchier, *Vesicular exocytosis under hypotonic conditions shows two distinct populations of dense core vesicles in bovine chromaffin cells*. *ChemPhysChem*, 2007. **8**(4): p. 578-585.
20. T. C. Rao, D. R. Passmore, A. R. Peleman, M. Das, E. R. Chapman, A. Anantharam, *Distinct fusion properties of synaptotagmin-1 and synaptotagmin-7 bearing dense core granules*. *Molecular biology of the cell*, 2014. **25**(16): p. 2416-2427.
21. J. G. Burchfield, J. A. Lopez, K. Mele, P. Vallotton, W. E. Hughes, *Exocytotic vesicle behaviour assessed by total internal reflection fluorescence microscopy*. *Traffic*, 2010. **11**(4): p. 429-439.
22. Ohara-Imaizumi, M., et al., *Monitoring of exocytosis and endocytosis of insulin secretory granules in the pancreatic β -cell line MIN6 using pH-sensitive green fluorescent protein (pHluorin) and confocal laser microscopy*. *Biochemical Journal*, 2002. **363**(1): p. 73-80.
23. M. Ohara-Imaizumi, Y. Nakamichi, T. Tanaka, H. Katsuta, H. Ishida, S. Nagamatsu, *The use of pHluorins for optical measurements of presynaptic activity*. *Biophysical journal*, 2000. **79**(4): p. 2199-2208.
24. Z. Zhang, Y. Wu, Z. Wang, F. M. Dunning, J. Reh fuss, D. Ramanan, E. R. Chapman, M. B. Jackson, *Release mode of large and small dense-core vesicles specified by different synaptotagmin isoforms in PC12 cells*. *Molecular biology of the cell*, 2011. **22**(13): p. 2324-2336.
25. S. P. Gandhi, C. F. Stevens, *Three modes of synaptic vesicular recycling revealed by single-vesicle imaging*. *Nature*, 2003. **423**(6940): p. 607.

26. P. P. Atluri, T. A. Ryan, *The kinetics of synaptic vesicle reacidification at hippocampal nerve terminals*. Journal of Neuroscience, 2006. **26**(8): p. 2313-2320.
27. R. I. Trouillon, A. G. Ewing, *Actin controls the vesicular fraction of dopamine released during extended kiss and run exocytosis*. ACS chemical biology, 2014. **9**(3): p. 812-820.
28. L. J. Mellander, R. Trouillon, M. I. Svensson, A. G. Ewing, *Amperometric post spike feet reveal most exocytosis is via extended kiss-and-run fusion*. Scientific reports, 2012. **2**: p. 907.
29. L. Wu, E. Hamid, W. Shin, H. Chiang, *Exocytosis and endocytosis: modes, functions, and coupling mechanisms*. Annual review of physiology, 2014. **76**: p. 301-331.
30. A. Elhamdani, F. Azizi, C. R. Artalejo, *Double patch clamp reveals that transient fusion (kiss-and-run) is a major mechanism of secretion in calf adrenal chromaffin cells: high calcium shifts the mechanism from kiss-and-run to complete fusion*. Journal of Neuroscience, 2006. **26**(11): p. 3030-3036.
31. E. Alés, L. Tabares, J. M. Poyato, V. Valero, M. Lindau, G. Alvarez de Toledo, *High calcium concentrations shift the mode of exocytosis to the kiss-and-run mechanism*. Nature Cell Biology, 1999. **1**(1): p. 40.

Chapter 5: General conclusion and perspective

Exocytosis is one of the most commonly used pathway for signal exchange in achieving intercellular communication. Generally, chemical/biochemical molecules acting as signal messengers carrying specific information are internalized into transmission carrier - vesicle at the beginning of exocytosis. Following the transportation of vesicle close to the release site adjacent to cellular membrane, coalescence of interfaced vesicular membrane and cellular membrane supported by SNAREs traction induces the formation of submicrometric fusion pore. As a signal channel connecting intracellular and extracellular space, the fusion pore is responsible for expelling these messengers. Within the mediation of some biological mechanisms like myosin II based one we focused on, the fusion pore enlargement or contraction is capable to be controlled and then release of various messengers with a multitude of molecule weight is further able to be regulated. Messenger discharge process as the crucial stage of exocytosis for dominating intracellular signal transmission attracts attention. Our research interest in this work is thus to analyze the exocytosis from PC12 cells particularly focusing on the secretory release and its associated fusion pore evolution.

Secretory release as the most intuitive and external manifestation of exocytosis process was first investigated. We have demonstrated the suitability of synthesized natural neurotransmitter analog FFN102 to be used as a probe for bioanalytical studies at a widely used secretory cell model - PC12 cells. With respect to the fact that cellular endogenous neurotransmitter dopamine and FFN102 are oxidized at different potentials, discrimination on the population of both species in FFN102 treated cells with amperometry is capable of being achieved. We realized that the uptake of FFN102 led to the partial replacement of dopamine in secretory vesicles. Moreover, the storage of FFN102 mostly occurred in fast diffusion compartment of the vesicles supported by the evidence that FFN102 was overreleased through the initial fusion pore. Furthermore, compared to traditional individual amperometric recording of small neurotransmitter release relying on dopamine, the availability of FFN102 as a bioanalytical probe expanded the diversity of secretory release measurement owing to its additional fluorescent property. The partial replacement of dopamine opened a new opportunity to monitor exocytotic events through electrochemical detection of dopamine and fluorescence detection of FFN102. This approach could be of interest to overcome the possible shortcoming of the high oxidation potential of FFN102.

The comprehensive observation of small neurotransmitter release is worth to shed light on fusion pore expansion that controls the recorded release process. Relying on a previously

established fast analytical model, fusion pore size was extracted from a given amperometric spike recorded during secretory release. The reconstruction afforded us a chance to analyze the behaviour of fusion pore with high temporal resolution during small neurotransmitter release at single vesicle level. The relative precision of fusion pore size restored from current spike provided its great potential to be applied in fusion pore regulation mechanism research. In our case, by statistical analysis of performance of fusion pore relying on reconstruction, we investigated the role of molecular motor myosin II in regulating fusion pore expansion. The inhibition of myosin II accelerated the fusion pore opening to its maximum during neurotransmitter release whereas the amount of cargo secreted remained similar. In addition, larger population of exocytotic events showed big fusion pore size with myosin II activity inhibition. Further in light of the relative unrestrained opening of fusion pore after interference on myosin II supported by higher occurrence of events with double exponential decay in amperometric recording.

Beyond the development of fusion pore size confined at the stage of small neurotransmitter release, we broadened our research scope to the fusion pore evolution in entire process of exocytosis. Via simultaneous monitoring of both neurotransmitter release with amperometry and the fate of vesicular membrane with TIRFM, the fusion pore state during exocytosis can be completely monitored and associated with the secretory release occurring through it. According to the literature on fusion pore action, exocytosis events were generally identified into two major modes: “open and close” and “full opening” of the vesicle membrane with the cellular membrane. The regular pattern of fusion pore development in each mode was summarized and further sustained by the associated neurotransmitter release. We observed that the fusion pore expansion experienced in a longer procedure than depicted by secretory release. It valuably supported that secretory release of small neurotransmitter occurred at the beginning of fusion pore expansion before its expansion. The systematic alignment of optical and electrochemical measurements from single vesicle allowed us to integrate information collected from different measurements with distinct time scale. The coupling method combining TIRFM/amperometry hence showed a promising prospect for inspection of exocytosis in a whole footprint. For instance, by altering the fluorescent labeled substance to vesicle cargo, one may selectively visualize release of differential vesicular content component that is unrevealed by electrochemical detection, and thus making great contributions to the understanding of secretory release.

Supporting information

I. Quantitative extraction of fusion pore expansion from amperometric spikes by means of simulation

Although several mature measurement techniques have been established for monitoring the trend of fusion pore development during exocytosis, the dynamics of fusion pore expansion as well as the actual size of the pore are still concealed beneath the detection. Extraction of these information represents a challenging problem in current research. In order to be informative on the kinetic fusion pore size from its corresponding amperometric spike, simulations become indispensable. Here, we would like to briefly illustrate the simulation procedure used in Chapter 3 for extracting the real time variations of fusion pore radius based on recorded current spikes. The theoretical model was established on chromaffin cell [1]. It was kindly supported by Alexander OLEINICK, our close collaborator.

1.1 Full simulations about diffusion through constant surface area

Diffusion from a spherical container has become a well known physicochemical problem for a long time. Dealing with sphere cooling system, Newton and Kelvin first proposed that the quantity diffused from within a spherical body with a full open surface follows an exponential law. In our earlier works, we promoted this exponential law to the case when diffusion occurring only through a fraction of spherical surface with the help of full scale simulations [2, 3]. Owing to the specific design of quasi-conformal mapping, the extreme curvatures of flux near the interface between the vesicle interior and extracellular space are easily resolved. This data model can be expected to be encountered in many situations such as the diffusion of the neurotransmitter molecules released by emptying the spherical vesicles in cell biology. Interestingly, through the full simulation, it was realized that neurotransmitter spatial distribution within the vesicle attain sufficiently rapidly quasi-steady state with respect to changes of the fusion pore size. Insights obtained from this formulation allowed us to develop a simple semi-analytical procedure that will deliver results instantly rather than time-consuming confined by full simulations. We compared the results obtained by full scale simulations with that by fast analytical procedure. They reached reasonable agreement when dealing with vesicular exocytosis. Hence, in the following I will elaborate directly the fast semi-analytical simulation.

1.2 Exponential behaviour on amperometric spike

The model we set up for the study of exocytotic event is described as the following. Exocytotic vesicle of radius R_{ves} is connected at time $t=0$ to the extracellular fluid by a lipidic cylindrical channel (the fusion pore) of internal radius R_{pore} and length L . Catecholamines stored in the vesicle dense core matrix may thus be released through the channel and diffused instantly to external space. The carbon fibre electrode is positioned about 100 nm close to the cell membrane to construct an artificial synaptic cleft and act as an electrochemical detector for amperometry.

In a general case, the released flux is kinetically regulated by: (i) the intrinsic transport rate constant:

$$\kappa = D_{ves} / R_{ves}^2, \text{ [Eqn 1]},$$

within the matrix, (ii) the radius of the fusion pore, R_{pore} , and (iii) the length of the fusion pore channel, L . With the data obtained from chromaffin cell, we have proved that unless L is longer than unrealistic 10^3 nm, otherwise the release flux should only be regulated by the convergent diffusion of catecholamine cations towards fusion pore entrance inside the matrix. Therefore, the length of channel is not considered as a limiting factor dealing with exocytosis, hence will be ignored in the following. The mathematical certification can be found in [1, 4].

By inspecting each single amperometric spike, we realized that most of the first falling stage of the individual current spike represents an exponential decay. In other words, if the current is plotted in a log-scale, it exhibits a linear decline with constant slope. In our previous work we have showed that the exponential decay of current corresponds to a fixed vesicle opening angle α (see inset in Fig. 1.1a) and depends on the diffusion rate κ within the matrix [2].

The current can be expressed as:

$$i \sim \exp[-k_{\rho}^{diff} t] = \exp[\pi^2 \Lambda(\alpha) \kappa t] = \exp[-\alpha \kappa t], \text{ [Eqn 2]},$$

where t is the time and k_{ρ}^{diff} is the slope of current decay in log plot (Fig. 1.20b). As shown in this equation, if the diffusion rate keeps constant during secretory release, the exponential decay of current directly corresponds to a fixed vesicle opening angle. Unfortunately, since no more limited condition exists to restrict the values of α and κ , there is an infinite number of pair values to reproduce the measured k_{ρ}^{diff} value.

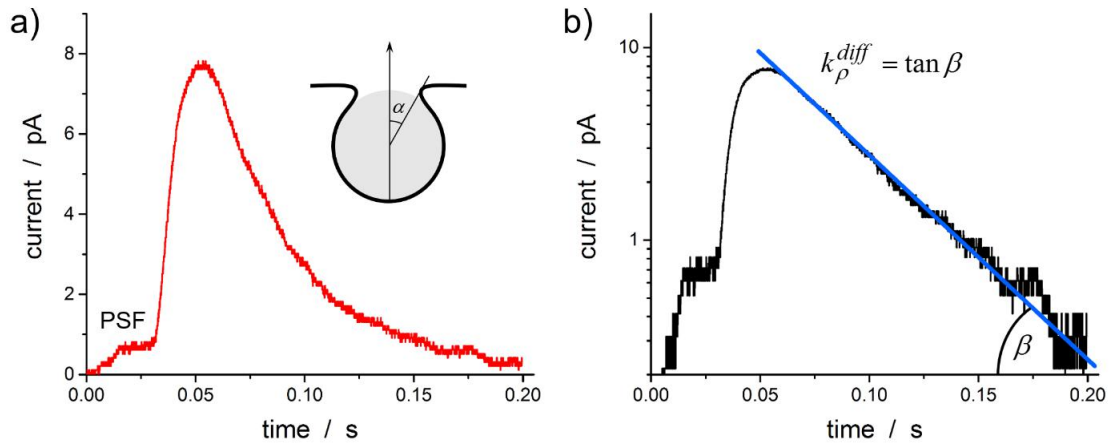


Fig. 1.1 Typical spike with PSF in real scale (a) and in log plot (b). Inset in (a) shows definition of vesicle opening angle.

1.3 Concentration profile in quasi-steady state diffusion regime

During exocytosis, the fusion pore opening creates the diffusion wave inside the matrix and cause the inhomogeneous concentration of molecules. As mentioned above, the transport rate of molecules (K) within the matrix is determined by its diffusion coefficient inside matrix, D_{ves} , as well as vesicle radius, R_{ves} . K value for chromaffin cells was recently determined as 415 s^{-1} based on the analyzed pre-spike feature intensities of amperometric spikes relating item to initial fusion pore size $R_{pore}^{initial}$ estimated by patch clamp [5]. The theoretical concentration profiles of neurotransmitter diffusion wave spanned over the complete interior of the matrix achieved at different times along the longest diffusional pathway of the spherical matrix were computed employing the K value measured above.

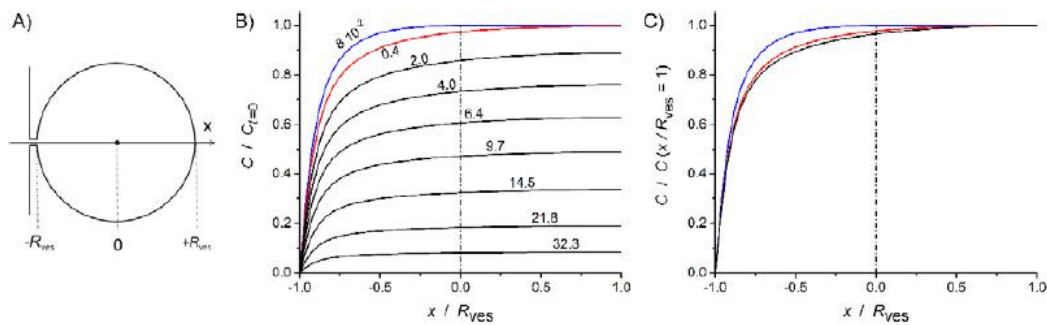


Fig. 1.2 A) Schematic representation of a fused vesicle with definition of the diametric axis x . B) Distribution of concentration along the diametric axis x at different $Kt = D_{ves}t/R_{ves}^2$ values (as marked on each curve) with the assumption that the fusion pore opened immediately to its maximum radius of $0.087R_{ves}$ (i.e., at a 5 degree half-cone angle). C) Normalization of concentration profiles in B) by corresponding concentrations at $x/R_{ves}=1$, noting that all curves shown black in B) strictly superimpose in C). Figure adapted from reference [1].

As we can realize from Fig. 1.2, after the diffusion wave hits the deepest place of vesicle membrane diametrically opposite to the pore (at $x/R_{ves}=1$), the shape of the concentration profiles maintains and only their amplitude varies. It is displayed as the same curvature of normalized concentration profile in Fig. 1.2C, that is the so called quasi-steady state regime. In other words, as soon as the diffusion spreads throughout the vesicle lumen, at any time the concentration at any point should become proportional to its average value within the matrix. In this quasi-steady state regime diffusion pattern, the relative concentration with respect to the average one depends only on the location inside matrix rather than dependent of time. Noting that $\kappa t=0.4$ (red curve in Fig. 1.2B)), the mean deviation from the quasi-steady state regime (ca. 1%) is much less than the precision on the amperometric current measurement. Even for the most severe condition like a rather large instant opening of the fusion pore (5 degrees, at a ca. 13.6 nm radius for a vesicle of mean radius $R_{ves}=156$ nm from chromaffin cell [6]), $\kappa t > 0.1$ is sufficient to ensure the achievement of quasi-steady state regime. It means that in a few tenths of a millisecond (i.e., $t > 0.1/415 \text{ s}^{-1}$ in chromaffin cell) after fusion pore opens to its maximum radius, quasi-steady state regime established in the secretory vesicle.

1.4 Quantitative extraction of fusion pore expansion

When release reaches a quasi-steady state regime, the diffusion-controlled neurotransmitter concentration pattern is established. Therefore during the spike's exponentially descending period, the concentration gradient at pore opening is proportional to the average quantity of releasable catecholamines remained inside vesicle matrix, $q_{ves}(t)$. Based on the previous work of Oleinick et. al. [7], $q_{ves}(t)$ is allowed to be expressed as:

$$dq_{ves} / dt = -\kappa \rho \times q_{ves}(t), \text{ [Eqn 3]},$$

with a time-dependent coefficient ρ that relies on the value of $R_{pore}(t)/R_{ves}$. Interestingly, when $R_{pore}(t)/R_{ves}$ is less than 0.7, a common condition applied to all treated amperometric events, the product ρ approximates with the ratio of $R_{pore}(t)/R_{ves}$. So that Eqn 3 can be rewritten as:

$$dq_{ves} / q_{ves} = -\kappa \left[R_{pore}(t) / R_{ves} \right] dt, \text{ [Eqn 4]}.$$

Noting that the total amount of releasable catecholamine cations stored inside vesicle:

$$q_{ves}^{tot} = 2F \int_0^{\infty} i(t) dt, \text{ [Eqn 5]},$$

Then the evolution of fusion pore is further represented as:

$$R_{pore}(t) = \left[i(t) \times R_{ves} / \kappa \right] / \left[q_{ves}^{tot} - \int_0^t i(u) du \right], \text{ [Eqn 6]},$$

with the dummy integration variable u related to the time. It is remarked that R_{ves} / κ is an independent index that is not quite necessary for comparing the trend of fusion pore expansion from similar vesicles belonging to a given cell type. When κ is unknown, $R_{pore}(t)$ obtained from the series of individual current spikes would be on a same relative scale. If the actual information about pore dimension is required, the following procedure was employed for determining κ .

1.5 Determination of molecule transport rate within intravesicular matrix

PC12 cells are reported to have dense core vesicles with diameter in a wide range (100nm~240nm) measured by electron microscopy. This wide range could be explained by the uniqueness of each exocytotic events. Compared with the amperometric spikes obtained by Ewing's lab, ours displayed smaller spikes with lower charge in average. It's possibly due to the small size of vesicles in our PC12 cells. Thus we reasonably applied 80nm, a bit smaller than average value reported previously, as vesicle radius in our reconstruction model.

The pre-spike feature from the amperometric spike reflects the initial fusion pore opening [8]. It appears approximately in one third of all exocytotic events, hence it is definitely a statistically representative fraction. The pre-spike feature often displayed a steady-state current lasting for several milliseconds, which represents a stable structure of initial fusion pore. We have proved that the pre-spike current is related to both initial fusion pore size and the transport rate of molecules inside matrix in our previous work [4]. Therefore, if the initial fusion pore radius is foreknown, it's easy to accomplish the calibration of a series of κ relied on independent single intense pre-spike features. Sharing similar vesicle structure, properties of neurotransmitter storage and exocytotic behaviour, PC12 cells is considered a promising substitute of adrenal chromaffin cells as cell model for neurosecretion research. Hence we applied 1.2nm [5], the initial pore radius of chromaffin cell measured by patch-clamp, as the approximate value of fusion pore radius in the first opening stage of PC12 cells. After calibration of well-defined foot portion on amperometric spikes, a set of κ values was obtained. The common diffusion rate constant value then was defined as the average value of this set for reconstruction of fusion pore enlargement.

1.6 Reference

1. A. Oleinick, I. Svir, C. Amatore, *'Full fusion'is not ineluctable during vesicular exocytosis of neurotransmitters by endocrine cells*. Proc. R. Soc. A, 2017. **473**(2197): p. 20160684.
2. C. Amatore, A. I. Oleinick, I. Svir, *Diffusion from within a spherical body with partially blocked surface: diffusion through a constant surface area*. ChemPhysChem, 2010. **11**(1): p. 149-158.

3. C., Amatore, A. I. Oleinick, I. Svir, *Reconstruction of aperture functions during full fusion in vesicular exocytosis of neurotransmitters*. ChemPhysChem, 2010. **11**(1): p. 159-174.
4. A. Oleinick, F. Lemaître, M. Guille-Collignon, I. Svira, C. Amatore, *Vesicular release of neurotransmitters: converting amperometric measurements into size, dynamics and energetics of initial fusion pores*. Faraday discussions, 2013. **164**: p. 33-55.
5. A. Albillos, G. Dernick, H. Horstmann, W. Almers, G. Alvarez de Toledo, M. Lindau, *The exocytotic event in chromaffin cells revealed by patch amperometry*. Nature, 1997. **389**(6650): p. 509.
6. R. Coupland, *Determining sizes and distribution of sizes of spherical bodies such as chromaffin granules in tissue sections*. Nature, 1968. **217**(5126): p. 384.
7. A. Oleinick, R. Hu, B. Ren, Z. Tian, I. Svir, C. Amatore, *Theoretical model of neurotransmitter release during in vivo vesicular exocytosis based on a grainy biphasic nano-structuration of chromogranins within dense core matrixes*. Journal of The Electrochemical Society, 2016. **163**(4): p. H3014-H3024.
8. C. Amatore, S. Arbault, I. Bonifas, M. Guille, F. Lemaître, Y. Verchier, *Relationship between amperometric pre-spike feet and secretion granule composition in chromaffin cells: an overview*. Biophysical chemistry, 2007. **129**(2-3): p. 181-189.

II. Cell transfection and selection

The monitor of exocytosis through TIRFM is regularly achieved by the fluorescent labeling of intracellular exocytosis-associated organelles. Here I would like to present our effort for labeling cellular organelles via cell transfection and polyclonal cell line selection. Owing to sufficient biological information supported by numerous research as well as massive analogous investigation surrounding exocytosis as reference, PC12 cell was chosen as our cell model for exocytosis study and thus became the marking object. TIRFM was applied as the detection tool to inspect labeling consequence.

2.1 cell transfection in optimized condition

PC12 cells were seeded in collagen4 coated μ -dish (ibidi) with 1×10^5 cells/mL in complete growth medium to ensure 70-90% confluent in the next day. Complete growth medium was replaced with non-penicillin streptomycin one before transfection. Lipofectamine 3000 reagent 8 μ L was well diluted in 125 μ L Opti-MEM. The master mix of DNA was prepared by diluting 3 μ g plasmid in another 125 μ L Opti-MEM, followed by adding 6 μ L P3000 Reagent (2 μ L/ μ g DNA) and gently mixing. Hereafter diluted DNA was further mixed with diluted Lipofectamine 3000 reagent within 1:1 ratio. Mixture was incubated 5 min at room temperature and then evenly dropped into cell sample. Cell sample was carefully transferred into the incubator with cell-friendly atmosphere and stored overnight for gene embedding.

2.2 Stable cell line selection

The efficiency of transfection manipulation no more than 60% even under ideal condition. In order to obtain a population of labeled cells, stable cell line selection can be taken into consideration. When plasmid contains a selectable marker which is resistant to specific antibiotic, antibiotic selection can be applied to sustain cells expressed the antibiotic-immune proteins introduced by transfection whereas the non-transfected cells are all killed by the long time incubation with antibiotic.

pCAGLifeAct - TagRFP encoding common neomycin phosphotransferase inhibition sequences purchased from ibidi were applied as test probe for optimizing antibiotic concentration. Transfected PC12 cells were aliquoted into collagen 4 coated 24-well plate with 10^4 cells /well in 0.5 mL complete growth medium one day before antibiotic selection. G418 as an analog of neomycin sulfate was used as a selective agent for PC12 cells and added into each well according to the dose gradient presented in Fig. 2.1 Left. Medium containing G418 was refreshed every two days till the end of seven days' selection. Number of cells in each well was then counted and drew into the killing curve of G418 as a function of antibiotic

concentration (Fig. 2.1 Right). Concentration of G418 from wells containing living cells completely labeled by RFP after selection was identified as optimal dose, which is around 500 $\mu\text{g}/\text{mL}$ read out from the curve. This dosage can be universally used to select PC12 cells transfected with various plasmids encoding neomycin resistance gene. Except for the biochemical selection, purification of fluorescence labeled PC12 cells can be further approached by flow cytometry selection. Although the polyclonal selection technique has not been used in this thesis, it is still an applied practice of manipulation. Aware of proper dosage of antibiotic makes profound benefit for future stable cell line acquirement, circumventing the repetitive time-consuming transfection with same vector required by experiment.

**PC12 G418 selection:
optimal concentration determination ($\mu\text{g}/\text{mL}$)**

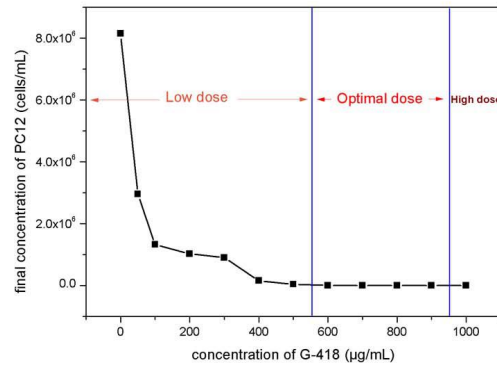
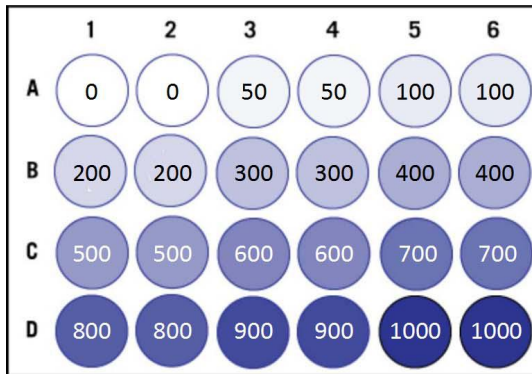


Fig. 2.1 Increasing amount of G418 applied in dose-response experiment based on PC-12 cells(left) and the corresponding kill curve (right).

Résumé

L'exocytose, la dernière étape du processus de sécrétion, a été étudiée sur des cellules neuroendocrines modèles (PC12). Nous avons caractérisé l'internalisation d'un analogue synthétique de neurotransmetteur (FFN102) dans les vésicules des cellules PC12. La différence de potentiel d'oxydation de la dopamine et de ce faux neurotransmetteur fluorescent a été exploitée pour montrer que l'internalisation de FFN102 s'effectue en remplaçant 10% de la dopamine endogène présente dans les vésicules. De plus, la cinétique de libération de FFN102 suggère son stockage dans un compartiment de la vésicule où sa diffusion est facilitée. Cette sonde électroactive et fluorescente associée aux cellules PC12 constitue donc un système de choix pour des études bioanalytiques impliquant la libération de neurotransmetteurs par exocytose. L'exocytose débute par la formation d'un pore formé par la fusion de la membrane vésiculaire avec la membrane de la cellule. Les mécanismes de régulation de l'expansion du pore de fusion ne sont pas complètement connus. Nous avons montré que la myosin II limite la vitesse d'expansion du pore en détectant la libération de la dopamine par ampérométrie et en traitant les cellules PC12 avec un inhibiteur pharmacologique. La mesure de la cinétique d'ouverture du pore à l'aide d'un modèle développé récemment a montré que la myosin II ne modifie pas la taille maximale du pore au cours de la libération de neurotransmetteurs. Ce suivi ampérométrique de l'expansion du pore est limité à une durée de quelques dizaines de millisecondes.

Afin d'étendre la durée du suivi de l'expansion du pore, nous avons réalisé des mesures simultanées de libération de la dopamine par ampérométrie et d'évolution de la membrane vésiculaire par TIRFM. La membrane des vésicules a été marquée par des protéines fluorescentes sensibles au pH et génétiquement encodées. Nous avons pu ainsi observer l'évolution du pore qui s'achève par une fermeture ou une expansion complète. La quantité de neurotransmetteurs détectée était plus importante dans le cas d'une expansion totale du pore.

Mots Clés

exocytose, libération sécrétoire, pore de fusion, vésicule, neurotransmetteur

Abstract

Exocytosis, the last step of the secretion process was investigated using the PC12 neuroendocrine cell model. We characterized the uptake of FFN102, a synthesized analog of neurotransmitter, in the secretory vesicles of PC12 cells. Relying on the different oxidation potentials of dopamine and FFN102, it was shown that FFN102 replaces ca. 10% of the dopamine stored in the vesicles. The release kinetics of FFN102 suggests that its storage occurred in a fast diffusion compartment of the vesicles. This electroactive fluorescent probe associated with the PC12 appears therefore as a valuable system for bioanalytical studies related to neurotransmitters release. Exocytosis starts when vesicular and cellular membranes fuse and lead to the formation of the fusion pore. The regulation mechanisms of the fusion pore expansion are not completely known. We have shown that myosin II slowed down the pore expansion using amperometric detection of released dopamine and inhibiting myosin II in PC12 cells treated with a pharmacological drug. A recently introduced model was used to measure the pore expansion kinetics and show that myosin II did not affect the extent of pore opening during neurotransmitter release. This monitoring of fusion pore expansion only span the tens milliseconds timescale. Simultaneous monitoring of both released dopamine using amperometry and stained vesicular membrane using TIRFM achieved to track the whole exocytotic events. The vesicular membrane was stained with genetically encoded pH-sensitive tagged proteins. Both "full opening" and closure of the pore were observed. The amount of released neurotransmitters was higher when the pore fully opened.

Keywords

exocytosis, secretory release, fusion pore, vesicle, neurotransmitter